

University of Arkansas, Fayetteville

ScholarWorks@UARK

Graduate Theses and Dissertations

12-2020

Fourier Transform Infrared Spectroscopy for the measurement of GeSn/(Si)GeSn

Solomon Opeyemi Ojo

University of Arkansas, Fayetteville

Follow this and additional works at: <https://scholarworks.uark.edu/etd>



Part of the [Electromagnetics and Photonics Commons](#), [Electronic Devices and Semiconductor Manufacturing Commons](#), and the [Semiconductor and Optical Materials Commons](#)

Citation

Ojo, S. O. (2020). Fourier Transform Infrared Spectroscopy for the measurement of GeSn/(Si)GeSn. *Graduate Theses and Dissertations* Retrieved from <https://scholarworks.uark.edu/etd/3901>

This Thesis is brought to you for free and open access by ScholarWorks@UARK. It has been accepted for inclusion in Graduate Theses and Dissertations by an authorized administrator of ScholarWorks@UARK. For more information, please contact scholar@uark.edu.

Fourier Transform Infrared Spectroscopy for the measurement of GeSn/(Si)GeSn

A thesis submitted in partial fulfillment
of the requirements for the degree of
Master of Science in Microelectronics-Photonics

by

Solomon O. Ojo
Obafemi Awolowo University
Bachelor of Science in Engineering Physics, 2005

December 2020
University of Arkansas

This thesis is approved for recommendation to the Graduate Council.

Shui-Qing Yu, Ph.D.
Thesis Co-Director

Zhong Chen, Ph.D.
Thesis Co-Director

Gregory Salamo, Ph.D.
Committee Member

Rick Wise, Ph.D.
Ex-Officio Member

The following signatories attest that all software used in this thesis was legally licensed for use by Solomon Ojo for research purposes and publication.

Mr. Solomon O. Ojo, Student

Dr. Shui-Qing Yu, Thesis Co-Director

Dr. Zhong Chen, Thesis Co-Director

This thesis was submitted to <http://www.turnitin.com> for plagiarism review by the TurnItIn company's software. The signatories have examined the report on this thesis that was returned by TurnItIn and attest that, in their opinion, the items highlighted by the software are incidental to common usage and are not plagiarized material.

Dr. Rick Wise, Program Director

Dr. Shui-Qing Yu, Thesis Co-Director

Dr. Zhong Chen, Thesis Co-Director

Abstract

Photoluminescence (PL) and Electroluminescence (EL) characterization techniques are important tools for studying the optical and electrical properties of (Si)GeSn. Light emission from these PL and EL measurements provides relevant information on material quality, bandgap energy, current density, and device efficiency. Prior to this work, the in-house PL set-up of this lab which involves the use of a commercially-obtained dispersive spectrometer was used for characterizing both GeSn thin film and fabricated devices, but these measurements were limited by issues bordering on low spectral resolution, spectral artifacts, and poor signal-to-noise ratio (SNR) thereby resulting in the possible loss of vital information and inaccurately reported parameters.

To maintain the progress of the GeSn material development toward replacing the group III-V semiconductors in the optoelectronics industry, high-resolution spectroscopy with high SNR are necessary to accurately determine the unknowns in the GeSn growth conditions, device fabrication, and material development. In this work, PL and EL characterization systems were designed, built, and aligned using a Bruker Fourier transform infrared (FTIR) set up to collect the emission from fabricated GeSn samples using an external source with an external photodetector.

This thesis presents an optical setup of a Bruker FTIR spectrometer aligned with external optical components and external light sources (532 nm laser and 1064 nm laser) to achieve high-resolution spectroscopy with high SNR. The setup employs the use of OPUS operational software for controlling the components of the FTIR hardware and a LabVIEW program for controlling all motorized devices on the external optical bench. An indium antimonide (InSb) external photodetector was used with the FTIR for a wider spectral range detection. Finally, a

step-scan mode of operation which required both lock-in and a chopper was used to measure various GeSn bulk and laser samples at high resolution. The results obtained from these characterizations demonstrate a high SNR spectrum compared to a dispersive spectrometer.

Acknowledgment

I would like to thank my advisor, Dr. Shui-Qing (Fisher) Yu, for his patience, support, and guidance. His faith in me has helped me develop strong research skills and the logic required to conduct experiments as a researcher. I am grateful to Dr. Gregory Salamo whose FTIR spectrometer has made this thesis possible. I would like to thank Dr. Zhong Chen for agreeing to be my thesis co-advisor and whose office is always open to me for discussion.

Special thanks to Dr. Rick Wise for giving me the opportunity to join the Microelectronics-Photonics program and for always providing excellent leadership. I would like to thank Renee Jones-Hearon whose support, interest, and generosity are to an extent unparalleled.

I would like to thank Dr. Yiyin Zhou for introducing me to the laser world. As the leading student when I newly joined the group, he brought me up to speed with the training and projects, and got me involved in characterization and fabrication. I am also thankful to him for his guidance on the Bruker Fourier transform infrared spectroscopy (FTIR) setup. I would like to thank Joshua M. Grant for introducing me to the UHCVD chamber and ensuring I become a certified grower. I would like to thank members of the research group for their support and help with various research tasks.

I would also like to thank my family whose immense support has made this degree possible. They have been a solid pillar in and out of season upon which I could always rely. To my mother who has always believed in the future and encouraged me all the way. To my parents-in-law, Mr. Felix Ilesanmi Fadayomi and Mrs. Oluremi Fadayomi, for always cheering me on. Special thanks to my wife who has been the greatest gift I could ever ask for, and you will always mean the world to me. I would like to acknowledge the love and support from my

daughters, IranlowoOluwa and Olamiposi, and my son, Aaron. You guys have been my source of encouragement and motivation to always want to be the best student and a better father.

I would like to thank the funding agency. This project was financially supported by the Air Force Office of Scientific Research (AFOSR) # FA9550-18-1-0045. Any opinions, findings, and conclusions or recommendations expressed in this material are those of the author and do not necessarily reflect the views of any of this funding agency. This research was made possible through the use of the High-Density Electronics Center (HiDEC) at the University of Arkansas, Fayetteville campus to fabricate GeSn laser devices.

Dedication

I dedicate this thesis to God Almighty, the source and the giver of life, the one in whom I live, move, and have my being. I also dedicate this work to my wife Olamiposi Antinuke Ojo, for her unending love and unconditional support. To my children IranlowoOluwa Ojo, Olamiposi Ojo, and Aaron Ojo for sticking with me through this journey and not loving me less, and finally to my mother Elizabeth Adedoyin Adelaja for praying me beyond my limitations.

When I think of success and accomplishment, you all come to mind because you made it possible. I am grateful.

Table of Contents

Chapter 1: Introduction	1
1.1 Motivation.....	1
1.2 Problem Statement and Objective.....	4
1.3 Scope and Organization of this Thesis	5
Chapter 2: FTIR Spectroscopy.....	7
2.1 Introduction.....	7
2.2 Principles of Operation	9
2.3 FTIR Modes of Operation.....	11
2.3.1 Continuous-Scan Mode.....	11
2.3.2 Step-Scan Mode	12
2.4 The Interferogram Mathematical Expression	13
2.5 FT-IR Advantages.....	14
Chapter 3: BRUKER IFS 66/S FTIR Project	16
3.1 Experimental Setup.....	18
3.1.1 Infrared Fourier Spectrometer IFS 66/S Setup and Internal Alignment	18
3.1.2 Optical Bench External Setup and Alignment	24
3.2 Optical Elements Construction for Step Scan Option	26
3.2.1 Optical Path Construction for Room-Temperature (RT) Measurement	27
3.2.2 Optical Pumping Measurement Setup	29
3.2.3 Electroluminescence Measurement Setup	30
Chapter 4: FTIR PL (EL) Measurements	33

4.1 FTIR Measurement for PL.....	33
4.1.1 Ge PL	33
4.1.2 GeSn PL	38
4.2 FTIR Measurement for GeSn Laser.....	39
4.2.1 Device Fabrication	40
4.2.2 Optical Pumping Measurement.....	46
4.2.3 Electroluminescence Measurement	51
4.3 Results and Discussion	61
Chapter 5: Conclusion and Future Work.....	64
References	65
Appendix A: Description of Research for Popular Publication	68
Appendix B: Executive Summary of Newly Created Intellectual Property	70
Appendix C: Potential Patent and Commercialization Aspects of Listed Intellectual Property Item	71
Appendix D: Broader Impact of Research	72
Appendix E: Microsoft Project for MS MicroEP Degree Plan	73
Appendix F: Identification of All Software Used in Research and Thesis Generation	74
Appendix G: All Publications Published, Submitted, and Planned	75
Appendix H: Bruker IFS 66/S Standard operating procedure for Yu Lab	78
Appendix I: Edge Emitting LED/Lasers Fabrication Traveler.....	88

List of Figures

Figure 1.1. Schematic of the electronic band structure for germanium (Ge) and silicon (Si) at room temperature	3
Figure 1.2. Plot showing the GeSn bandgap energy as a function of Sn concentration	3
Figure 2.1. Example of a typical infrared spectrum.....	7
Figure 2.2. Schematic diagram of a dispersive spectrometer; a monochromator	8
Figure 2.3. Michelson interferometer.	9
Figure 2.4. Infrared Interferogram	11
Figure 2.5. Relative phase relationship of waves from fixed (solid) and movable (dashed) mirrors at different δ values: (a) zero path difference; (b) path difference of one-half wavelength	11
Figure 2.6. (a) continuous-scan mode and (b) step-scan mode illustration	12
Figure 3.1. View of ENRC 2933A laboratory showing the Bruker IFS 66/S spectrometer and other optical elements.	17
Figure 3.2. External view of the IFS 66/S distinguished compartments	18
Figure 3.3. Inside view of the BRUKER IFS 66/S Interferometer Compartment.....	19
Figure 3.4. (a) Sine wave signal observed on the oscilloscope (b) Unlit TC20 processor board.	20
Figure 3.5. Bruker IFS 66/S Optical Layout.....	21
Figure 3.6. OPUS Stepper Motor control.	22
Figure 3.7. Bruker IFS 66/S Interferogram display at room temperature.....	22
Figure 3.8. Side view of IFS 66/S He-Ne laser alignment with the optical table plane.	24
Figure 3.9. Light box showing (a) the parabolic mirror within, (b) the detector holder with threaded nut, and (c) a detector securely seated in its holder.	25
Figure 3.10. IFS 66/S alignment from the alternative output port using a white light source.....	26
Figure 3.11. 532 nm green laser alignment from source to sample holder.....	28
Figure 3.12. Bruker IFS 66/S room temperature PL schematic diagram.....	28

Figure 3.13. Bruker IFS 66/S Optical Pumping schematic diagram.....	30
Figure 3.14. FTIR PL spectroscopy and Optical pumping schematic	31
Figure 3.15. IFS 66/S optical path for EL measurement.	32
Figure 4.1. Normalized Ge RT PL spectrum with LN ₂ cooled InGaAs detector.	34
Figure 4.2. Ge RT PL spectra measured with (a) 8 cm ⁻¹ and (b) 4 cm ⁻¹ resolutions, respectively.	35
Figure 4.3. Ge spectrum from step-scan measurement.....	35
Figure 4.4. Ge PL spectra measured with (a) iHR320 spectrometer and (b) FTIR spectrometer.	36
Figure 4.5: Ge PL spectra from (a) iHR320 and (b) FTIR spectrometer using pulsed laser.	37
Figure 4.6. Ge RT PL spectra comparison.....	38
Figure 4.7. GeSn PL spectra from (a) iHR320 and (b) FTIR spectrometer using a pulsed laser.	39
Figure 4.8. GeSn PL spectra using (a) iHR320 and (b) FTIR spectrometer with a pulsed laser..	39
Figure 4.9. LED device fabrication process flow.	40
Figure 4.10. (a) Si wafer cleaved into four quarters. (b) A quarter wafer cleaved into 1x1 inch ² squares.....	41
Figure 4.11. Four (1-inch x 1-inch) etched samples of GeSn.....	43
Figure 4.12. Schematic diagram of a standard photolithography process.	44
Figure 4.13. Sample image after the development of the negative photoresist.	44
Figure 4.14. Sample image after metal deposition.	45
Figure 4.15. Wire bonded device.....	46
Figure 4.16. (a) Side facet of a cleaved device. (b) Mounted cleaved sample.	47
Figure 4.17. Cryostat stabilization for optical pumping measurement.	48
Figure 4.18. Temperature-dependent L-L curve for GeSn laser.....	48
Figure 4.19. Spectra of GeSn laser at 77 K.....	49
Figure 4.20. Spectra of GeSn laser at 90 K.....	49
Figure 4.21. Spectra of GeSn laser at 110 K.....	50

Figure 4.22. 77 K Spectra of GeSn laser at (a) 8 cm ⁻¹ and (b) 4 cm ⁻¹ resolution.	50
Figure 4.23. Pth spectrum across temperatures.	51
Figure 4.24. Light emission by application of electric field to the p-n junction.....	52
Figure 4.25. Cross-sectional schematic of samples (a) F and (b) G laser devices.....	52
Figure 4.26. Temperature-dependent I-V curve for sample F with 11% Sn composition.....	53
Figure 4.27. LI curves of 0.8 mm cavity length and 80 μm ridge at 77 K and 100 K.....	54
Figure 4.28. EL spectra of various current injections at 77 K.	55
Figure 4.29. 3D view of EL spectra of various current injections at 77 K.	55
Figure 4.30. EL spectra of various current injections at 100 K.	56
Figure 4.31. 3D view of the EL spectra of various current injections at 100 K.	56
Figure 4.32. EL spectra from microHR dispersive spectrometer at 77 K.....	57
Figure 4.33. Lasing spectra from microHR spectrometer compared with lasing spectra from FTIR spectrometer at 77 K.	57
Figure 4.34. Temperature-dependent I-V curve for sample G with 11% Sn composition.	58
Figure 4.35. LI curves of 1.0 mm cavity length and 80 μm ridge from 10 K and 120 K.....	58
Figure 4.36. EL spectra from microHR dispersive spectrometer at 10 K.....	59
Figure 4.37. EL spectra from microHR dispersive spectrometer at 77 K.....	59
Figure 4.38. EL spectra from microHR dispersive spectrometer at 100 K.....	60
Figure 4.39. EL spectra from microHR dispersive spectrometer at 110 K.....	60

List of Tables

Table 2.1. Pros and cons of a continuous-scan and step-scan modes of interferometer operations.....	13
Table 3.1. IFS 66/S FTIR compartments	17
Table 3.2. IFS 66/S room temperature internal alignment configuration.	23
Table 4.1. Room temperature PL characterization summary of Ge buffer growths.....	61
Table 4.2. Summary of Sample (E) and Lasing Characterization Results at 77 K.....	61
Table 4.3. Sample G summary at 110 K.....	62
Table 4.4. The FWHM characteristics at 10 K, 77 K, and 110 K.....	63

Chapter 1: Introduction

1.1 Motivation

Since the potential of integrated silicon photonics was first demonstrated in 1985[1], [2], the prospect of developing silicon-based light emitters for optoelectronics devices and on-chip communication has attracted special interest and motivated further research efforts both theoretically and experimentally. Silicon remains a prominent semiconductor material for electronic devices because of its earthly abundance which makes it readily available and affordable (low cost), its formation of stable high-quality oxides with ease (suitable for IC fabrication techniques), and its doping capability. In spite of the remarkable success of silicon technology, it has reached its upper limits for data transmission as transistors continue to scale in agreement with Moore's Law prediction. With the current state of the art pushed to its limit, silicon electronics face major challenges as the electrical interconnects have become the limiting factor for performance while additional transistors enhance computational performance[3]–[5]. This gave rise to the concept to integrate electronics with optical components on a Si chip. Achieving this approach involves the substitution of electrical interconnects with optical interconnects on silicon chips to overcome the technical barrier posed by Moore's Law prediction. The benefits of using optical interconnect includes: increased high-speed data transmission using photons (light signals), a significant reduction in power consumption [6], increased interconnect energy efficiency, improved clock and signal timing, and very low data loss for relatively long-distance [5]. To achieve a cost-effective process for the replacement of electrical interconnects with optical interconnects, monolithic integration on silicon and Si complementary metal-oxide-semiconductor compatibility (CMOS) is necessary to make a variety of optical and optoelectronic devices.

However, the dearth of a monolithic Si-compatible laser source has since hindered the development of optoelectronic integration with metal-oxide-semiconductor compatibility (CMOS) [7], [8]. The reason for this drawback is due to the indirect bandgap of silicon which makes it an inefficient light source. To overcome this challenge and achieve the set goal of fabricating efficient Si-based light laser, researchers employed a hybrid solution that utilizes direct bandgap III–V lasers as light sources through monolithic integration steps as wafer-bonding or selective area growth [9]–[14]. However, the complexity and low compatibility of III-V materials with Si complementary metal-oxide-semiconductor (CMOS) technology increases fabrication costs and is time-consuming which makes the method expensive.

As a result, group IV materials are particularly desirable because of their similar electronic properties with Si, for achieving monolithic integration of lasers on silicon CMOS-compatible technology at a lower cost [15]. More recently, GeSn binary alloys [16]–[21] have been investigated extensively for exhibiting a direct bandgap with Sn composition above 6% [15]. The GeSn material system shows immense potential as an optoelectronic material that can be integrated monolithically on a low-cost Si platform by CMOS technology [22], [23]. The uniqueness of GeSn material, despite group IV's low light-emitting efficiency due to indirect bandgap, lies in its ability to transition from indirect-to-direct bandgap material with the incorporation of sufficient Sn (another group IV material). Therefore, it makes for an excellent light emitting devices. Figure 1.1 illustrates the band structure of Si and Ge as examples of group IV materials with indirect band gap, while Figure 1.2 [24] depicts the transition of GeSn material from indirect to direct bandgap material as a function of Sn concentration. The GeSn alloy material has a flexible bandgap that can be tuned to enhance its optical properties by varying the Sn composition; hence, its bandgap and strain engineering attribute. The material wavelength

covers a broad range in mid-infrared (MIR) because of its bandgap tunability, which makes it suitable for a wide range of device applications in the IR range.

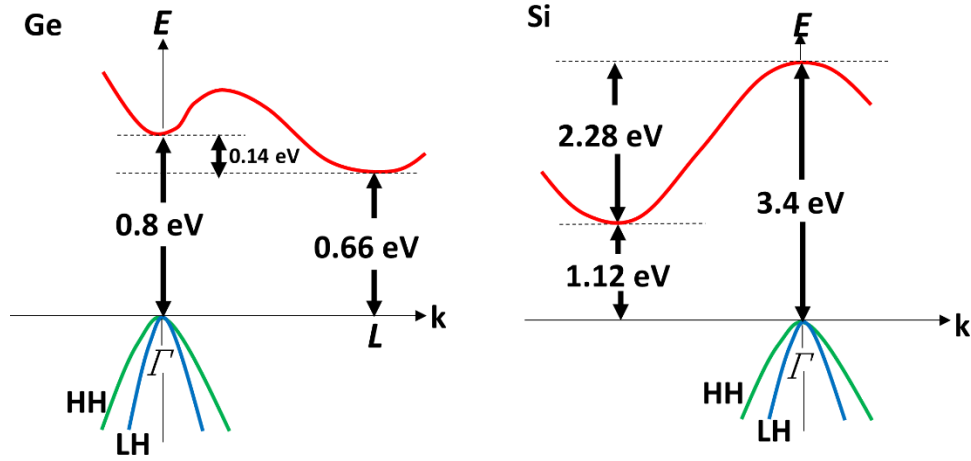


Figure 1.1. Schematic of the electronic band structure for germanium (Ge) and silicon (Si) at room temperature [25].

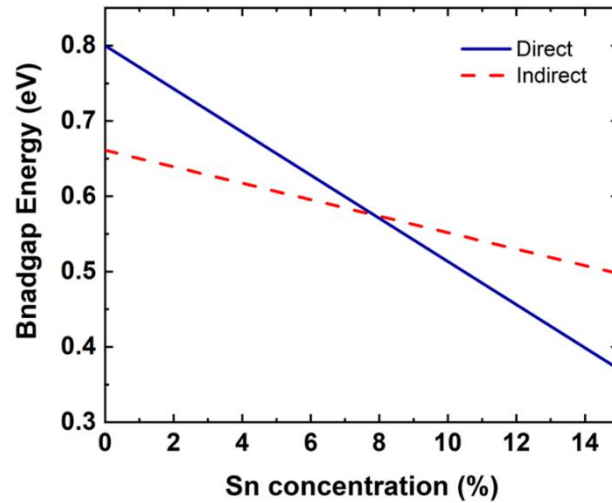


Figure 1.2. Plot showing the GeSn bandgap energy as a function of Sn concentration [26].

Opportunities and significant characteristics of GeSn such as directness and bandgap tunability, wide wavelength range, and compatibility with state-of-the-art CMOS technology, make GeSn an attractive group IV emitting material for laser devices and various optoelectronic applications.

1.2 Problem Statement and Objective

Optical and electrical characterization of germanium tin (GeSn) and silicon germanium tin (SiGeSn) alloy materials with different structures and various Sn compositions have been performed extensively in Dr. Fisher Yu's lab (University of Arkansas, Fayetteville), to investigate the quality of the layers and Sn concentrations and to gain a greater understanding of the material properties.

The standard protocol for this characterization is achieved with the use of dispersive infrared spectrometers. However, the resolution of most infrared spectra from (Si)GeSn samples measured on dispersive spectrometers is of low quality and low signal-to-noise (SNR) ratio. In addition to this, GeSn laser measurement exhibits a wide laser linewidth (FWHM) from the acquired spectrum in a slow process that measures every wavelength individually across the spectrum with a dispersive spectrometer. All these are because dispersive infrared spectrometers, otherwise known as grating or scanning spectrometers, are slit-based spectrometers.

The slit on a dispersive spectrometer greatly limits the amount of energy reaching the (Si)GeSn sample and, ultimately, the detector, hence a small signal-to-noise ratio (SNR) of the measured infrared spectrum is attained. The limitation of the throughput energy is responsible for the low signal-to-noise ratio (SNR) which is insensitive to small peaks and gives little or blurry details of the sample spectrum making it difficult to distinguish unique peaks in the spectrum. Also, the feasibility of high-resolution measurement on a dispersive spectrometer at an extremely small slit is difficult. The reason has been that a slit-based spectrometer cuts off the light significantly, such that the device does not have sufficient intensity to get a meaningful spectrum at high-resolution, resulting in a low-quality spectrum. Thus, more features and vital information on the structures and properties of (Si)GeSn material are still elusive and insights on the

improvement of the material growth and performances are difficult to obtain.

One way to overcome these challenges and gain deeper insights toward a better understanding and improvement of the (Si)GeSn material is the use of a Fourier-transform infrared (FTIR) spectrometer. A FTIR based spectrometer does not cut the device signal significantly and is capable of measuring at high-resolution. The aim is to conduct both optical and electrical characterization of (Si)GeSn using the FTIR based spectrometer to achieve a high-resolution measurement of infrared spectra with greater quality and higher signal-to-noise ratio.

1.3 Scope and Organization of this Thesis

In this research, the performance of an FTIR spectrometer over a dispersive infrared spectrometer was explored toward obtaining a higher quality resolution and narrow laser linewidth (FWHM) for (Si)GeSn alloys. The main motivation was to obtain a higher signal-to-noise ratio, clearer and more distinguishable spectrum details in the FTIR spectrum, than the dispersive spectrum of the (Si)GeSn same sample.

In Chapter 2 of this thesis, a brief introduction to FTIR spectroscopy is presented — its working principles and the instrumentation. The chapter also includes the benefits of the FTIR spectrometer over dispersive spectrometer.

Chapter 3 provides detailed information on the experimental setup of the spectrometer (Bruker IFS 66/S FTIR), its alignment to an external light source, and the design for various experiments using a single setup. The experimental procedure for device characterization is specified and the results from the material measurement are compared with previous results from a dispersive spectrometer.

Chapter 4 looks at the fabrication process and characterization of the GeSn edge-emitting LED (light-emitting diode). The resulting spectrum is analyzed and compared based on different

spectrometers.

Finally, Chapter 5 discusses and presents a summary of all results. Conclusions, new capabilities, and recommended future work are also presented there.

Chapter 2: FTIR Spectroscopy

2.1 Introduction

Infrared spectroscopy (IR) is a technique for studying the interactions between the molecules of material and light in the infrared region of an electromagnetic spectrum. It involves the absorption measurement of distinct infrared frequencies of a sample irradiated with monochromatic infrared electromagnetic radiation or placed in the optical path of an IR beam. The absorbed radiation corresponds to the vibration of specific molecular bonds. As shown in Figure 2.1, the absorbed IR radiation of the material sample is measured with a spectrometer and plotted against specific wavenumbers (wavelength) in the IR region.

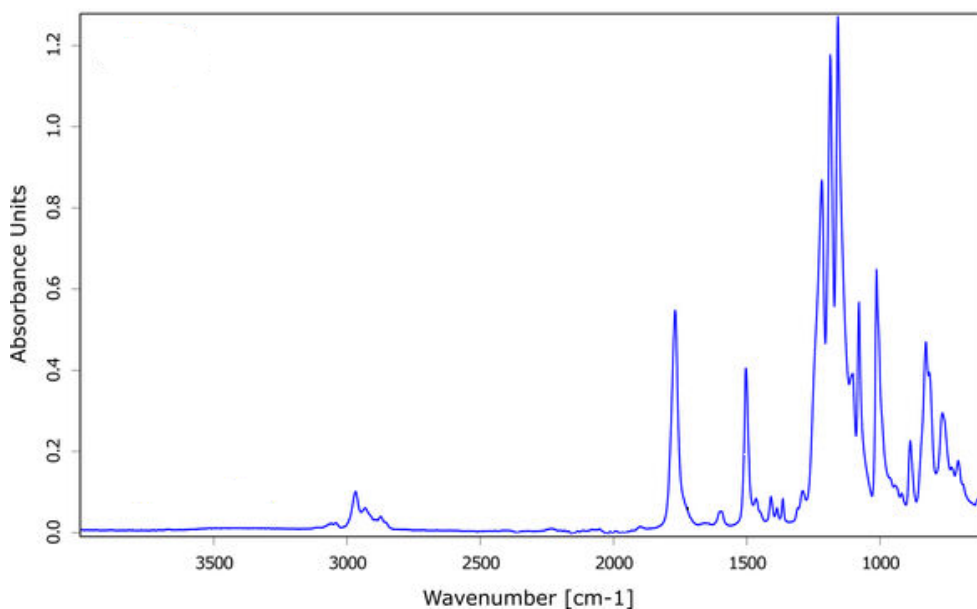


Figure 2.1. Example of a typical infrared spectrum.

The plot in Figure 2.1 results in a spectrum that provides a unique molecular characteristic (fingerprint) used to identify and quantify components of unknown samples and to obtain structural information on a sample with specific regard to its chemical composition and respective concentrations.

There are two main methods for performing infrared spectroscopy [27]. The first method makes use of a dispersive spectrometer to generate spectra; by using diffraction grating to optically separate (disperse) the incoming light into constituents of different wavelengths (colors) of the electromagnetic spectrum. A scanning monochromator with small slit width at the entrance and the exit port of the spectrometer is then used to direct the required wavelength range of the dispersed light to a detector as shown in Figure 2.2. The spectral resolution of this spectrometer is a function of the groove frequency of the grating, which also determines its wavelength coverage.

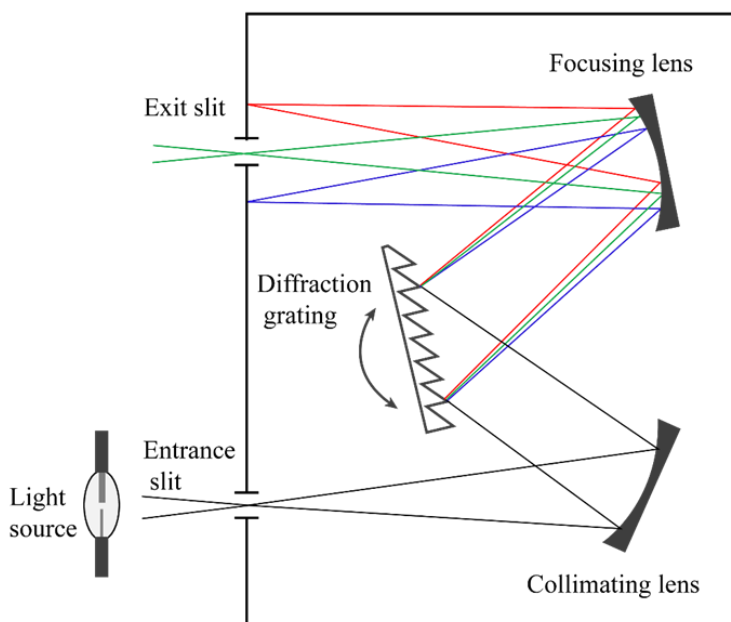


Figure 2.2. Schematic diagram of a dispersive spectrometer; a monochromator [28].

The second method involves using a Fourier-transform (FT) spectrometer to study the absorptive and emissive properties of materials. This spectrometer uses a Michelson interferometer to modulate the radiation signal and encode the wavenumber details from the source radiation. A Fourier-transform (FT) is performed on the data coding to obtain a frequency

domain infrared spectrum. This method is referred to as Fourier transform infrared (FTIR) spectroscopy because of the key role of the Fourier transformation [29], [30].

2.2 Principles of Operation

The Fourier transform (FT) spectrometer core component is the Michelson interferometer. As shown in Figure 2.3, the Michelson interferometer consists of a light source (S), a detector (D), a beam splitter, and two perpendicular plane mirrors. One of the mirrors, M_1 , is a fixed mirror, and the other a movable mirror, M_2 , which can move in the direction indicated by the arrow. As a collimated beam of radiation from a coherent light source enters the interferometer, the incoming beam impinges the beam-splitter and then splits into two beams of equal amplitude (50/50). One beam (50%) is transmitted through the beam-splitter to a mirror and the other 50% is reflected to the second mirror. These beams (transmitted and reflected) are then reflected off the mirrors M_1 and M_2 shown in Figure 2.3, respectively, and retraces the path to the beam-splitter. Each of these beams hits the beam-splitter a second time, where they recombine and passed to the infrared detector, D .

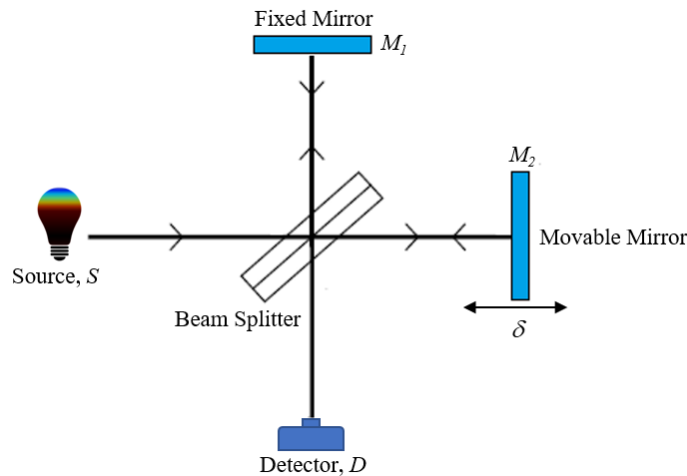


Figure 2.3. Michelson interferometer.

When scanning, the optical path length of the beam from the movable mirror (M_2) changes as its position varies with the traveled distance of the moving mirror compared to the light beam from the fixed mirror, M_1 . This light traversal to and from the beam-splitter and the two plane mirrors M_1 and M_2 leads to an optical path difference (OPD), also known as the retardation δ . When the beams recombine at the beam-splitter, interference occurs and the changes in retardation (δ) creates an interference pattern of the IR beam accordingly. This interference pattern is called an interferogram $I(\delta)$ (Figure 2.4), and it represents the intensity of the IR signal reaching the detector (D) as a function of the retardation δ . The two beams can interfere constructively or destructively depending on the difference of their optical beam path. When the path difference between the movable mirror (M_2) and the fixed mirror (M_1) is zero (i.e. equidistant from the beam-splitter), the condition is referred to as zero path difference (ZPD) and beams are said to be in phase. At ZPD, all wavelengths of the light for the two beams will interfere constructively and the photodetector records a high-intensity IR signal (Figure 2.5a). In contrast, if the retardation (δ) is half the wavelength of the light, the two beams will interfere destructively, and the detector will record a zero signal as depicted in Figure 2.5b. In practice, the intensity modulations on the detector (D) of the FTIR spectrometer is dependent on the phase difference of the two beams resulting from the varying changes in their optical beam path.

In FTIR spectrometers, a monochromatic light beam, often Helium-Neon (HeNe) laser, is used as the internal reference in addition to the infrared beam. The HeNe laser beam travels the same optical path through the interferometer as the infrared beam with a unique wavelength of 633 nm ($15,800\text{ cm}^{-1}$) and generates a sinusoidal signal (interferogram) when modulated by the Michelson interferometer. This signal provides an accurate measurement of the interferometer displacement (δ), and it is extremely useful as a standard alignment laser in FTIR spectrometers.

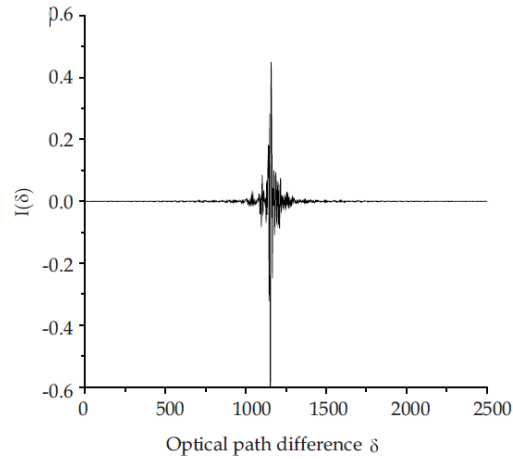


Figure 2.4. Infrared Interferogram [31].

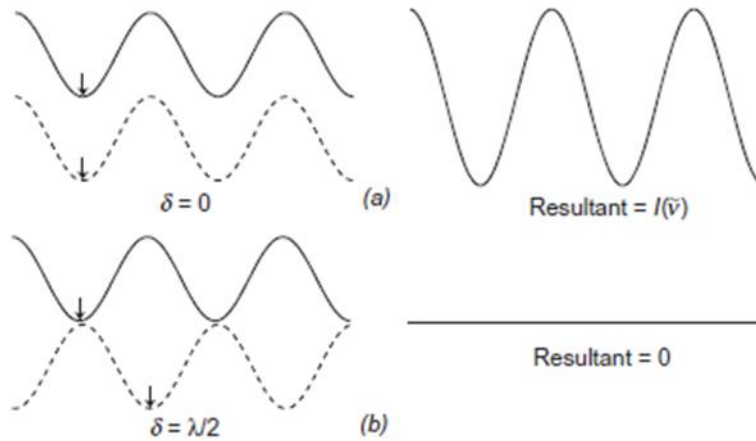


Figure 2.5. Relative phase relationship of waves from fixed (solid) and movable (dashed) mirrors at different δ values: (a) zero path difference; (b) path difference of one-half wavelength [30].

2.3 FTIR Modes of Operation

There are two main operation techniques in FTIR spectroscopy for controlling the OPD of the interferometer: continuous-scan mode and step-scan mode.

2.3.1 Continuous-Scan Mode

Under the continuous-scan mode method of operation, the movable mirror travels back and forth at a constant velocity. The optical path length difference (OPD) of the movable mirror is controlled by the generated signal (sinusoidal interference pattern) of the reference HeNe laser

which is also used in determining the position of the moving mirror. Data are acquired as the mirror moves at a constant speed and the detected signal of the HeNe reference interferogram is amplified at zero crossings and AC coupled. The signal-to-noise ratio (SNR) of this technique is improved as data from the same positions are aggregated and averaged. This method gives accurate measurement and it is easily repeatable because of the stabilized frequency of the HeNe laser reference with a center wavelength of 633 nm.

2.3.2 Step-Scan Mode

In a step-scan mode, the movable interferometer mirror advances incrementally in a stepwise manner from one optical retardation position to a new position and then halts for a defined period known as stabilization delay allowing the sample data to be acquired at each position. In this mode, optical path difference (OPD) is held constant while a measurement is made, after which the OPD is quickly advanced to the next position. The process is repeated until all data needed are acquired for the specified wavelength/wavenumber range. The step-scan mode option is helpful but not limited to the following research areas; FT-Raman spectroscopy, Photoluminescence (PL) spectroscopy, Signal modulated experiments, Photoacoustic spectroscopy (PAS) and Time Resolved Spectroscopy (TRS).

Figure 2.6 shows the illustrations of both scan modes for interferometer operations and Table 2.1 gives the pros and cons of both modes of operations, respectively.

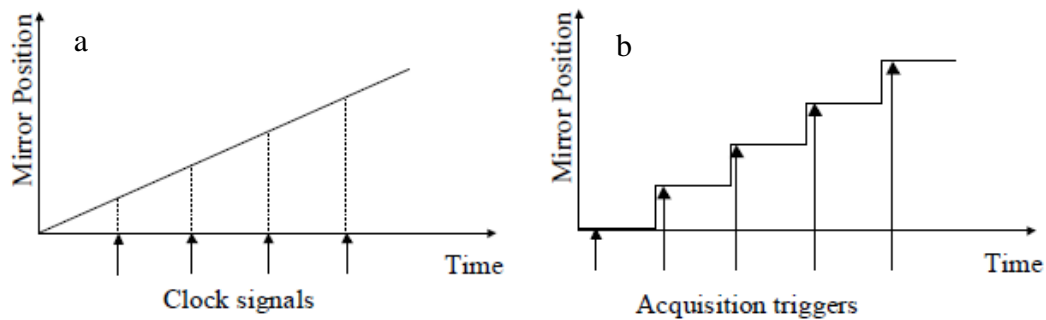


Figure 2.6. (a) continuous-scan mode and (b) step-scan mode illustration [29].

Table 2.1. Pros and cons of a continuous-scan and step-scan modes of interferometer operations.

Step-scan	Continuous-scan
A lock-in amplifier (LIA) and a mechanical chopper can be used with this option. It provides a greater degree of noise rejection to improve the measurement signal.	This option uses filtering techniques. It does not differentiate the noise and the signal based on their phases.
The DC (direct current) signal is modulated to improve the SNR.	The signal is already modulated by the moving mirror speed and the radiation wavelengths.
The measurement duration is proportional to the sampling frequency. Higher resolutions will increase the Interferogram size (data points) and scan time.	Scan time is generally faster. Measurement duration is not affected by the sampling frequency.
Allows the use of pulsed and continuous-wave (CW) lasers.	Only a continuous-wave laser is allowed in this mode.

2.4 The Interferogram Mathematical Expression

At the detector, a Fourier transform spectrometer generates an output intensity $I'(\delta)$ as a function of retardation from the measured beam at a wavenumber $\tilde{\nu}_0$. From Figure 2.3, the intensity at any position where $\delta = n\lambda$ is proportional to the intensity of the source $I(\tilde{\nu}_0)$, where n is an integer and λ is the wavelength of the radiation. Assuming the interferometer has an ideal beamsplitter in with an equal percentage of transmittance and reflectance (50%), and an ideal mirror with 100% reflectance, then

$$I_1 = I_2 = 0.5 I(\tilde{\nu}_0) \quad (\text{Equation 2.1})$$

where I_1 and I_2 represents the detected intensities from the fixed and movable mirror, respectively. Thus, the quantity $I'(\delta)$ measured with ideal optics (interferometer) is expressed as

$$I'(\delta) = 0.5 I(\tilde{\nu}_0) (1 + \cos 2\pi \tilde{\nu}_0 \delta) \quad (\text{Equation 2.2})$$

By integrating Equation 2.2, one obtains the aggregate intensity over the range of

frequencies defined by the moving mirror positions in the interferometer output

$$I'(\delta) = \int_0^\infty 0.5 I(\tilde{\nu}_0) (1 + \cos 2\pi \tilde{\nu}_0 \delta) d\tilde{\nu}_0$$

$$I'(\delta) = \int_0^\infty 0.5 I(\tilde{\nu}_0) d\tilde{\nu}_0 + \int_0^\infty [0.5 I(\tilde{\nu}_0) \cos 2\pi \tilde{\nu}_0 \delta] d\tilde{\nu}_0 \quad (\text{Equation 2.3})$$

Equation 2.3 shows the quantity $I'(\delta)$ has two components: a constant component (DC) $= 0.5 I(\tilde{\nu}_0)$ and a modulated component (AC) $= 0.5 I(\tilde{\nu}_0) \cos 2\pi \tilde{\nu}_0 \delta$. In FTIR spectroscopy, only the AC-modulated component is important:

$$I(\delta) = 0.5 I(\tilde{\nu}_0) \cos 2\pi \tilde{\nu}_0 \delta \quad (\text{Equation 2.4})$$

This real quantity of an inverse Fourier transform $I(\delta)$ is referred to as the interferogram.

2.5 FT-IR Advantages

The three fundamental advantages of Fourier transform spectrometer over dispersive infrared spectrometer (grating spectrometer) are the multiplex, throughput and Connes advantages.

1. Multiplex Advantage:

The multiplex advantage, also known as Fellgett advantage, results from the capability of the FTIR instrument to collect the complete infrared spectrum during each scan of the moving mirror in the interferometer. The successive scans are then combined and averaged to obtain a spectrum with a better signal-to-noise ratio compared to a dispersive spectrometer.

2. Throughput Advantage:

The throughput advantage, also referred to as Jacquinot advantage, arises because the FTIR instrument has fewer mirrors and does not require slit devices which attenuate the IR light reaching the sample and detector. Hence, more radiation energy reaches the

sample and detector, yielding a higher SNR and a more distinguishable sample spectrum compared with a dispersive spectrometer.

3. Connes Advantage:

This Connes advantage refers to the use of a helium-neon (He-Ne) laser as a standard laser for the instrument's internal reference. The He-Ne laser wavelength is an accurately known value and the x-axis of the FTIR spectrum is referenced to this value to determine the accurate wavelength positions. The Connes advantage ensures internal precision is maintained and provides stable calibration for all wavelengths. The assigned FTIR spectrum wavelength is repeatable and can be compared to libraries of identified spectrum wavelengths.

Chapter 3: BRUKER IFS 66/S FTIR Project

The purpose of setting up a FTIR spectrometer was to further explore the optical characteristics of the (Si)GeSn material grown at the University of Arkansas chemical vapour deposition (CVD) laboratory, and samples grown by a collaborating foundry. This project aimed to use the FTIR internal optical components with an external light source and photodetector to answer the following fundamental questions towards a deeper understanding of the GeSn material:

1. How does one build the setup to align with external optical components for FTIR spectroscopy?
2. Using FTIR, can one obtain a better resolution laser spectrum?
3. If yes, how does one measure the laser-output versus pumping-laser-input (L-L) curve?
4. Using FTIR, can one get a better SNR electroluminescence (EL) spectrum?
5. How could one accommodate all the needs to reconfigure the system?

The presented results and discussion in this chapter were obtained using the high-resolution Bruker IFS 66/S (Bruker Optics Inc., Fremont, CA) Fourier transform spectrometer located at the Engineering Research Center (ENRC) lab 2933A, University of Arkansas, Fayetteville. Figure 3.1 shows the table view of ENRC 2933A laboratory with the Fourier transform spectrometer Bruker IFS 66/S, N₂ gas cylinders, external optics components, two external light sources (532 nm and 1064 nm lasers), cryostat, and computers (desktop and laptop) all on the optical bench. The spectrometer comes with a Microsoft Windows 2000 operating PC system, installed with an extensive analytical spectroscopic software package: “OPUS-NT” for controlling the spectrometer and spectra acquisition/manipulation. The IFS 66/S features a digital signal processor (DSP) for the optics bench, an acquisition processor (AQP) which operates

independently from the PC data system.

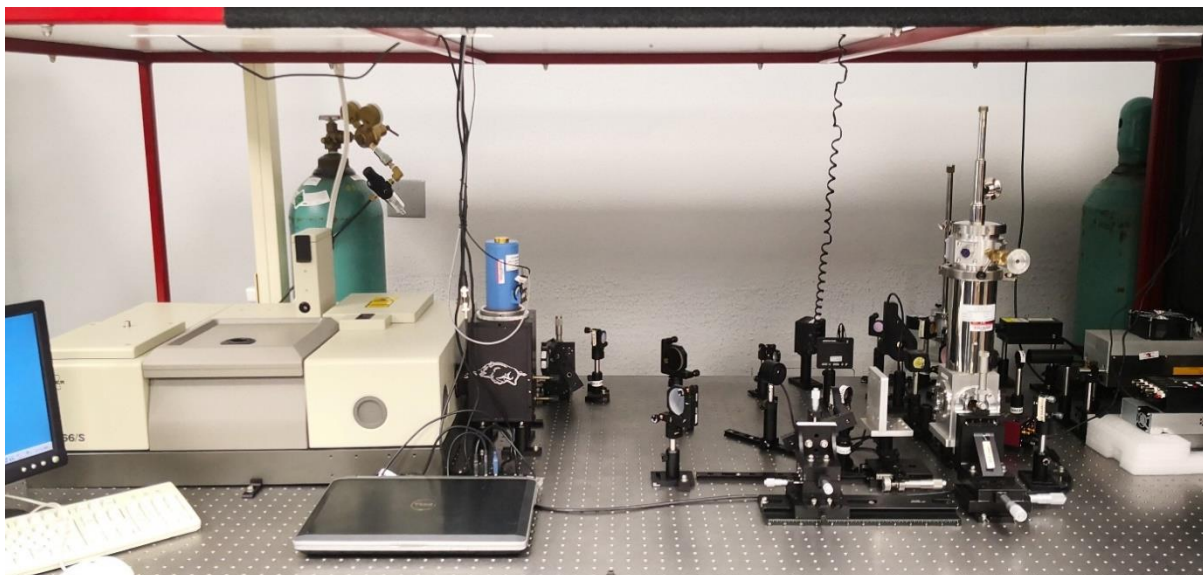


Figure 3.1. View of ENRC 2933A laboratory showing the Bruker IFS 66/S spectrometer and other optical elements.

This Fourier transform spectrometer is a bench-top instrument with a flexible spectral range that can be expanded from the far-infrared (FIR) region to the near ultraviolet (UV) region, with several different modules and accessories required for operation. Its standard frequency range is from 7500 cm^{-1} to 370 cm^{-1} with an option for range extension. Figure 3.2 shows the external view of the IFS 66/S spectrometer with its distinguished compartments described in Table 3.1.

Table 3.1. IFS 66/S FTIR compartments

Compartment	Description
A	Sample Compartment
B	Interferometer Compartment
C	Electronics Compartment
D	Detector Compartment
E	Beamsplitter storage box
F	Optional exit ports (and one input port)

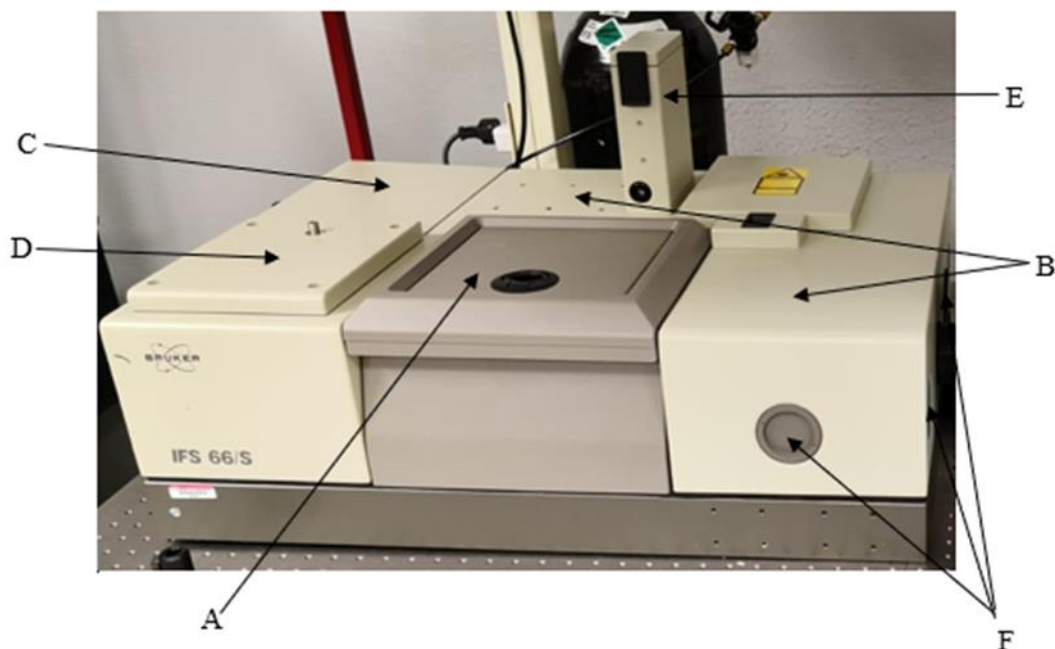


Figure 3.2. External view of the IFS 66/S distinguished compartments.

3.1 Experimental Setup

The goal of the experimental setup was to have the internal optical plane of the FTIR spectrometer align to the external optical bench plane. This was achieved by creating optical paths using the right transmissive and reflective optical components to guide the external beam source to the FTIR instrument.

3.1.1 Infrared Fourier Spectrometer IFS 66/S Setup and Internal Alignment

The FTIR spectrometer was placed on a sturdy optical table with enough space to accommodate a computer, samples, tools, and other optical components. Figure 3.3 shows the interferometer compartment of the Bruker IFS 66/S Fourier transform spectrometer. The instrument is equipped with two water-cooled internal sources: Glowbar (Bruker Optics Inc., Fremont, CA) for Mid-infrared (MIR) and tungsten lamp for Near-infrared (NIR) and visible (VIS) spectroscopy. To align the internal He-Ne laser, the purge gas (N_2) was opened at 100 psi to sustain the purging flow rate in the spectrometer and then turned on by pressing the power

switch on the electronics unit (ELU). This was followed by connecting an oscilloscope to test point A (LSA2) or B (LSB2) and the signal ground (AGND) on the TC20 processor board (Fig. 3.4 (b)) to adjust the fixed mirror on the interferometer. From the oscilloscope, the least expected peak-to-peak amplitude was 1.4 V for test point A and 2 V for test point B or more. Before starting the adjustment, the moving mirror (scanner) was stopped by switching it off from the TC20 board.

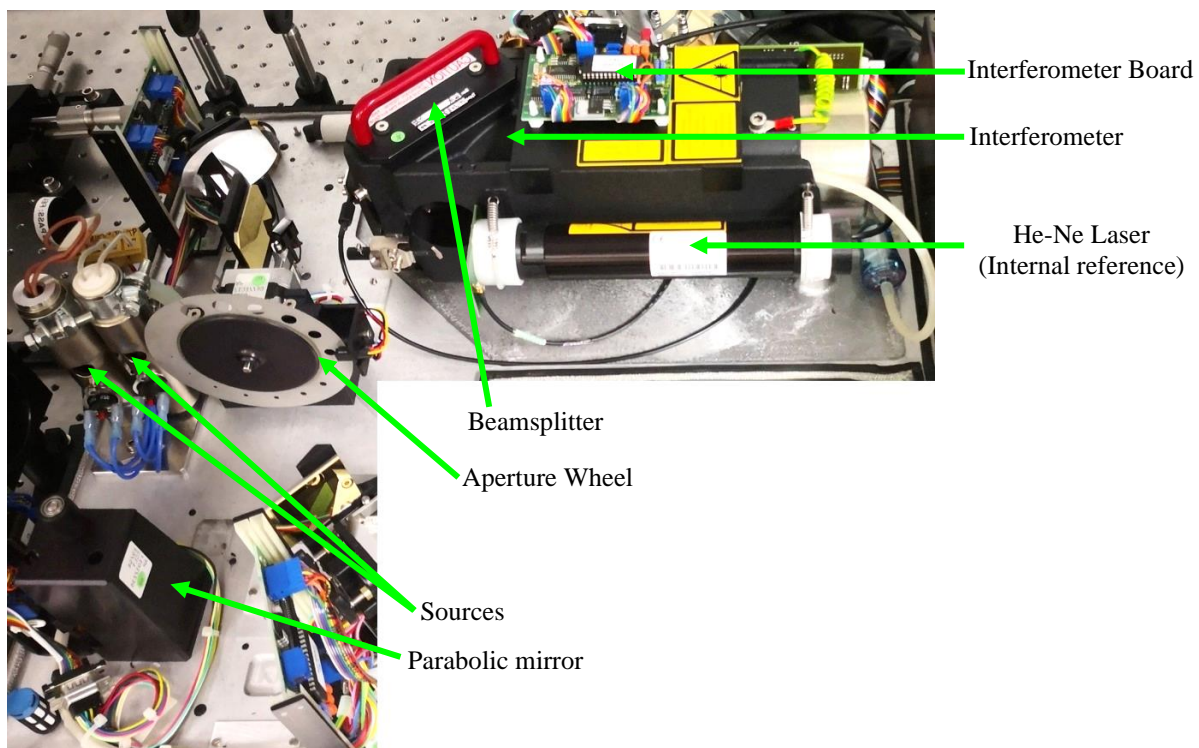


Figure 3.3. Inside view of the BRUKER IFS 66/S interferometer compartment.

By slowly moving the scanner and gently turning the x and y knobs for the fixed mirror, Figure 3.4 (a) shows the observed sine wave signal on the oscilloscope with the corresponding test point amplitude. Once the mirror limit was reached for either test point, the test lights LAE (A) and LBE (B) on the TC20 board became unlit and the spectrometer blinked a green light at the front indicating the scanner was functioning properly.

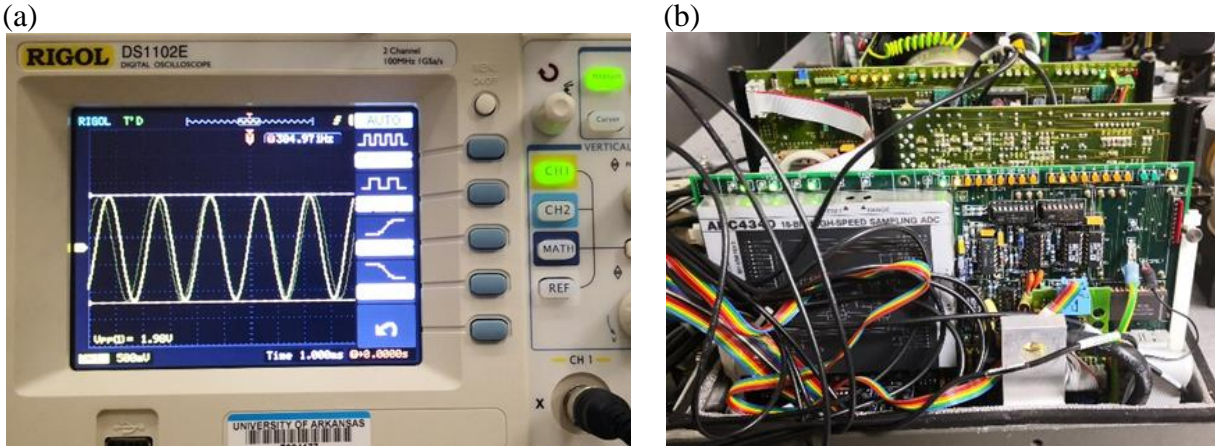


Figure 3.4. (a) Sine wave signal observed on the oscilloscope. (b) Unlit TC20 processor board.

The tungsten lamp source for the NIR and the visible region was switched-on by selecting the NIR switch on the ELU and heated to about 1500 K to produce continuous radiation with maximum intensity. The IFS 66/S optic bench instrument is made up of optics (normal, parabolic, and concave mirrors) that provides a complete optical path from the internal light source(s) to the two internal detectors. Hence, to guide the IR light to the detector, the OPUS software was started to configure and adjust the spectrometer optics for the internal alignment experiment with the following steps:

1. Start OPUS software.
2. Click Measurement on the OPUS toolbar.
3. Select the Basic tab from the Measurement Dialog box and load the existing experiment file for internal alignment: DTGS_NIR.XPM
4. Check the Advanced, Optic, Acquisition, and FT tabs to confirm their inputs corresponds to Table 3.2
5. Select Check Signal to confirm the position of the interferogram
6. Save interferogram using the “Save peak Position button” after adjustment.

The IR light from the tungsten lamp source was collected by a parabolic mirror and

reflected through an adjustable aperture to focus on a second curved mirror which collimated the light through the interferometer and followed the optical path to the detector as shown in Figure 3.5. Once the interferogram was observed in step 5, the stepper motor was then adjusted manually using the OPUS software until the maximum amplitude was located. The adjustment of the amplitude and peak position could also be done using the Auto-Align button. It was important to save the maximized peak position and amplitude using the save peak position button to ensure auto internal self-alignment could subsequently be performed without opening the instrument.

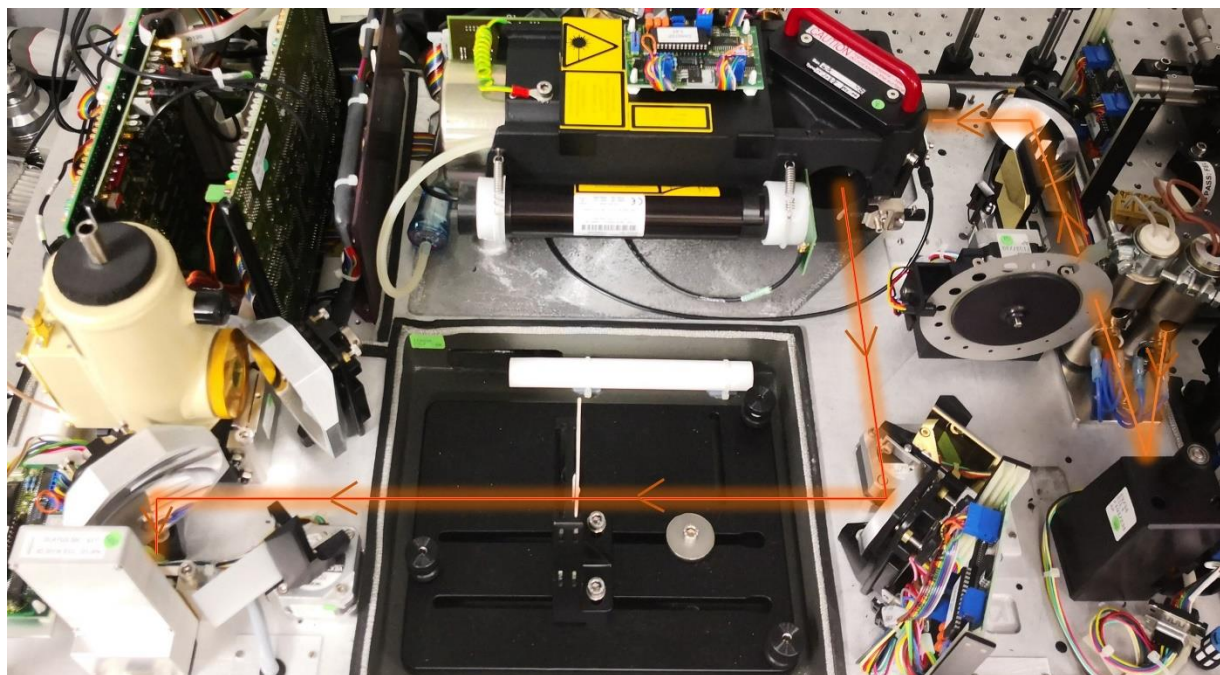


Figure 3.5. Bruker IFS 66/S optical layout.

Using the OPUS software, Table 3.2 summarizes the experimental conditions for the spectrometer internal alignment at room temperature. The result was observed from the Check Signal page and optimized via the stepper motor control shown in Figure 3.6.

As shown in Figure 3.7, the centerburst of the displayed interferogram is proportional to



Figure 3.6. OPUS stepper motor control.

the intensity of the IR light incident on the deuterated triglycine sulfate (DTGS) detector. The choice of a DTGS detector was because it is a pyroelectric IR detector that responds swiftly to changes in temperature and operates at room temperature. Obtaining the largest amplitude possible with the smallest aperture size is desired for the internal alignment of the IFS 66/S FTIR spectrometer.

The configuration settings in Table 3.2 were saved as DTGS_NIR.XPM file with the interferogram position and amplitude values recorded. This could be used as a benchmark for subsequent internal alignment prior to measurement.

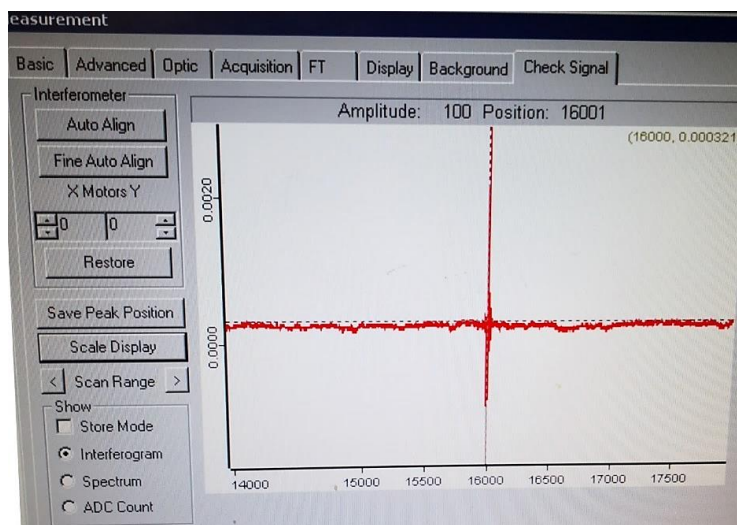


Figure 3.7. Bruker IFS 66/S interferogram display at room temperature.

Table 3.2. IFS 66/S room temperature internal alignment configuration.

Parameter	Value
Resolution (cm^{-1})	4
Sample/Background Scan Time	32
Resolution Spectrum	Transmittance
External Synchronization	OFF
Source Setting	NIR-Source
Beamsplitter (BS)	KBr (Potassium bromide)
Aperture Setting (mm)	0.25
Measurement Channel	Front
Detector Setting	DTGS
Scanner Velocity	1.6 kHz
Sample/Background Gain	Automatic
Delay after device change	0
Delay before measurement	0
Frequency range (cm^{-1})	9000 to 4000
Low Pass Filter	16 kHz
Acquisition Mode	Double Sided, Fast Return
Correlation Mode	No
Phase Resolution	32
Phase Correction Mode	Power Spectrum
Apodization	Blackman-Harris 4-Term
Zerofilling Factor	2

3.1.2 Optical Bench External Setup and Alignment

To set up the external optical components, the FTIR spectrometer was adjusted to ensure the internal He-Ne laser was parallel to the optical bench plane. A 200 mm focal length calcium fluoride (CaF_2) plano-convex lens was placed at the focus point from the spectrometer's input port to collimate the He-Ne laser coming through the port. A calibrated alignment screen was then placed at the other end of the collimating lens to align the He-Ne laser beam horizontally and measure its height parallel to the table. Several movements of the alignment screen parallel to the optical table were done to ensure the height and spots remained the same in different positions. Once the He-Ne laser beam was confirmed parallel to the table, the adjusted position of the spectrometer was secured using Thorlabs L-shape (CL5) table clamp (Thorlabs Inc., Newton, NJ). Figure 3.8 shows the schematic diagram of aligning the He-Ne laser with the optical table plane. For this setup, a light box was attached to the IFS 66/S spectrometer optional exit port as shown in Figure 3.9. The light box was built with a 2 inch 90° off-axis gold protected parabolic mirror (MPD249-M01) and a 3 inch precision kinematic mirror mount (KS3) to control the mirror positions for maximum beam collection from the FTIR spectrometer and direct it toward the mounted detector. The box has a detector holder with an exterior thread and a threaded lock nut for holding it to the top plate and adjusting the detector's height.

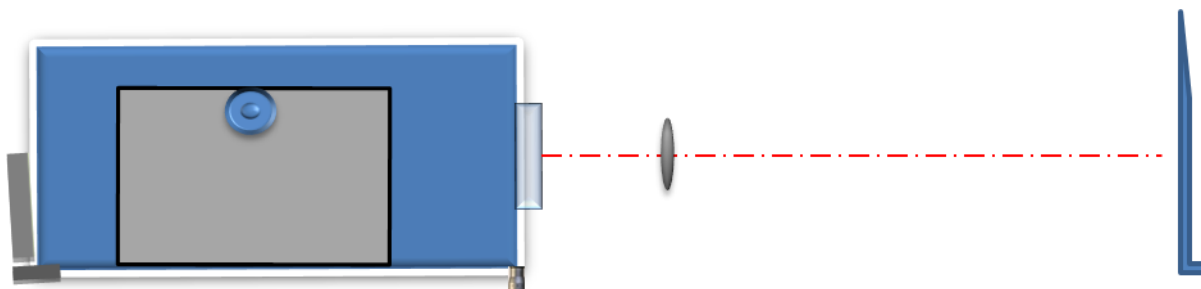


Figure 3.8. Side view of IFS 66/S He-Ne laser alignment with the optical table plane.

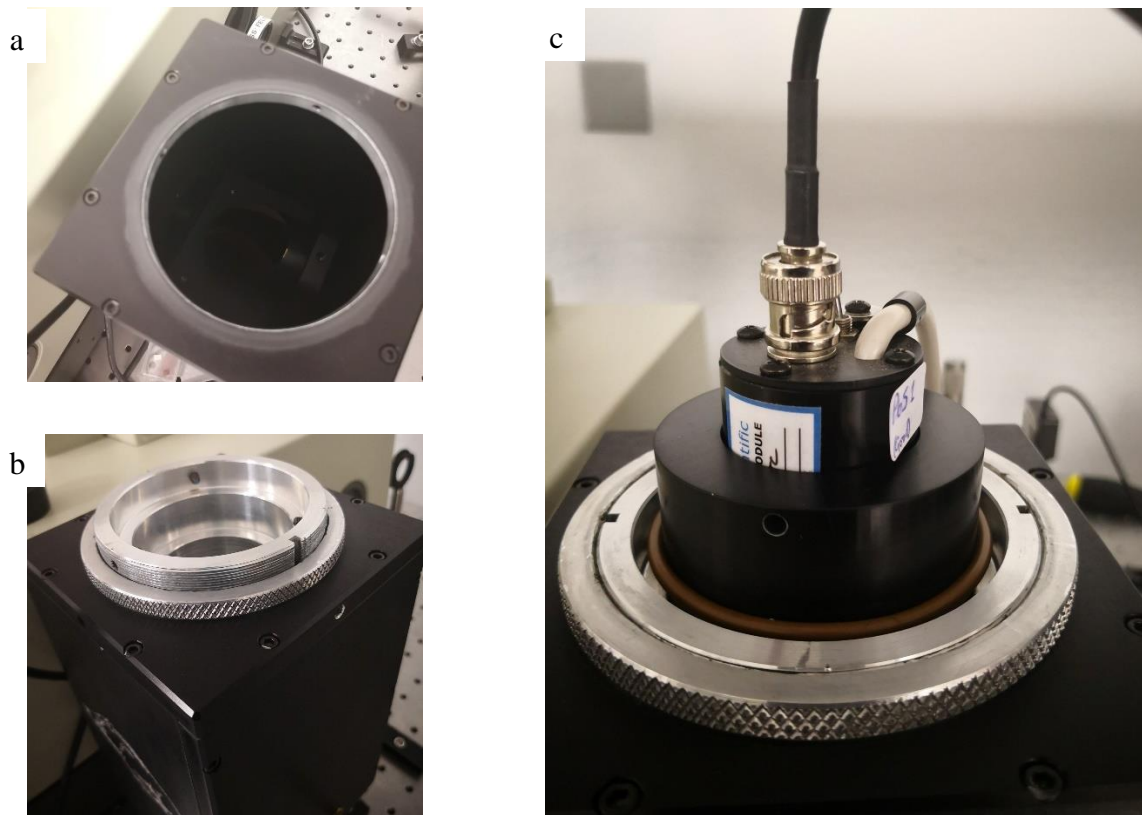


Figure 3.9. Light box showing (a) the parabolic mirror within, (b) the detector holder with threaded nut, and (c) a detector securely seated in its holder.

To ensure the light box was properly positioned at the output port of the spectrometer, a white light source was used for further alignment. The spectrometer configuration setting was adjusted with OPUS software (Bruker Optics Inc., Fremont, CA) to create an optical path from the input port to the output port by adjusting the internal mirrors. A white light was then transmitted through two pinholes and a collimating lens and collected from the input port as shown in Figure 3.10. The source path was adjusted to ensure light collected from the input port focused on the exact spot as the He-Ne laser on the alignment screen.

In this setup, two pumping lasers, 500 mW 532 nm continuous-wave green laser and a 1064 nm pulsed laser, were installed on the optical bench as external light sources. A laser leveler was used to carefully adjust the height of the laser mounts to ensure the pumping lasers

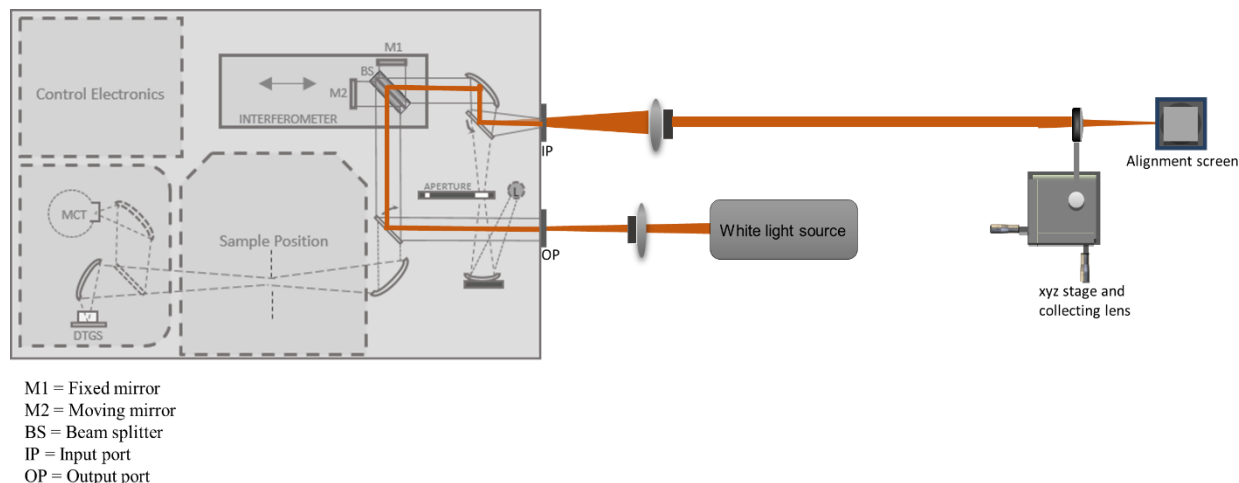


Figure 3.10. IFS 66/S alignment from the alternative output port using a white light source

were parallel to the bench surface plane and the laser beam had the same height as the focused He-Ne laser. To achieve optimal performance, the laser leveler, kept at the same height as the laser source, was used to adjust the mirror/lens posts and post holders to guide the laser rays through the precise center of the mirrors, lenses, and other optical elements to the FTIR external light entrance (input port). A one-inch premium bandpass (BP) filter (FLH532-10) with a 552 – 1200 nm blocking region was put at the entrance of the input port to isolate the external laser lines.

3.2 Optical Elements Construction for Step Scan Option

The optical elements arrangement was critical to maximizing the space on the optical table to accommodate different measurement setups. This setup was mainly built for the step scan option to greatly reduce the noise and improve the signal using both a mechanical chopper and a lock-in amplifier. The components were thoughtfully arranged to create the optical path for room temperature measurement, optical pumping measurement, and electroluminescence measurement.

3.2.1 Optical Path Construction for Room-Temperature (RT) Measurement

The laser beam from the 532 nm green laser was first filtered through a 532 nm BP filter and then incident upon a UV/VIS mirror. Two pinholes with their iris closed to ~1 mm were then used to align the reflected parallel beam off the first mirror at an angle of 45° onto a second UV/VIS mirror that could be flipped in and out of the beam path. Following the two successive UV/VIS mirrors, the beam was then walked from the second mirror to a third UV/VIS mirror using two pinholes. The pinholes were always placed at either end of a rail which helped adjust the angle of the mirror to guide the beam through the iris to the next mirror. A mechanical chopper was also placed along this path to modulate the light beam. From the third mirror (at 45°), the beam traversed a 1-inch CaF_2 convex lens with a 7.5 cm focal length to focus on the sample holder as shown in Figure 3.11.

The sample holder was assembled to allow X and Y translational motion for moving across a sample surface for different spot measurements. To define the optical path from the sample to the FTIR spectrometer, a good reflective material was placed on the sample holder and the light from the sample was walked through two pinholes to a 2 inch protected gold (IR) mirror. A 2 inch plano-convex lens with a 7.5 cm focal length installed on a 3D stage and mounted on a precision optical rail was introduced between the sample and the first protected gold (IR) mirror to collimate the light from the sample. The collimated light was then guided onto a second protected gold (IR) mirror before finally traversing through another 15 cm focal length plano-convex lens as depicted in Figure 3.12. For the 1064 nm pulsed laser, the laser beam traversed through a 1064 BP filter, then through a polarizing beamsplitter cube (VA5-1064) before it was incident on the first NIR mirror. The angle of the first NIR mirror was then adjusted to transmit the 1064 nm beam to a second NIR mirror as seen in Figure 3.12. From the

second NIR mirror, the beam followed the same optical path as the green laser after flipping the green laser's second UV-VIS mirror out of the beam path.

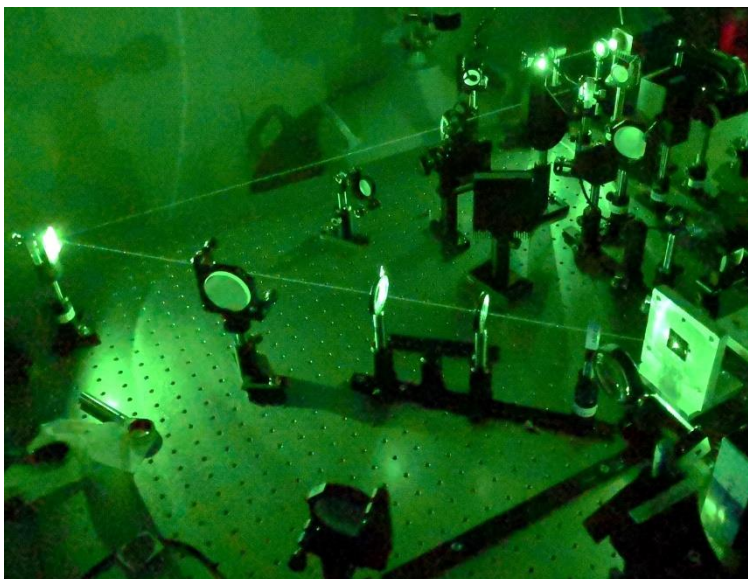


Figure 3.11. 532 nm green laser alignment from source to sample holder.

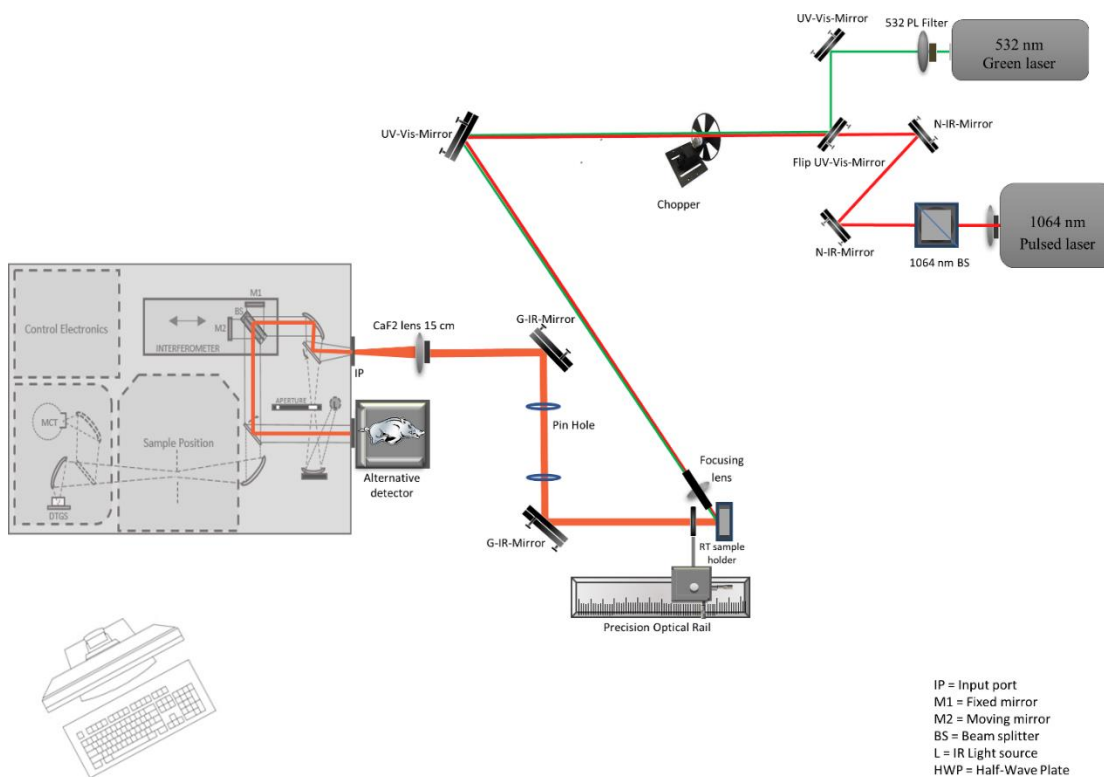


Figure 3.12. Bruker IFS 66/S room temperature PL schematic diagram.

3.2.2 Optical Pumping Measurement Setup

The optical pumping setup required an ST-100 Optical Cryostat (Janis Research, Woburn, MA) using liquid helium or liquid nitrogen (LN_2) for accurate temperature control of sample measurement. The cryostat was positioned on the optical table beneath the flexible transfer line opening in the overhead shelf. As a result of the cryostat position, the optical path was created by placing a 1-inch flip NIR mirror right after the mechanical chopper and in between the lasers common path to send the laser beam to a NIR mirror directly across the cryostat as shown in Figure 3.12. The mirror was then adjusted by using two pinholes to align the beam as it traversed through a half-wave plate in a motorized precision mount, a polarized BS, and collimated to a narrow stripe ($\sim 20\text{ }\mu\text{m}$ width and 0.3 cm length) through a cylindrical lens that focused the beam onto the sample waveguide in the cryostat. The half-wave plate was used to transmit light and modify its polarization state without attenuating or deviating the beam. The IR light from the sample was then collected following the same path described for sample holder to FTIR spectrometer in the RT setup. This was achieved by simply removing the sample holder from the beam path and the adjusting collimating lens as shown in Figure 3.13.

Prior to the creation and alignment of the pulsed laser for device pumping, the 532 nm laser was used for the optical pumping measurement setup and initial alignment. The reason was that the 532 nm laser is visible, collimated, and bright. Once the path was established, the pulsed laser (1064 nm) was then aligned for optical pumping following the same path with the help of a handheld VRC2 IR detector card (Thorlabs Inc., Newton, NJ) for easy location of the pulsed laser beam and its focal point. As a critical step for ensuring maximum laser energy reached the device, the cryostat was adjusted to ensure the collimated narrow beam beyond the cylindrical lens passed through the center of the cryostat incident window.

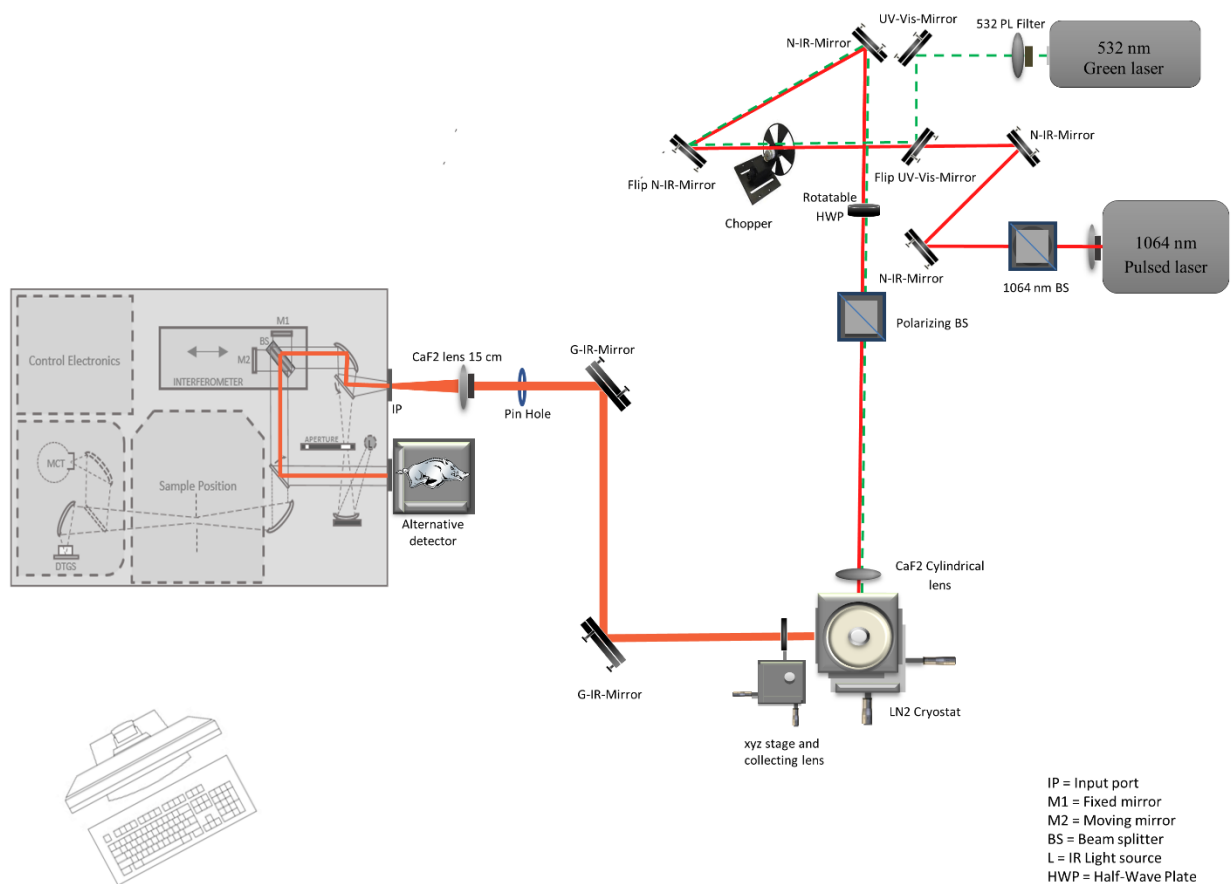


Figure 3.13. Bruker IFS 66/S optical pumping schematic diagram.

In optimizing the setup for different experiment measurements, a common optical path was adopted by using flip mirrors to fold the beam path in the desired direction and using a precision optical rail to freely adjust the collimating lens collecting the IR light from the sample without having to take it off when switching between different experiments. Figure 3.14 shows all the paths and optical elements of the complete setup for the FTIR table using external laser sources. This setup improves the efficiency of the FTIR table and greatly reduced the turnaround time for switching between different optical characterization setup.

3.2.3 Electroluminescence Measurement Setup

The electroluminescence (EL) measurement setup followed the exact optical path from

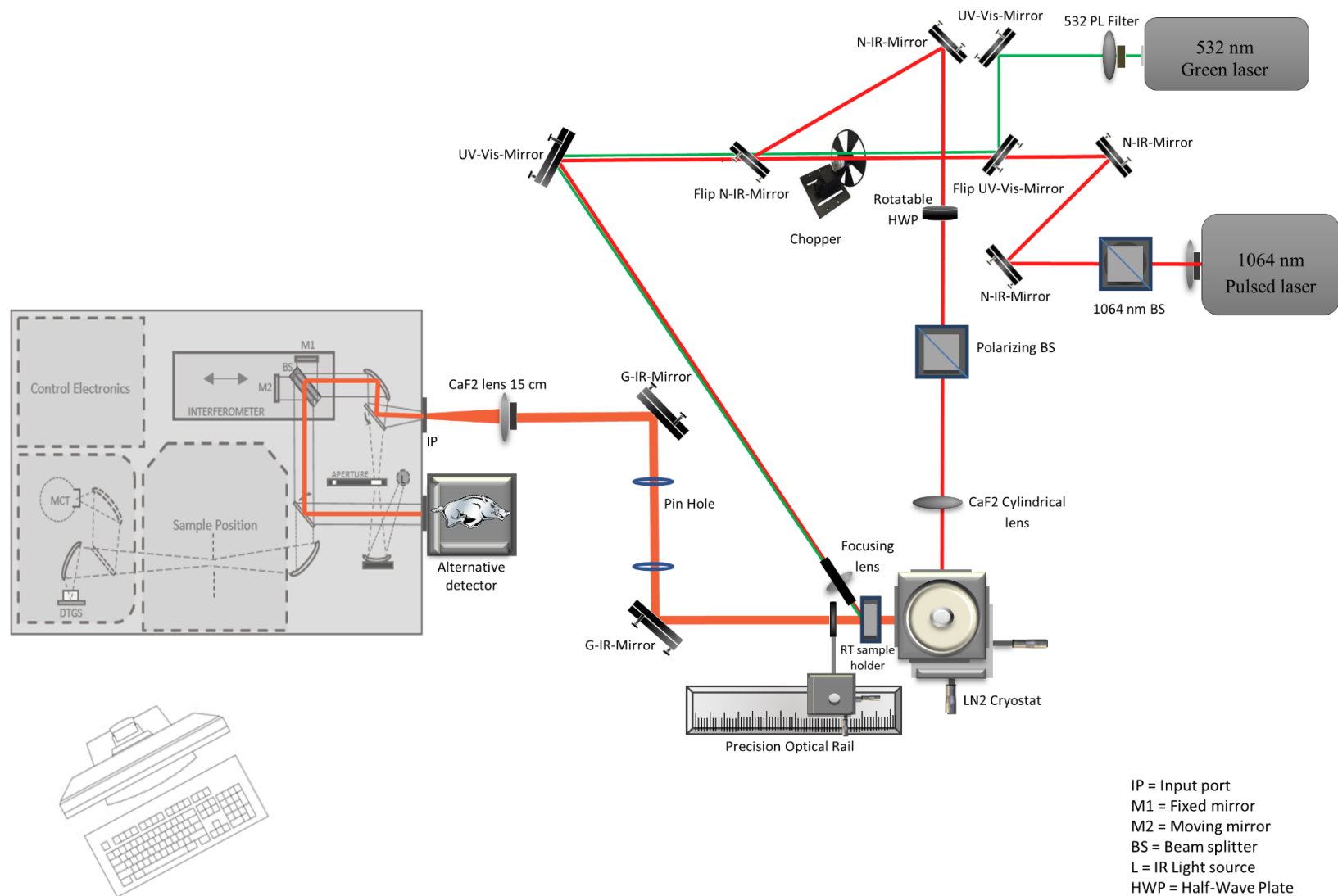


Figure 3.14. FTIR PL spectroscopy and optical pumping schematic.

Chapter 4: FTIR PL (EL) Measurements

Spectra of Ge, (Si)GeSn samples, and GeSn laser were measured with the Bruker FTIR IFS 66/S setup with an external laser source and externally mounted detector.

4.1 FTIR Measurement for PL

4.1.1 Ge PL

A Ge reference sample was measured using the continuous-scan mode at room temperature with a KBr beamsplitter and a LN₂ cooled InGaAs external detector (DSS-IGA(2-2)010L). The detector had a spectral range of 1.3 μm – 2.2 μm , a 1 mm² active area, and a specific detectivity (D^*) value of $8.86 \times 10^{12} \text{ cm}(\text{Hz})^{1/2}\text{W}^{-1}$. Both the mechanical chopper and lock-in amplifier were not used for the Ge RT measurement in the continuous-scan mode. The Ge reference sample mounted on the sample holder was irradiated with a 500mW green (532 nm) CW laser via the RT optical path described in Section 3.2.1 of Chapter 3. A 9000 cm⁻¹ to 4000 cm⁻¹ scan range, 8 cm⁻¹ resolution, 1.6 kHz scanner velocity, 7 mm aperture size, 16 kHz low-pass electronic filter, and a double-sided fast return acquisition mode were used as the OPUS parameters for the measurement. A power spectrum phase correction, Blackman-Harris 4-term apodization function, and zero filling factor of 2 was used for the Fourier transform. For the step-scan spectra, a Stanford Research Systems (SR830) (Bell Electronics, Renton, WA) lock-in amplifier was used for detector signal demodulation. A standard operating procedure was developed for the step-scan mode using the Bruker FTIR (see Appendix H). The lock-in amplifier was set up with a 12 dB and 100 ms time constant configuration and the interferogram size was set to 444 points by selecting lower resolution (128 cm⁻¹) for a quick step-scan measurement. After the stabilization delay (at least 6 times the time constant of the LIA) had elapsed, the output signal of the LIA was digitized at intervals based on the value entered in the

Number of Coadditions field (200 according to Appendix H). These values are then summed and averaged. For measurement signals that exceeded the analog-to-digital converter (ADC) input voltage range, the OPUS software always displayed an error message: Signal too large for ADC. To prevent this from saturating the detector and leading to artifacts in the spectra, “Automatic” was selected from the drop-down menu in the *Sample Signal Gain* field of the Optic tab. Figure 4.1 shows the Ge sample spectrum obtained from the RT measurement using continuous-scan mode with the CW laser, while Figure 4.2 shows the PL spectra obtained from the same sample at room temperature with different resolutions.

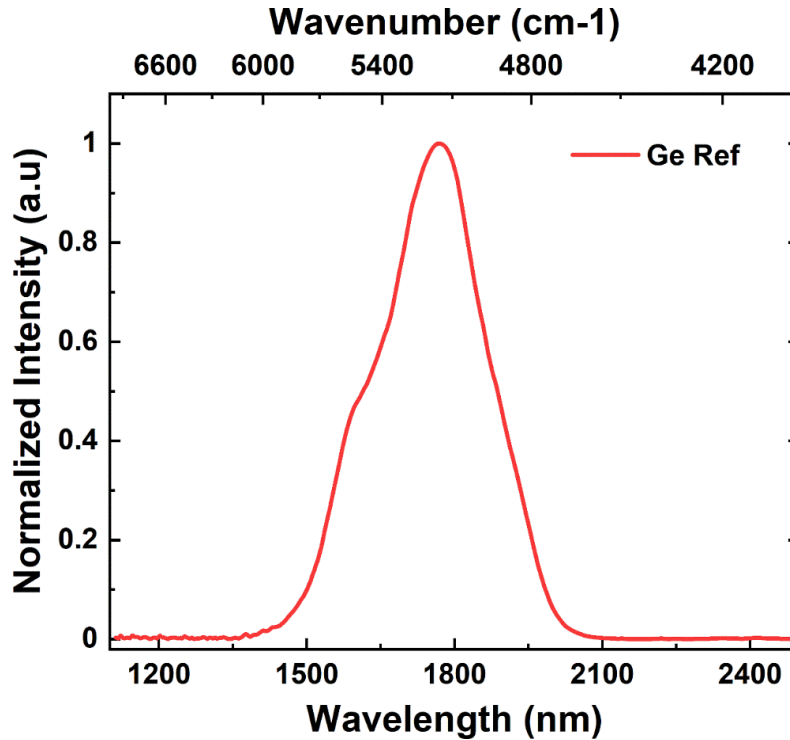


Figure 4.1. Normalized Ge RT PL spectrum with LN₂ cooled InGaAs detector.

Figure 4.3 shows the spectrum of the same Ge sample from step-scan measurement using a 1064 nm pulsed laser with a 45 kHz repetition rate, 60% lasing power, and 300 mW average power.

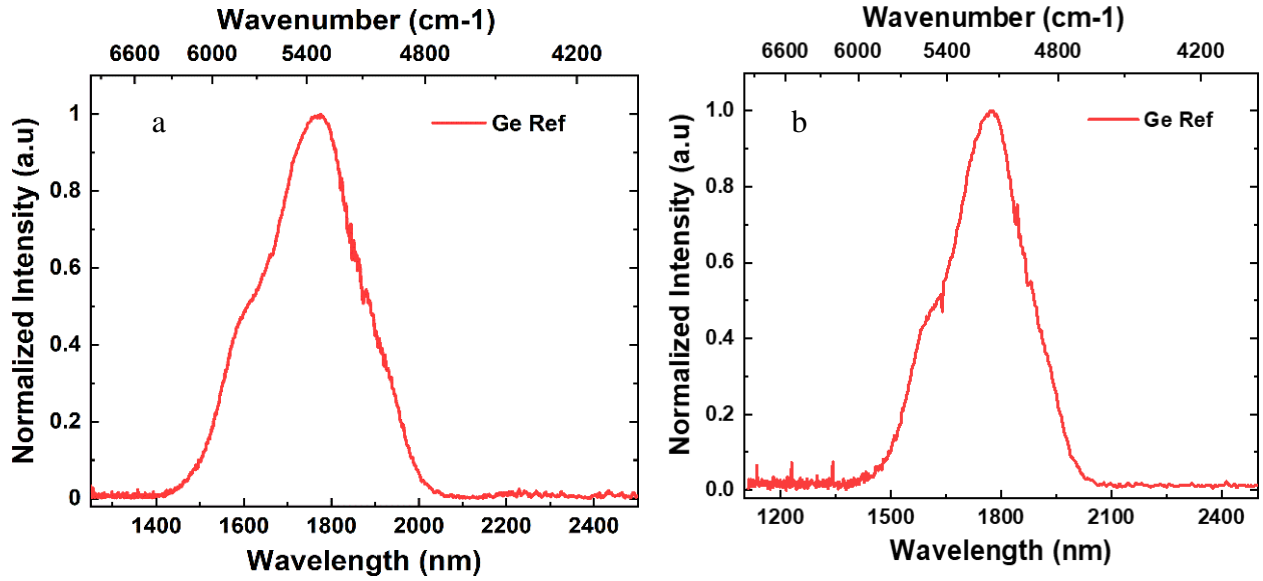


Figure 4.2. Ge RT PL spectra measured with (a) 8 cm^{-1} and (b) 4 cm^{-1} resolutions, respectively.

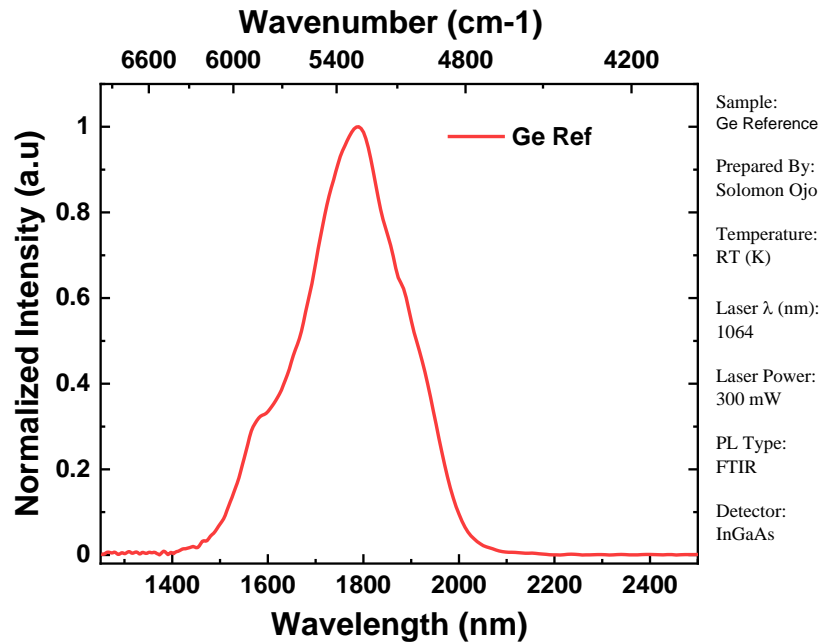


Figure 4.3. Ge spectrum from step-scan measurement.

To compare the spectra from an existing dispersive (iHR320) spectrometer setup to the spectra from the Bruker FTIR spectrometer measurement, two Ge samples were measured separately on both setups. The first Ge sample (A) was grown by a collaborating foundry and the

second sample (B) was grown at the University of Arkansas (UARK) CVD laboratory in Fayetteville. To ensure uniform conditions for measurement at RT, both spectrometers were mounted with a lead sulfide (PbS) thermoelectrically (TE) cooled detector (DSS-PS020T) (Horiba, Piscataway, NJ). The detector had a spectral range of $1\mu\text{m} - 2.8\mu\text{m}$, a $2\times 2\text{ mm}^2$ active area, and a detectivity (D^*) value of $6.67\times 10^{12}\text{ cm}(\text{Hz})^{1/2}\text{W}^{-1}$. Figure 4.4 shows the RT spectra for sample A from both setups using a CW-532 nm laser with 500 mW laser power. The PL spectra from each setup were then fit with a Gaussian function for comparison.

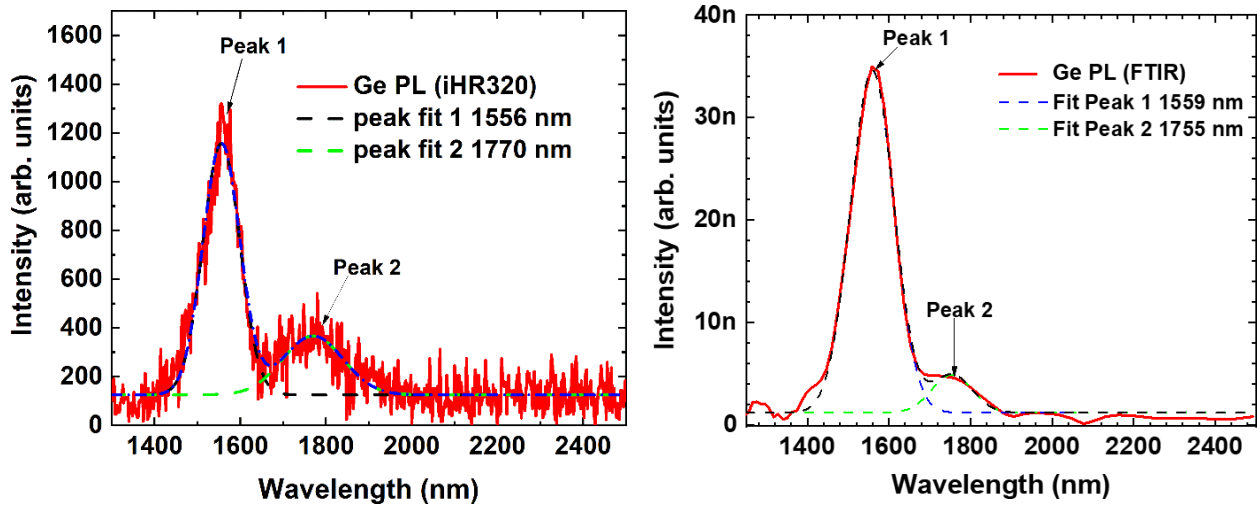


Figure 4.4. Ge PL spectra measured with (a) iHR320 spectrometer and (b) FTIR spectrometer.

Peaks 1 and 2 from Figure 4.4 represents the Ge direct bandgap and indirect bandgap transitions, respectively. As seen from the spectra, the wavelengths for both peaks were relatively close with $\sim 3\text{ nm}$ to 5 nm difference. The iHR320 spectrometer measurement was noisy compared to the FTIR spectrum which had high SNR and distinct peaks under the same conditions. Another room temperature experiment was also conducted for a UARK grown sample (B) on both setups using the step-scan mode. For this measurement, a 300 mW pulsed (1064 nm) laser was used to irradiate the sample at three different spots: wafer center, mid-point

between the center and edge of the wafer, and near the edge of the wafer to confirm the quality and uniformity of the growth. Figure 4.5 shows the spectra for the measured sample from both setups.

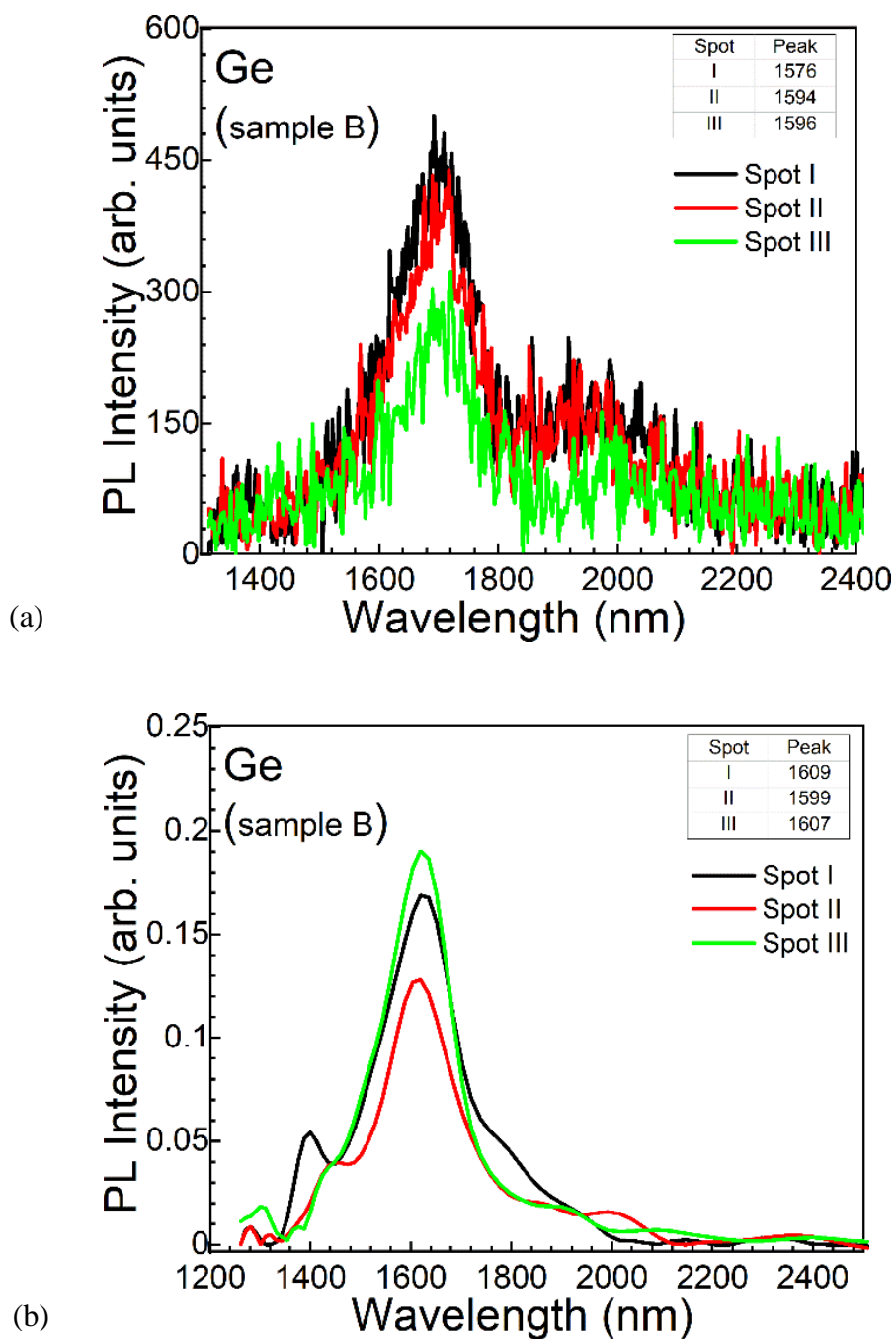


Figure 4.5: Ge PL spectra from (a) iHR320 and (b) FTIR spectrometer using pulsed laser.

An old benchmark Ge sample grown at UARK was remeasured with the FTIR spectrometer at RT following the steps in Appendix H. Figure 4.6 shows the comparison between the spectra.

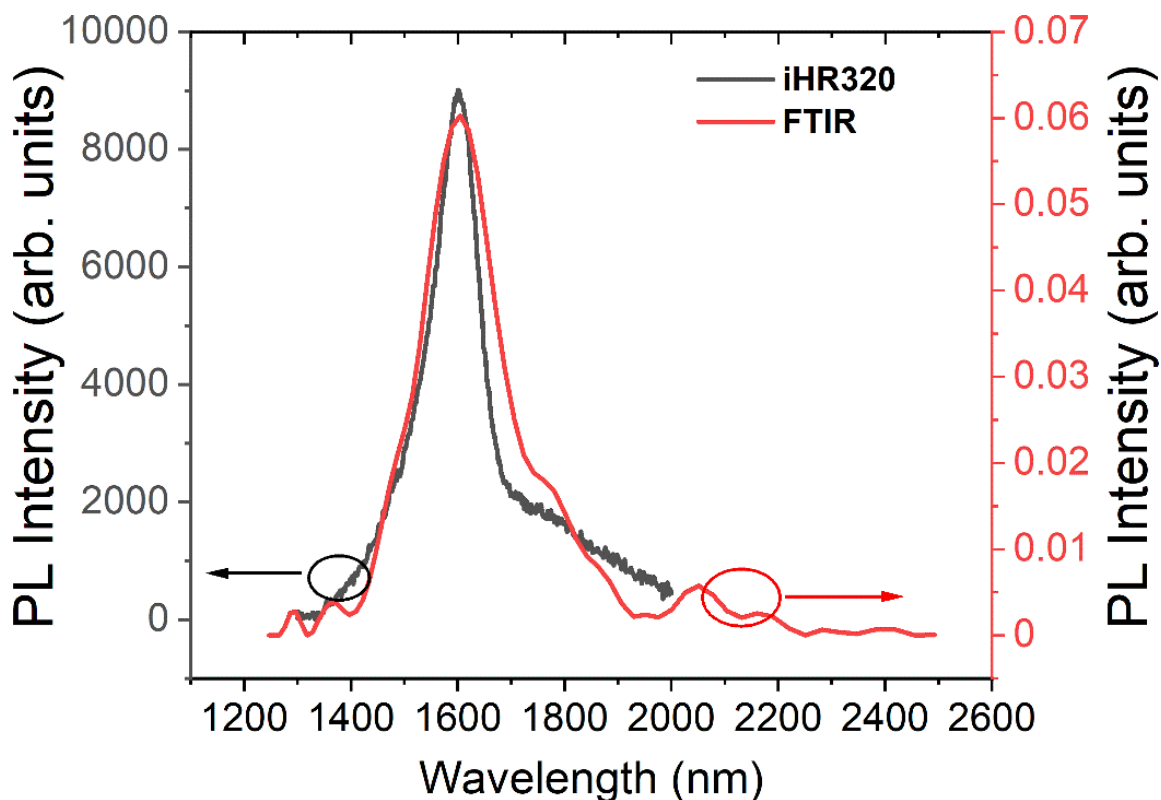


Figure 4.6. Ge RT PL spectra comparison.

4.1.2 GeSn PL

Following the result obtained from the Ge measurement using the FTIR setup, GeSn growths were then characterized at room temperature with the same setup. Using the steps described in Appendix H with a PbS photodetector, the RT PL of GeSn grown samples (C and D) were measured. For consistency and comparison with the old (dispersive spectrometer) setup, a 1064 nm laser with a laser power of 300 mW and a repetition rate of 45 kHz was used for the characterization. Figures 4.7 and 4.8 show the spectra for the measured GeSn samples.

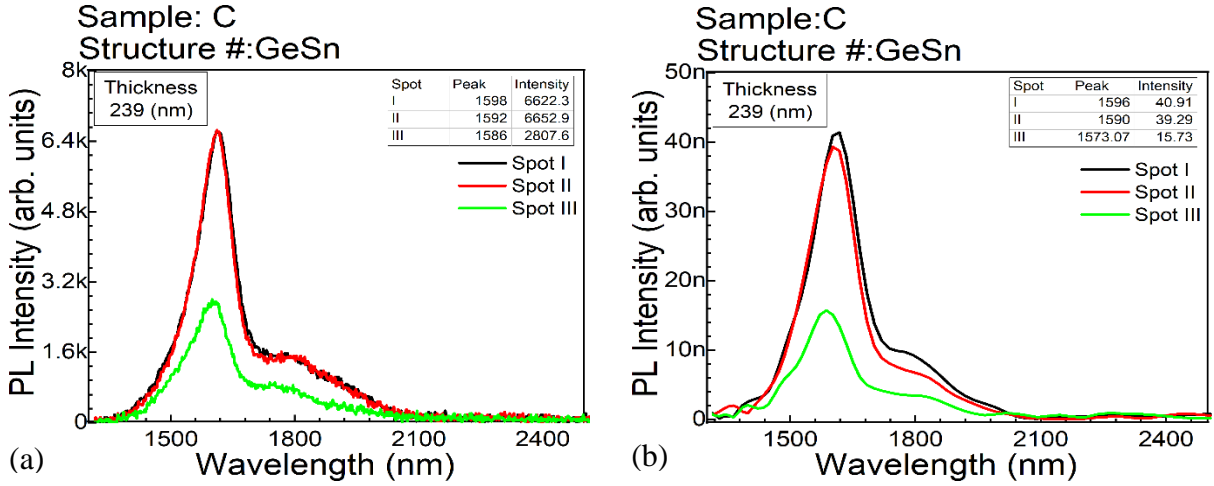


Figure 4.7. GeSn PL spectra from (a) iHR320 and (b) FTIR spectrometer using a pulsed laser.

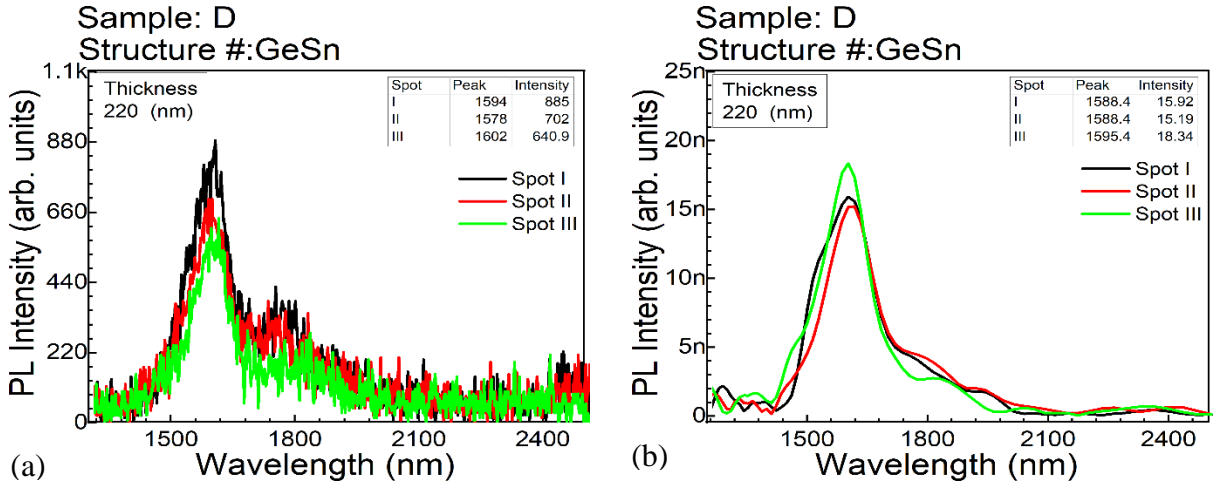


Figure 4.8. GeSn PL spectra using (a) iHR320 and (b) FTIR spectrometer with a pulsed laser.

4.2 FTIR Measurement for GeSn Laser

A double-heterostructure (DHS) was fabricated into an edge-emitting device for carrier confinement in the active region. The goal was to obtain a high-resolution spectrum from both electroluminescence (EL) and optical pumping measurements of the light-emitting devices to deepen knowledge of optical and electrical properties of GeSn material at different temperatures based on growth conditions, structures, and fabrication methods using the FTIR setup.

4.2.1 Device Fabrication

For the temperature-dependent optical pumping measurement, a 910 nm thick GeSn sample with 14.4% average Sn composition previously fabricated into a ridge-waveguide based edge-emitting laser device was used. The sample was grown using an industry-standard ASM Epsilon 2000 PLUS (ASM, Phoenix, AZ) reduced pressure chemical vapor deposition (RPCVD) reactor and fabricated by standard lithography and etching processes. As previously reported, the top and bottom of the ridge waveguide was 2 μm and 5 μm , respectively, with an etched depth of 800 nm and was lapped down to 70 μm thickness [32]. The edge-emitting LED device fabrication for EL characterization was carried out in a class 100 cleanroom to minimize contamination by particles. Figure 4.9 shows the LED device fabrication process flow from the grown sample to wire bonding. This process was developed into an easy-to-follow traveler (Appendix I) to avoid omitting any fabrication step. For electrical pumping, a mask was already designed by the research group with ridge width 40 μm , 80 μm , and 120 μm . The edge LED mask had two sections on it labeled as I and II that were used both for the positive and negative photolithography, respectively.

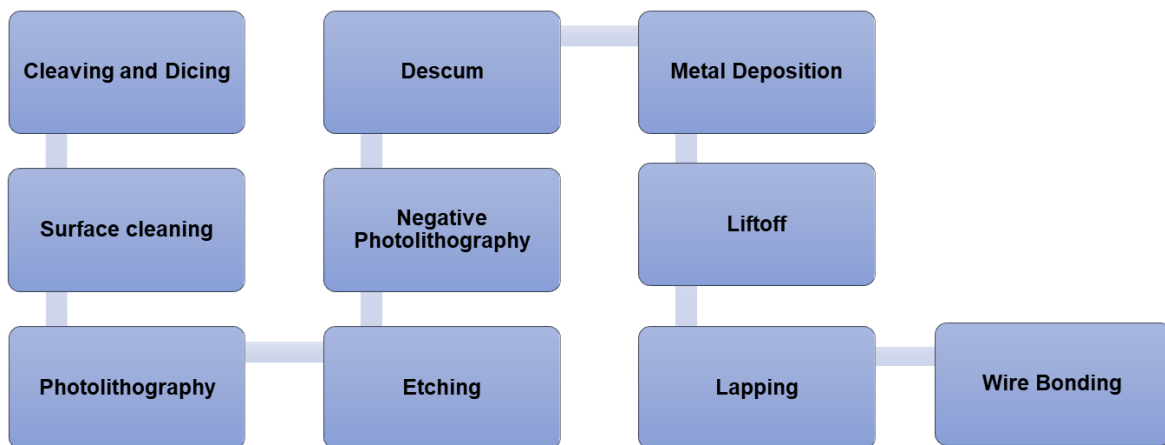


Figure 4.9. LED device fabrication process flow.

Cleaving and Dicing

The GeSn material was grown on 200 mm Si wafers. The Si wafer was first cleaved into four quarters and labeled as shown in Figure 4.10 (a) using a diamond scribe. The diamond scribe was suitable for cleaving and dicing because it cuts the sample along the crystal orientation. A one-piece full quarter was then further cleaved and diced into a 1-inch by 1-inch sized piece for characterization as seen in Figure 4.10 (b). This was followed by sample labeling before they were kept in a pre-cleaned 1-inch by 1-inch sample box. The remaining quarter wafer pieces were put into wafer holders with sample IDs written on them for ease of identification. Properly labeling the samples was important for ensuring the same region characterization.

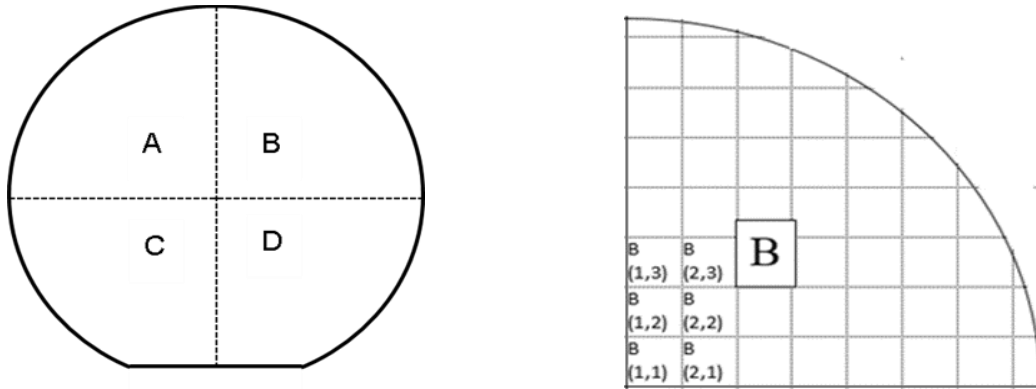


Figure 4.10. (a) Si wafer cleaved into four quarters. (b) A quarter wafer cleaved into 1x1 inch² squares.

Surface Cleaning

To remove any contamination due to organic residues from growth and/or particles on the surface of the sample due to cleaving, the sample was dipped into acetone and placed in an ultrasonic bath sonicator for 5 minutes to agitate and disperse the contaminants from the sample surface. The sample was then dipped into isopropyl alcohol (IPA) and finally rinsed off in deionized water (DI water). A N₂ gun was then used to dry the sample by blowing the water off the surface, followed by a 2 min hotplate bake of the sample at 95 °C.

Photolithography

Once the cleaning was done, the sample was prepared for positive photolithography by covering its surface with hexamethyldisilazane (HMDS) and then a positive photoresist using a spin coater. The HMDS served as an adhesive required to prevent the photoresist delamination. The sample was soft baked for 50 seconds at 110 °C as a curing process and transferred to the aligner brought in contact with the pre-defined photomask labeled as I where it was exposed to Ultraviolet (UV) light for 11 seconds. After exposure, the sample was put into the AZ-MIF-300 (Integrated Micro Materials, Argyle, TX) photoresist developer for 50 seconds to form the desired pattern. The sample was then rinsed in DI water and N₂ dried followed by a hard bake at 130 °C for 15 minutes. A descum process was then performed where the sample was placed in a vacuum chamber to allow oxygen plasma flowing through the chamber to burn off any photoresist residue layer from the sample and get rid of them.

Etching

To form mesas on the coated sample and open-up the waveguide strip, a chemical wet etch was performed. A solution of hydrochloride acid and hydrogen peroxide was a good etchant for the GeSn material. The solution was prepared with HCl:H₂O₂:H₂O=1:1:20 ratio and allowed to stabilize for 40 minutes. A thermometer was used to monitor the temperature of the reactants and the developed samples were dipped in the solution at 0°C. Figure 4.11 shows four samples dipped in a solution of HCl:H₂O₂:H₂O=1:1:20 during the etching process. The etch depth was a function of time and dependent on the sample thickness. Once the desired etch depth was determined based on the grown sample structure, a 10-minute dummy run was performed to determine the etch rate. The rate was then multiplied by the desired depth to determine the etch time.



Figure 4.11. Four (1-inch x 1-inch) etched samples of GeSn.

Negative Photolithography

To form the metal contacts for the device, the samples were covered with a negative photoresist using the spin coater and then baked for 50 seconds at 95 °C. The sample was then exposed for 5 seconds under the second section (II) of the pre-defined chrome mask. The second alignment was adjusted carefully to ensure there was no overlap between the first pattern and the second pattern to ensure proper liftoff after metal deposition. The samples were then baked for 2 minutes at 105 °C after exposure. To switch the properties of the photoresist between the exposed and unexposed area, a flood exposure without masks was performed on the samples for 60 seconds. Figure 4.12 shows the standard photolithography process from cleaning to development.

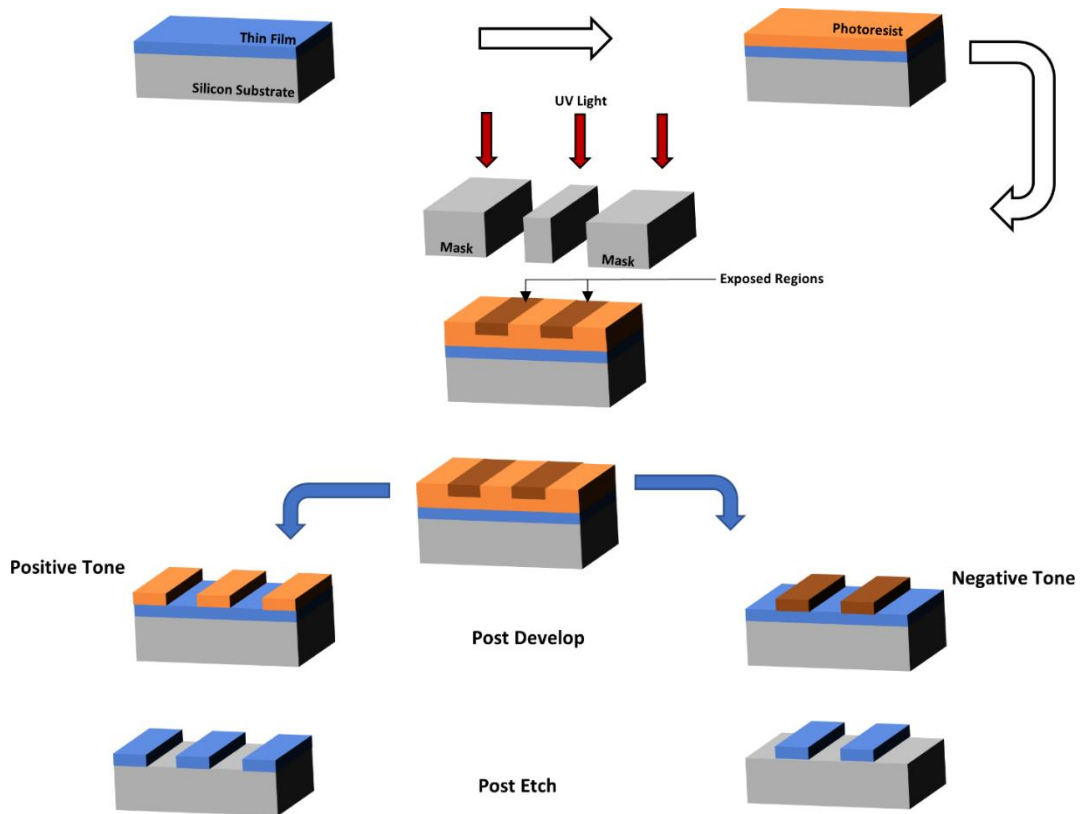


Figure 4.12. Schematic diagram of a standard photolithography process.

Descum

A second descum was done following the exposure and the wafers were dipped into the developer for ~2 minutes to expose the contacts. It was then rinsed with DI water and dried with N₂. The developed features were then inspected under the microscope as shown in Figure 4.13.

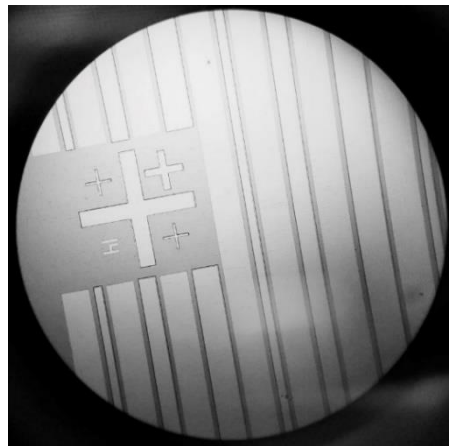


Figure 4.13. Sample image after the development of the negative photoresist.

Metal Deposition

Metallization was done in a vacuum chamber using the electron beam evaporation method. A 10 nm chromium (Cr) layer was deposited to form ohmic contact and then a 350 nm gold (Au) layer was deposited on top for better electrical conductivity. Figure 4.14 shows the sample after the metal deposition process.

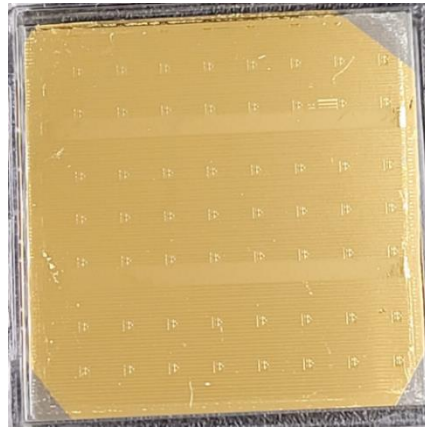


Figure 4.14. Sample image after metal deposition.

Liftoff

After the metallization process was complete, the samples were soaked in acetone for ~30 minutes. Cleanroom swabs were used to gently liftoff the peeling metals from the sample surface. This was followed by cleaning the samples in IPA and then DI water.

Lapping

The samples were grown on a 735 μm thick Si substrate. Hence, to ensure a uniform flat facet when cleaved after fabrication, and to reduce the series resistance of the edge-emitting LED caused by the substrate thickness, the Si substrate was lapped down to ~100 μm thickness using a 15 μm alumina powder.

Wire bonding

After lapping, the fabricated device was cut into smaller sizes and fit onto a chip carrier

by using thermally conductive epoxy. The sample was then bonded to the chip holder with either Ag or Au wire using the ball bonding method. Bonding the fabricated samples to the chip holder made it easier to mount the sample into the cryostat for characterization and secured the device in position compared to when the probes were used without a chip holder. It also helped preserve the device for future use after initial characterization. Figure 4.15 shows a wire-bonded sample after cleaving.

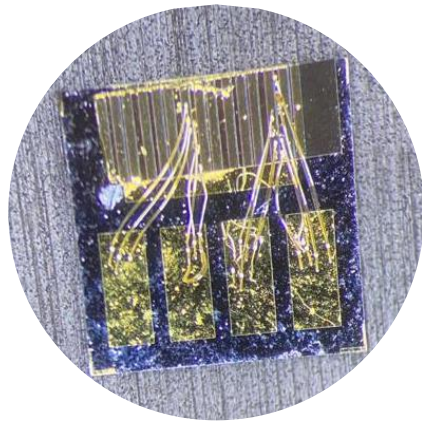


Figure 4.15. Wire bonded device.

4.2.2 Optical Pumping Measurement

The optical pumping characterization was performed with the fabricated edge-emitting device using the defined optical path described in Figure 3.13, and pulsed laser conditions listed below:

- 1064 nm laser source
- Pulse width = 2 ns
- Repetition rate = 10 kHz
- Spot size = 20 μm x 3 mm
- PbS detector (1 - 3 μm)
- Spectrometer: Bruker FTIR

The sample was cleaved into ~ 1.0 mm cavity length device with 20 μm , 40 μm , 60 μm , 80 μm , and 100 μm ridge widths and the cleaved sides formed mirror-like flat facets on both sides as shown in Figure 4.16 a. It was then mounted with a thermal grease onto a Si chip carrier as shown in Figure 4.16 b and placed into a cryostat with a continuous flow of LN_2 for low-temperature measurement.

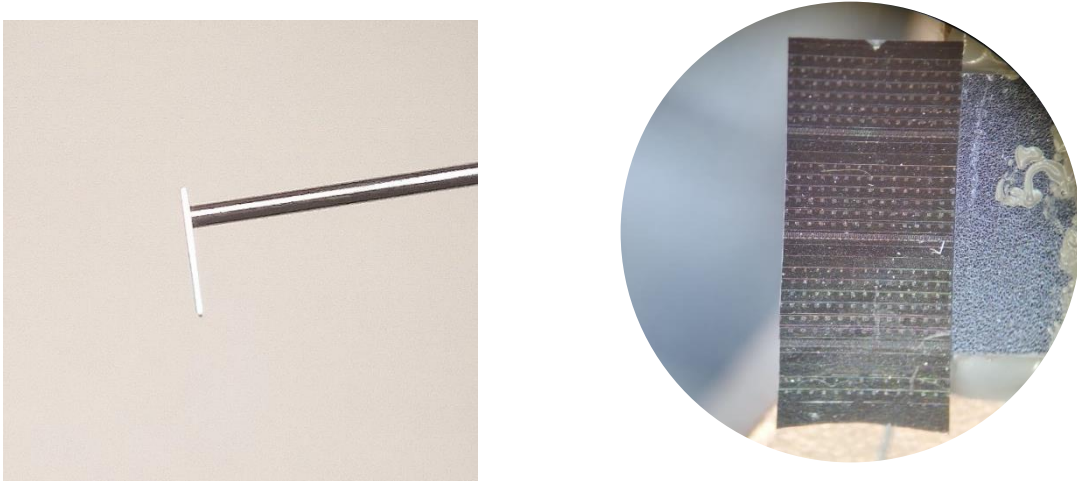


Figure 4.16. (a) Side facet of a cleaved device. (b) Mounted cleaved sample.

During measurement, the lock-in signal was highly unstable at different temperatures due to vibrations. The signal was improved and stabilized by changing the 3-D stage for mounting the cryostat to the optical bench to a lab jack as shown in Figure 4.17. The lab jack was then placed on two adjustable mounting stages to make a possible x, y, and z-axis adjustment for the cryostat. Once the signal stabilization was achieved, the GeSn sample (E) with 0.95 mm cavity length was then optically pumped at different temperatures ranging from 77 K to 160 K using the 1064 nm pulsed laser along with a lock-in amplifier chopped at 79 Hz.

The L-L data was collected by an existing LabVIEW program (National Instrument, Austin, TX) and the average power collected at each temperature measurement was converted to the peak power density and plotted against the obtained intensity as shown in Figure 4.18.

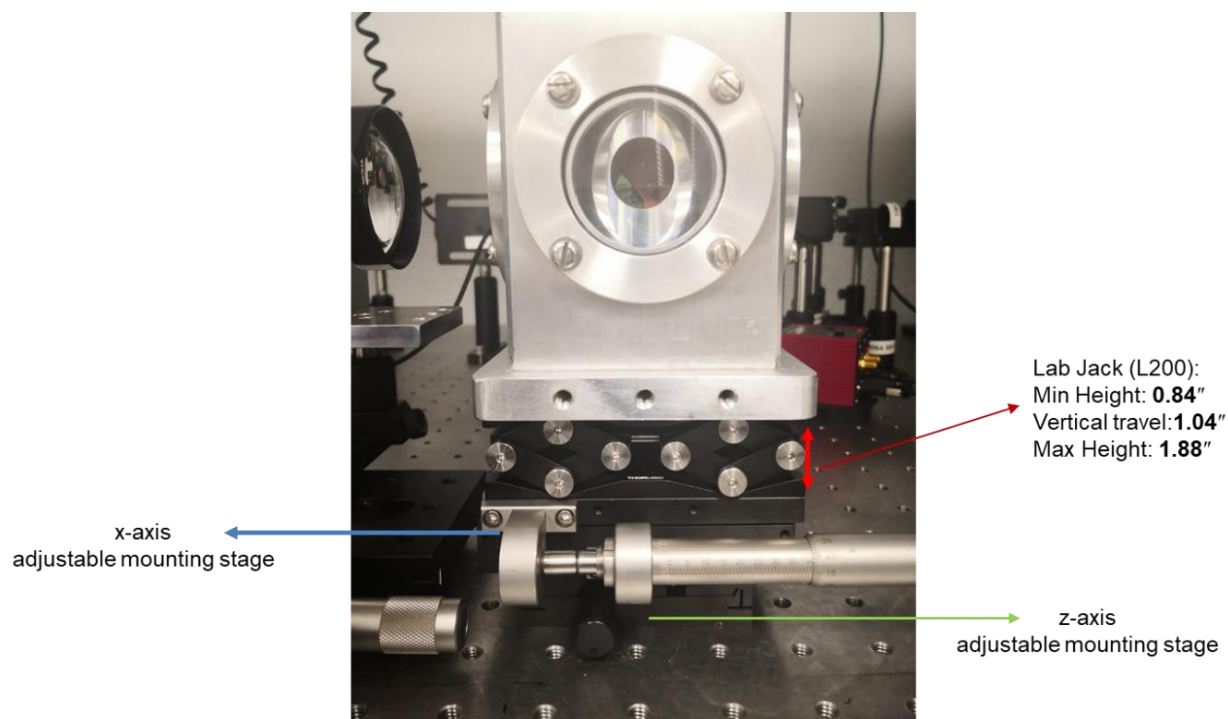


Figure 4.17. Cryostat stabilization for optical pumping measurement.

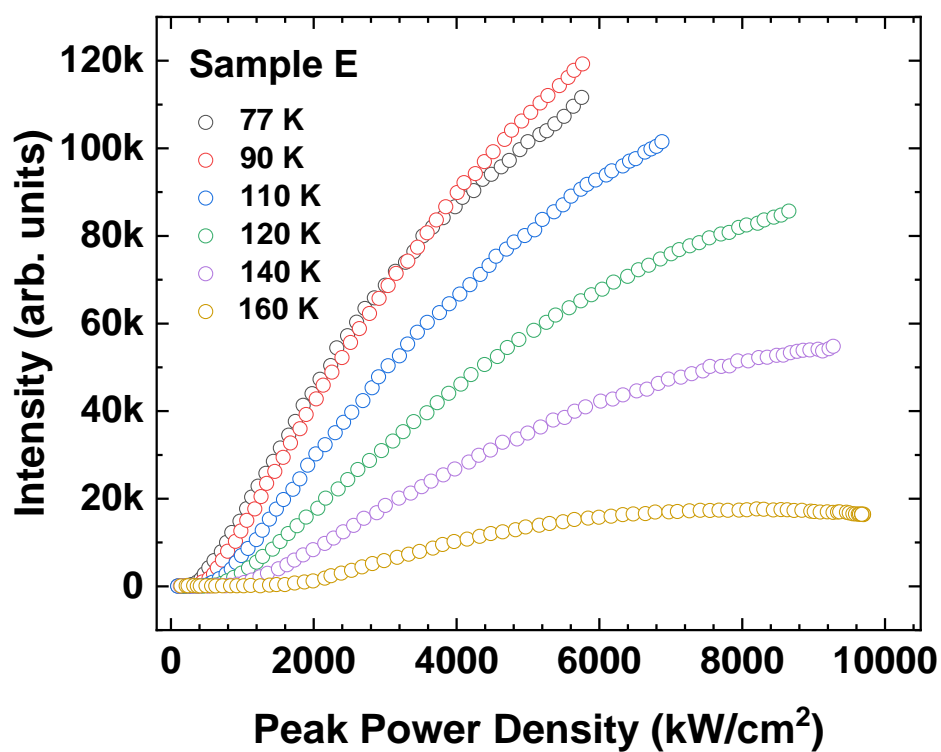


Figure 4.18. Temperature-dependent L-L curve for GeSn laser.

The sample spectrum was measured at the lasing threshold power density (P_{th}) for each temperature to investigate the lasing mode characteristics. Figures 4.19 to 4.21 shows the spectra at 77 K to 110 K at ~ 7 nm resolution.

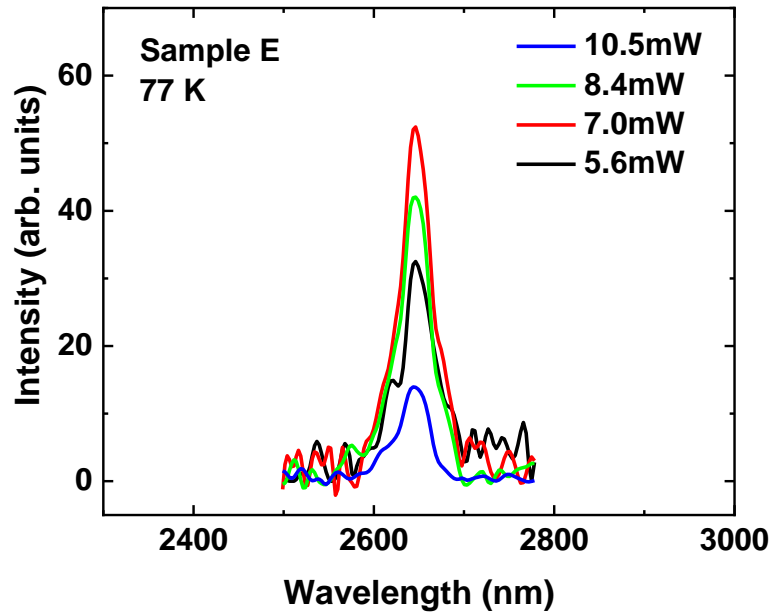


Figure 4.19. Spectra of GeSn laser at 77 K.

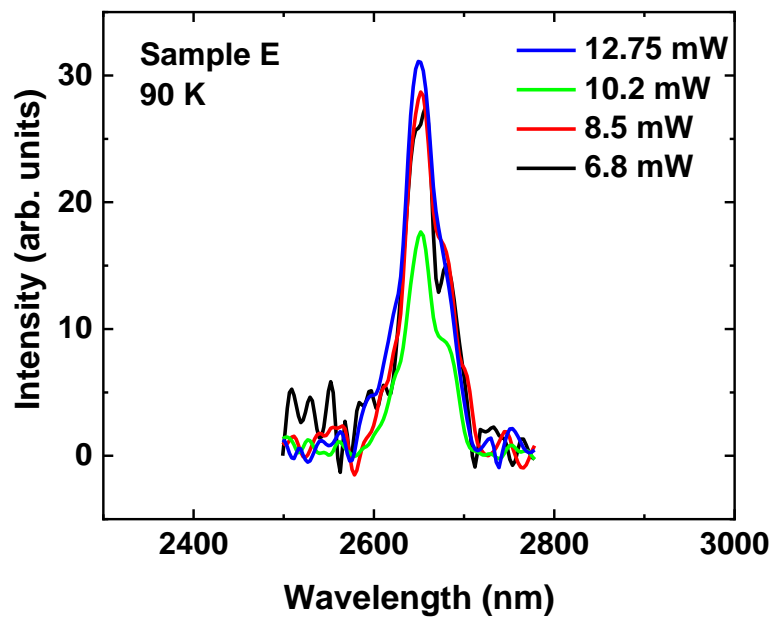


Figure 4.20. Spectra of GeSn laser at 90 K.

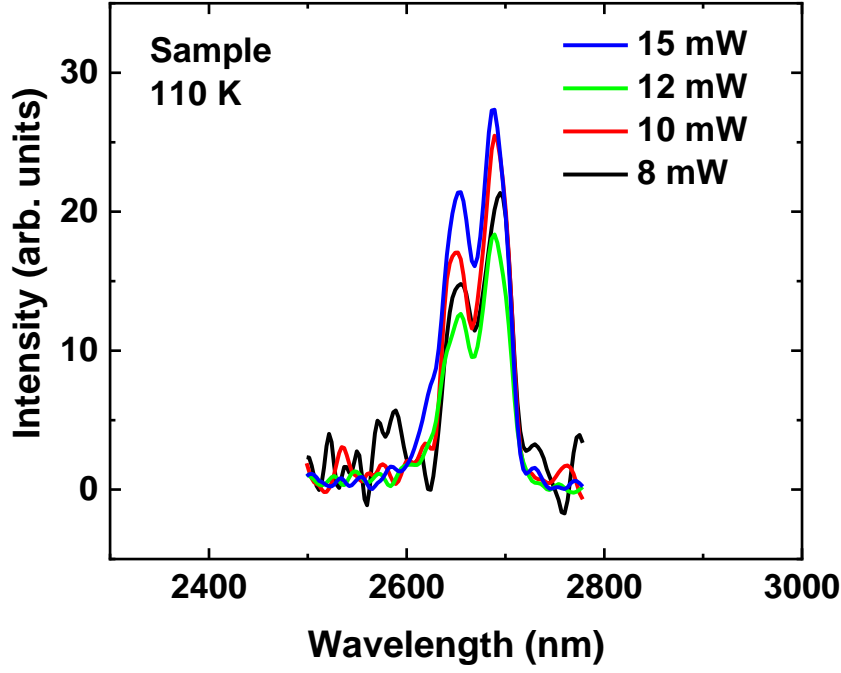


Figure 4.21. Spectra of GeSn laser at 110 K.

The sample was further measured at 8 cm^{-1} and 4 cm^{-1} resolutions at 77 K with 88 mW pumping power to investigate the sample characteristics at higher resolutions as shown in Figure 4.22. The lasing threshold power (P_{th}) spectrum for the sample was then plotted to observe the peak wavelength trend across different temperatures as shown in Figure 4.23.

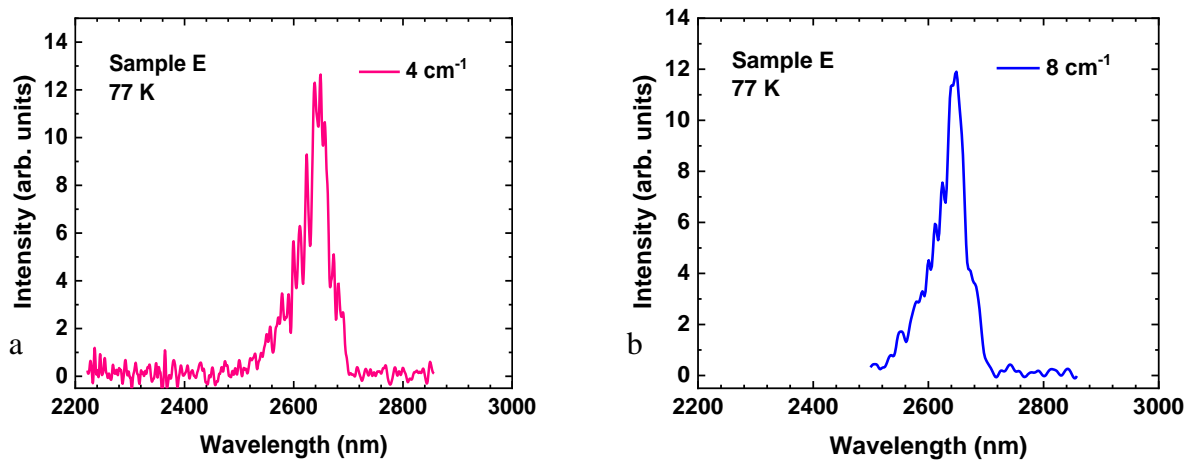


Figure 4.22. 77 K Spectra of GeSn laser at (a) 8 cm^{-1} and (b) 4 cm^{-1} resolution.

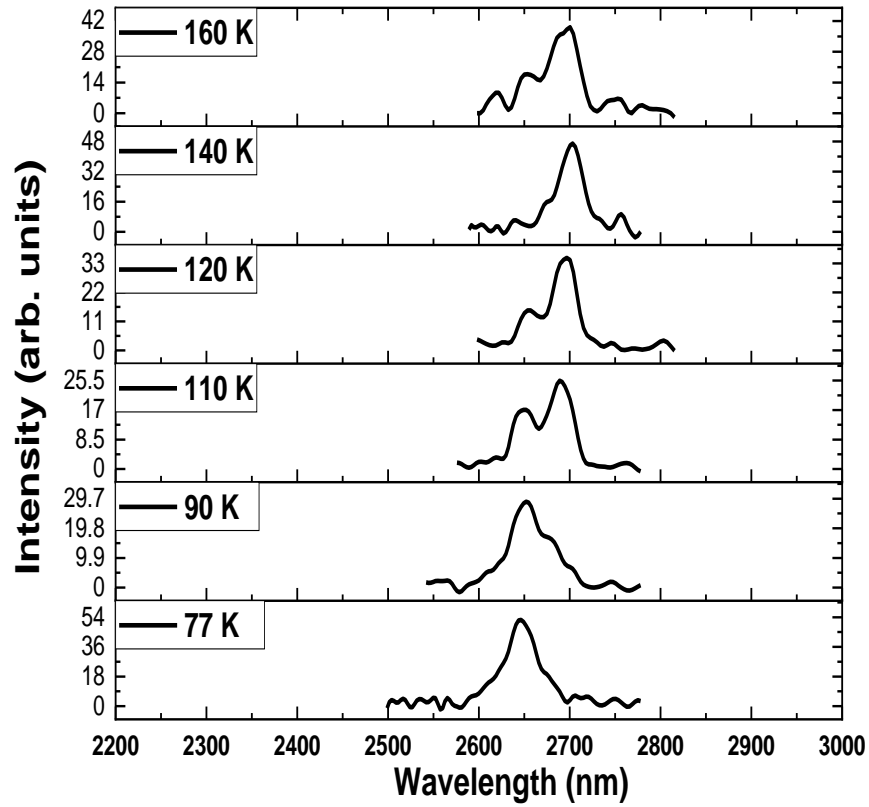


Figure 4.23. P_{th} spectrum across temperatures.

4.2.3 Electroluminescence Measurement

Electroluminescence (EL) is the emission of light by application of a forward bias to a device junction as illustrated in Figure 4.24. When an electric field is applied to a device, the junction barrier is lowered, and the injected electron and holes recombine radiatively. The radiative recombination then causes photons to be emitted from each electron-hole pair. Two GeSn laser diode samples (F and G) grown in an industry-standard chemical vapor deposition reactor using commercially available precursors are discussed in the remainder of this chapter.

The laser device structures, doping profiles, and their nominal thickness values are shown in Figures 4.25 (a) and (b), respectively. The samples were etched at 1.45 μm and 1.97 μm for F and G devices, respectively to expose the GeSn buffer layer for metal contacts. This was followed by the electron beam deposition of 10 nm Cr and 350 nm Au on the device to form the

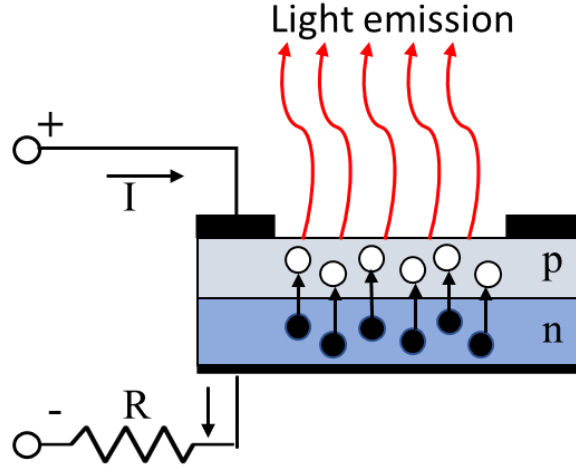


Figure 4.24. Light emission by application of electric field to the p-n junction.

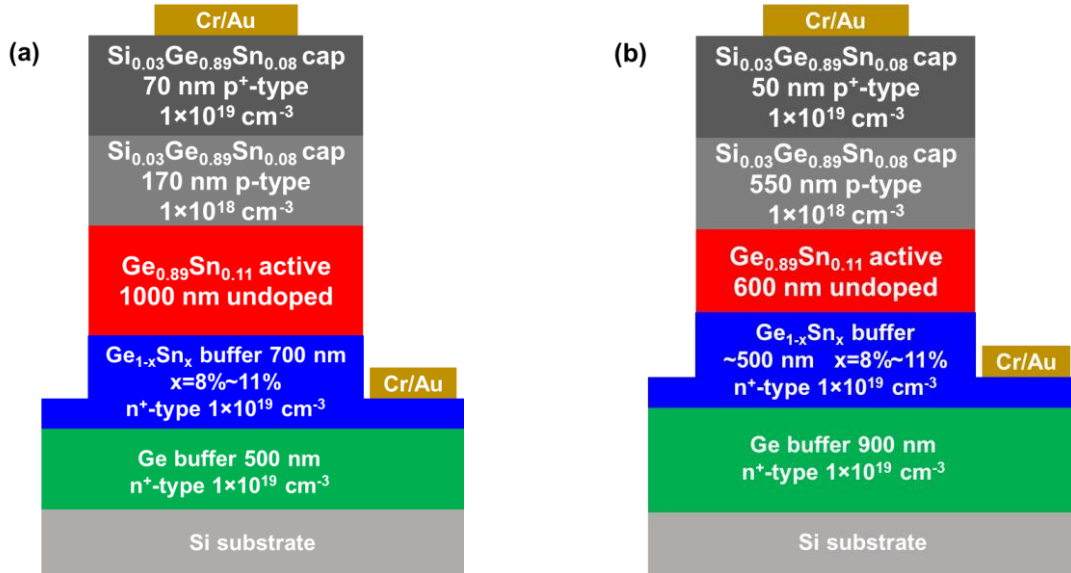


Figure 4.25. Cross-sectional schematic of samples (a) F and (b) G laser devices.

p and n electrodes after liftoff. Both samples F and G were then lapped down to $\sim 138 \mu\text{m}$ and $110 \mu\text{m}$ thickness, respectively, before cleaving individually into 0.8 mm and 1.0 mm cavity lengths with $40 \mu\text{m}$, $80 \mu\text{m}$, and $100 \mu\text{m}$ wide ridges. The devices were then wire bonded using the $80 \mu\text{m}$ ridge width and placed in cryostat after mounting with the probe station. The electrical properties were first observed by measuring the current-voltage (I-V) of the devices using a Keithley source measurement unit (SMU) connected to the setup shown in Figure 3.15. The

Keithley source served as the voltage source and current measurement unit, and the generated data for I-V characteristics were extracted via a LabVIEW program and the rectify behavior was observed. If the measured I-V at room temperature showed reverse bias, the wire polarity connecting the device under test (DUT) to the Keithley source was interchanged to correct the reverse bias to a forward bias outcome before proceeding to lower temperatures measurements.

Starting with sample F whose layer thickness had been confirmed with transmission electron microscopy (TEM), the I-V measurement was performed from 300 K to 77 K and plotted as shown in Figure 4.26.

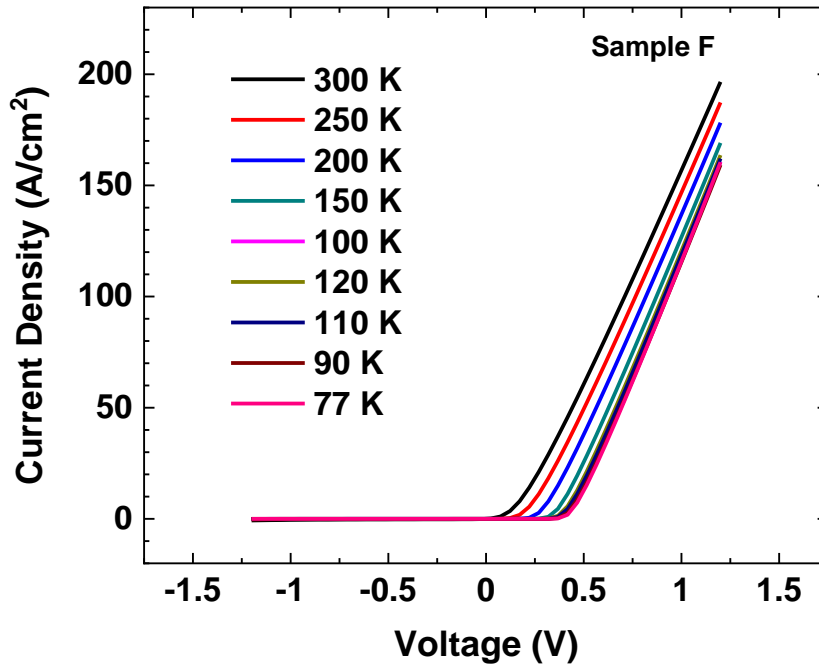


Figure 4.26. Temperature-dependent I-V curve for sample F with 11% Sn composition.

After measuring the I-V characteristics for sample F, the Keithley was disconnected and the DUT was connected to the pulse generator as shown in the EL measurement setup (Figure 3.15). The device was then tested for lasing or PL by supplying random voltage from the pulse generator. Once a reading was observed on the lock-in amplifier, the setup was maximized by

improving the alignment to get the highest possible reading on the lock-in. Using a PbS detector, the light output power versus current injection (LI) was measured at 77 K and 100 K, respectively, using a 1 kHz repetition rate and 700 ns pulse width. Figure 4.27 shows the LI curves of sample F. The power calibration was done by measuring the light emission from the device with the power meter. The average power was then calculated by dividing the measured power by the duty cycle. Since the FTIR spectrometer took in all the light, the moving mirror was stopped (for stability) to record the detector signal value of the laser diode from the lock-in.

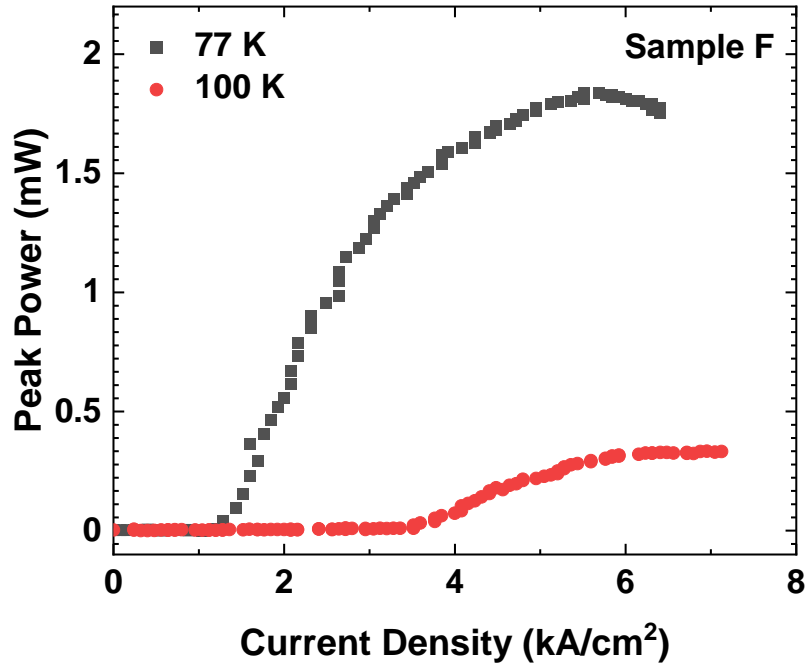


Figure 4.27. LI curves of 0.8 mm cavity length and 80 μm ridge at 77 K and 100 K.

The peak power using the FTIR spectrometer was then obtained from the ratio of the detector signal reading to the laser diode reading (when stopped) multiplied by the average power. The maximum power output was calculated to be 1.8 mW under 5.8 kA/cm² (40 V) at 77 K. The EL spectrum of the device was then taken at various current injections above and below the current density threshold at 77 K and 100 K to observe the emission profile as shown in

Figures 4.28 to 4.31. The experiment was also repeated using a microHR dispersive spectrometer setup with LN₂ InSb detector for comparison. Figure 4.32 shows the spectra at 77 K using the dispersive spectrometer. The 77 K lasing threshold spectra from both spectrometers were then plotted together in Figure 4.33 to clearly show the resolution difference.

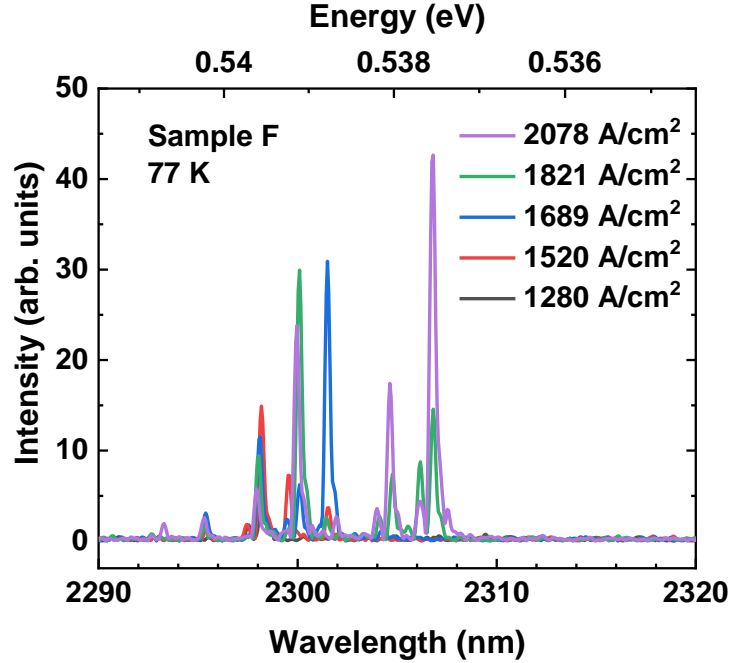


Figure 4.28. EL spectra of various current injections at 77 K.

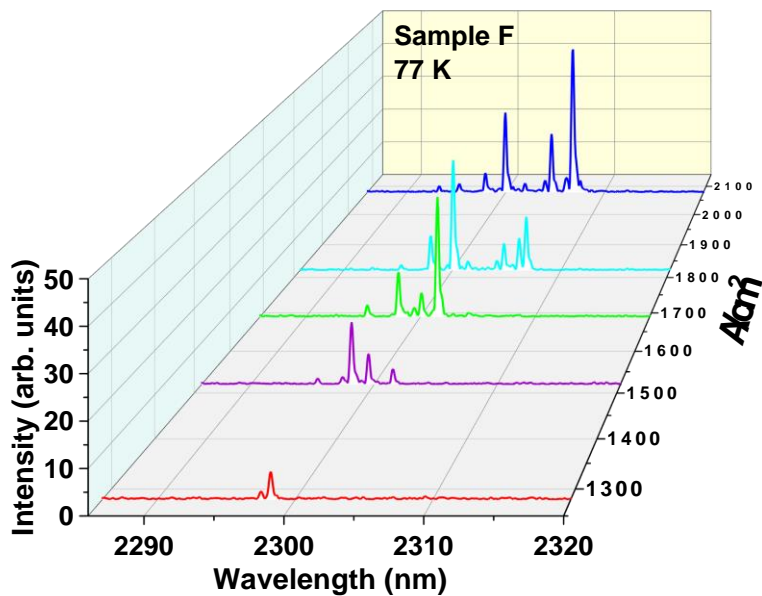


Figure 4.29. 3D view of EL spectra of various current injections at 77 K.

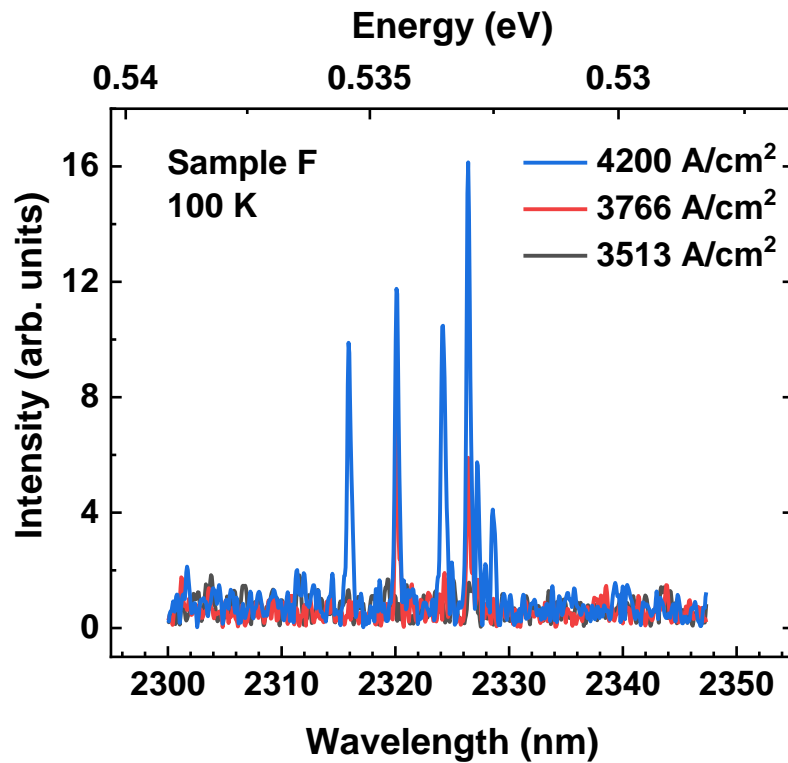


Figure 4.30. EL spectra of various current injections at 100 K.

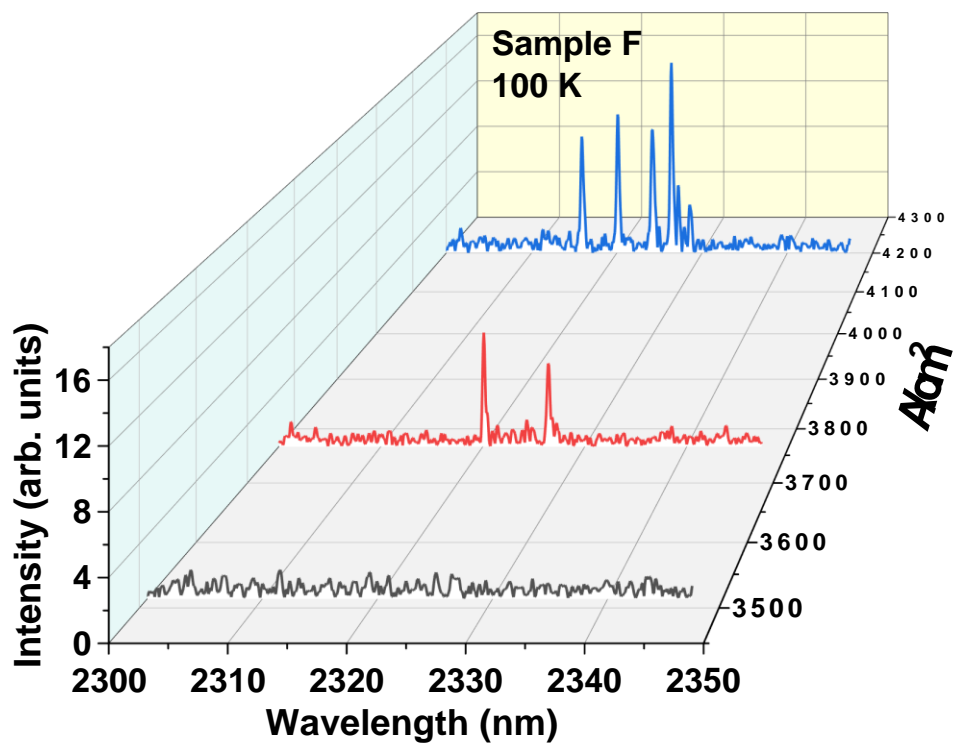


Figure 4.31. 3D view of the EL spectra of various current injections at 100 K.

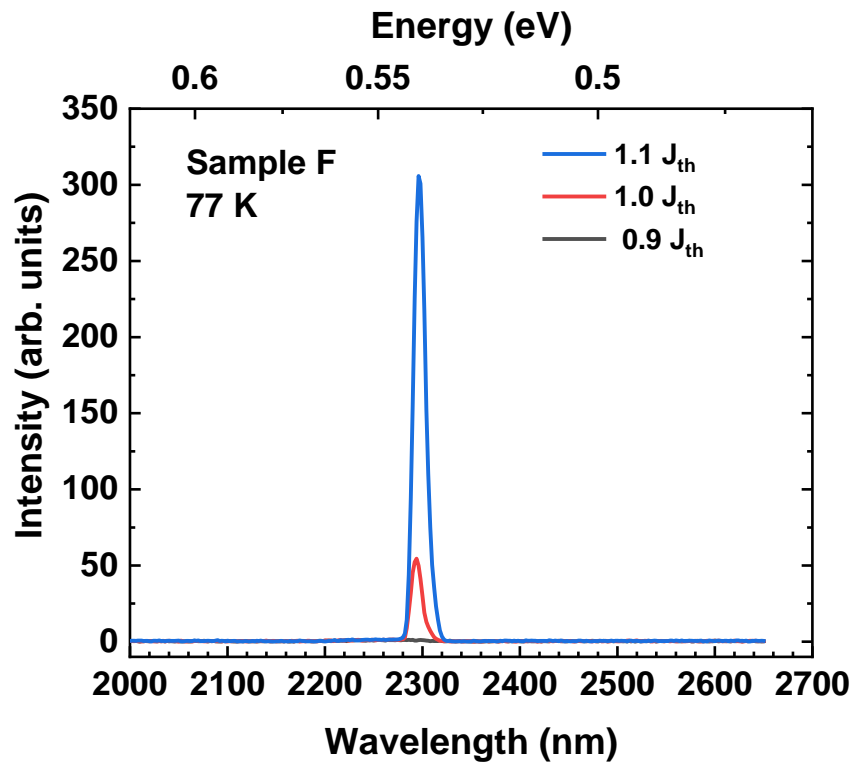


Figure 4.32. EL spectra from microHR dispersive spectrometer at 77 K.

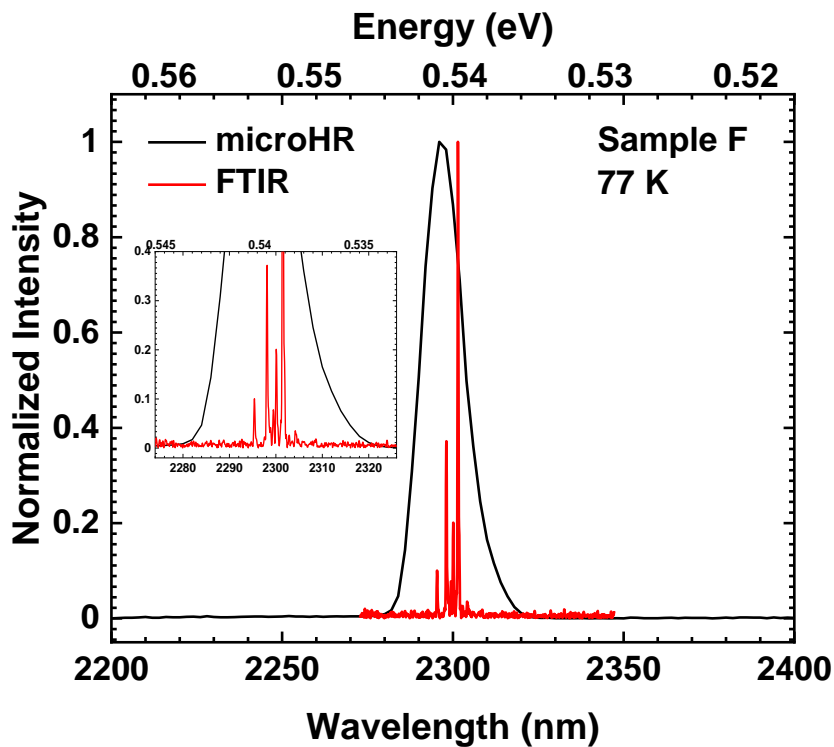


Figure 4.33. Lasing spectra from microHR spectrometer compared with lasing spectra from FTIR spectrometer at 77 K.

For sample G, the temperature-dependent I-V was measured from 300 K to 10 K following the same steps, and the LI measured with the same duty cycle using the microHR dispersive spectrometer setup. Figures 4.34 and 4.35 show the I-V characteristics plot and the LI curve, respectively. The electroluminescence signal was then collected, and the emission profile plotted across temperatures at various current injections. Figures 4.36 to 4.41 show the EL spectra from 10 K to 115 K.

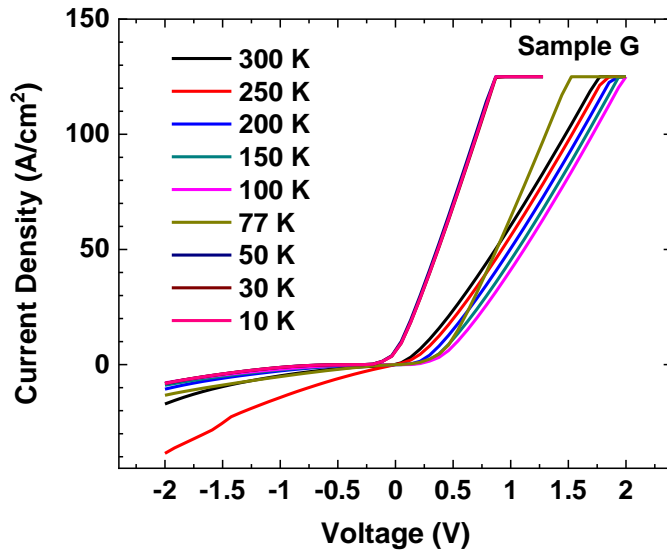


Figure 4.34. Temperature-dependent I-V curve for sample G with 11% Sn composition.

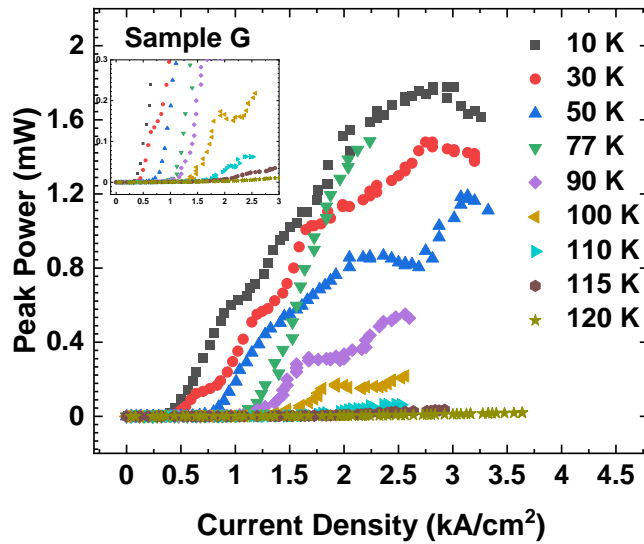


Figure 4.35. LI curves of 1.0 mm cavity length and 80 μm ridge from 10 K and 120 K.

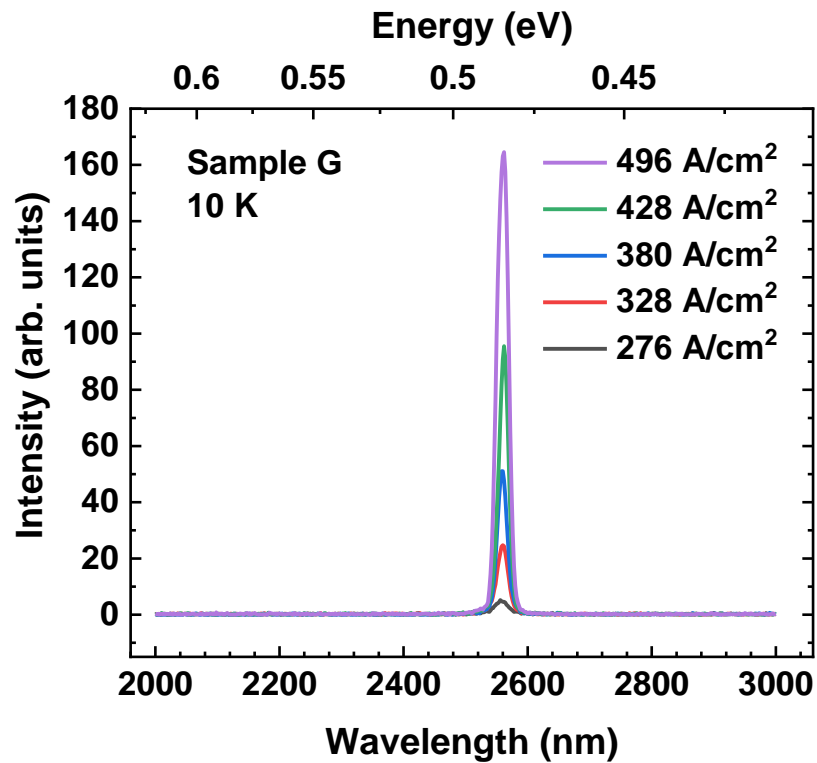


Figure 4.36. EL spectra from microHR dispersive spectrometer at 10 K.

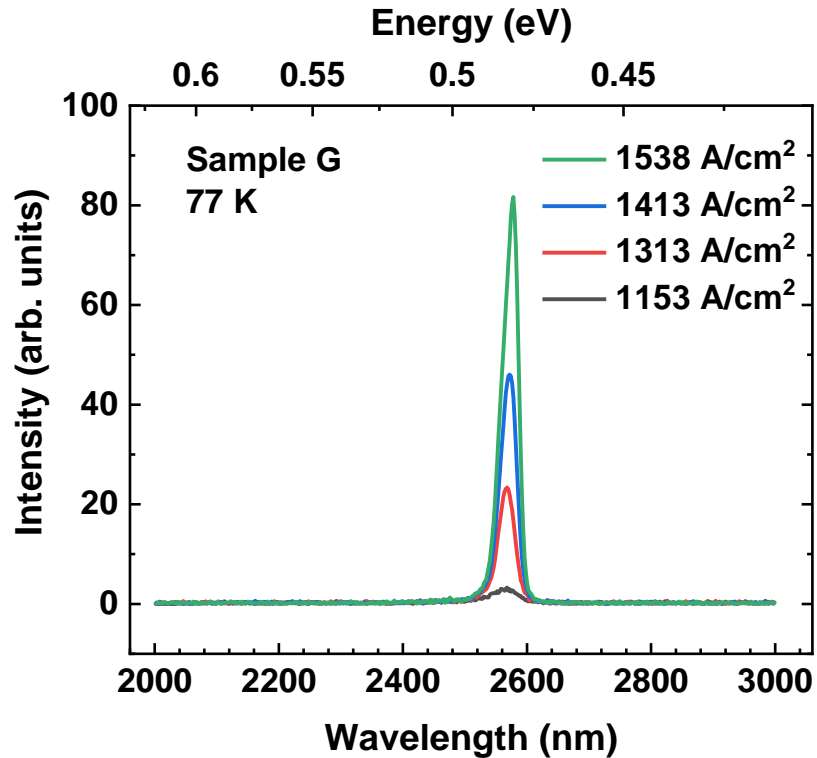


Figure 4.37. EL spectra from microHR dispersive spectrometer at 77 K.

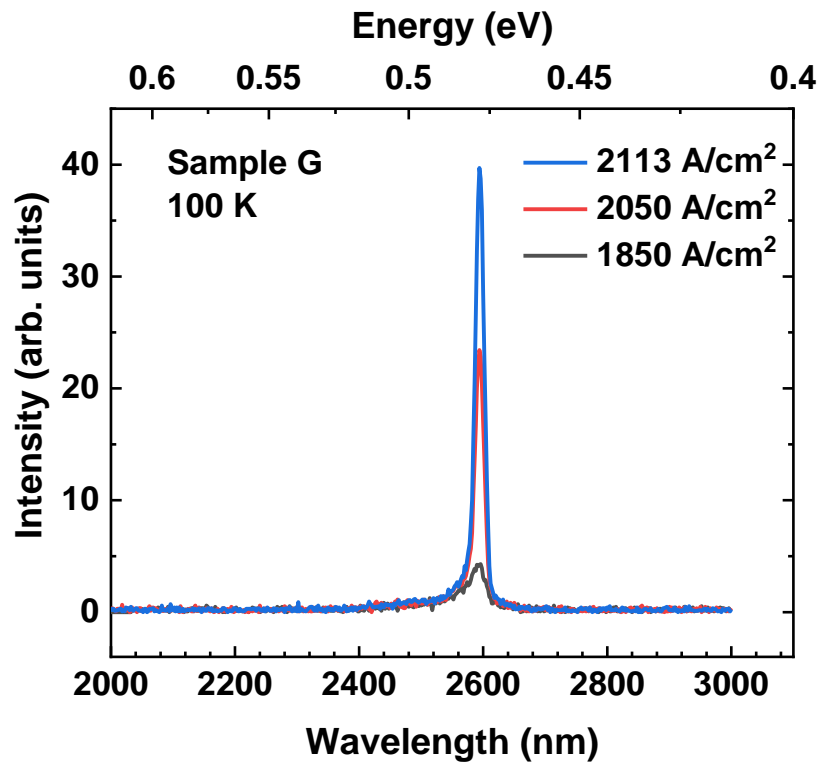


Figure 4.38. EL spectra from microHR dispersive spectrometer at 100 K.

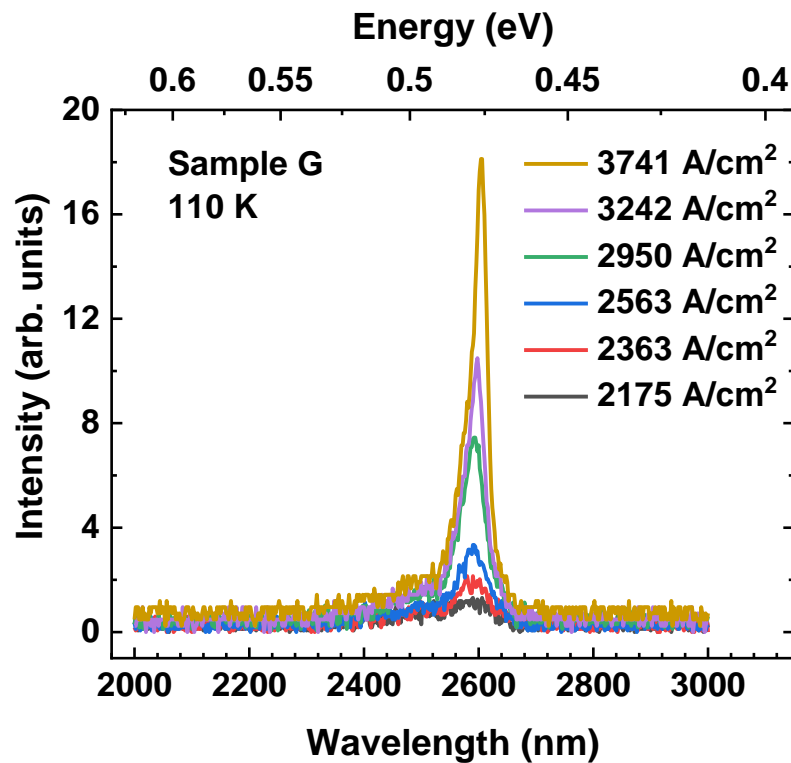


Figure 4.39. EL spectra from microHR dispersive spectrometer at 110 K.

4.3 Results and Discussion

The accuracy of the measured wavelength of the CVD Ge buffer growth samples was confirmed by the Ge reference sample with the FTIR spectrometer as shown in Table 4.1. The Ge and GeSn PL measurements showed a high signal-to-noise ratio (SNR) with a successfully suppressed background noise and optimal signal intensities. This was achieved by a suitable optical setup with the careful calibration of the Bruker FTIR spectrometer setup and a lock-in amplifier.

Table 4.1. Room temperature PL characterization summary of Ge buffer growths.

Sample ID	Thickness (nm)	Peak Wavelength (nm)	Growth to Ref Ratio
0333-UAF	972	1604	1/2.5
0861-UAF	1126	1604	1/2.5
0862-UAF	1054	1620	1/2.8
0863-UAF	1065	1604	1/3
0864-UAF (Annealed)	1083	1604	1/4

By using LabVIEW with the optical pumping and EL setup for components movement and signal reading in the step-scan mode, the setup was able to measure light emission from fabricated GeSn devices with high intensity, narrow Full-Width Half-Maximum (FWHM), and low background noise making made it possible to distinguish between minor excitation peaks and modes from the measured samples. The parameters of the optically pumped GeSn device (E) and the characterization results at 77 K are shown in Table 4.2.

Table 4.2. Summary of Sample (E) and Lasing Characterization Results at 77 K.

GeSn 1st layer		GeSn 2nd layer		Lasing Wavelength (nm)	Threshold at 77 K (kW/cm ²)
Sn %	Thickness (nm)	Sn %	Thickness (nm)		
10.5	250	14.4	670	2644	367

The device showed similar results with the previously reported measurement [32], with both operating at a maximum lasing temperature of 160 K and a lasing wavelength of ~ 2640 nm. The threshold for this device at 77 K was ~3x the previously reported value [32] because of the difference in the duty cycle. Sample E was measured with a 33% less duty cycle compared to the previous measurement. A 45 kHz repetition rate with a 6 ns pulse was used for the previously reported measurement [32], compared to a 10 kHz repetition rate and a 2 ns pulse width used in this thesis research project. The lasing peak blue-shift observed in Figure 4.23 with temperature decrease was due to the typical band filling effect of direct bandgap lasers usually observed from III-V lasers. Finally, at higher resolutions with a slightly higher pumping power, multi-peaks showing the lasing modes were observed as shown in Figure 4.22. For EL measurement, sample F had a maximum lasing temperature of 100 K. The peak FWHM for the EL measurement of sample F at 77 K was 79 nm below the threshold and ~14 nm above the threshold with 2294 nm lasing wavelength using the microHR spectrometer. This broad linewidth was due to microHR spectral resolution of ~10 nm. The higher resolution spectra from the FTIR spectrometer setup clearly showed the multimode lasing characteristics of sample F above the threshold as shown in Figure 4.33 inset, with a 0.3 nm FWHM for the individual peaks.

Sample G, however, showed better results and set a new world record lasing temperature at 110 K. The possibility of this sample lasing at 115 K was dependent on the high-resolution spectra where one can clearly identify the lasing characteristics. Table 4.3 shows the sample summary and EL characterization results at maximum lasing temperature for sample G. From the

Table 4.3. Sample G summary at 110 K.

Sample #	Cap material	Cap Thickness	Active Sn composition	Maximum operating temperature	Threshold at 110 K (A/cm²)
G	SiGeSn	~ 600 nm	11 %	110 K	1699

EL spectra at each temperature, the FWHM was narrowed as the injection current density increased, and the peak intensities were also observed to increase. This behavior indicated the lasing characteristics of the device. Table 4.4 shows the FWHM below and above the threshold with the peak wavelength at 10 K, 77 K, and 110 K, respectively.

Table 4.4. The FWHM characteristics at 10 K, 77 K, and 110 K.

Operating Temperature	FWHM below threshold (nm)	FWHM above threshold (nm)	Peak wavelength (nm)
10 K	29	19	2564
77 K	57	32	2574
110 K	112	60	2596

Chapter 5: Conclusion and Future Work

In this thesis research, an FTIR setup was designed and built with functions for PL and EL measurements at high resolutions. The Bruker IFS 66/S was aligned with external light sources and used with an external photodetector coupled with a lock-in amplifier that was modulated by a chopper. The pump laser from the optical bench was guided through the mirrors and lens to excite the sample / pump the laser device, while the emitted light was collected and guided to the FTIR spectrometer. The EL measurement was achieved by biasing the fabricated device and the collected EL was led to the FTIR spectrometer. The PL/EL data showed the expected result with a much higher SNR and low background noise. For efficient working protocol, the LabVIEW program was employed to control motorized components and interface the workstation with the setup for signal reading.

Further improvements could be made with a better understanding of the OPUS operating software and the Bruker trigger function setup for measurement. Time-resolved step scan with the internal ADC and trigger function knowledge would improve spectra quality with much higher resolution and save time.

Results from this batch of experiments were very promising and the proposed improvement with the time-resolved step scan with the internal ADC will provide finer outcomes.

References

- [1] R. A. Soref and J. P. Lorenzo, “Single-crystal silicon: a new material for 1.3 and 1.6 μm integrated-optical components,” *Electron. Lett.*, vol. 21, no. 21, p. 953, 1985, doi: 10.1049/el:19850673.
- [2] G. T. Reed, W. R. Headley, and C. E. J. Png, “Silicon photonics: the early years,” San Jose, California, United States, Mar. 2005, p. 1, doi: 10.1117/12.596921.
- [3] D. A. Miller, “Physical reasons for optical interconnection,” *Intel J Optoelectron.*, vol. 11, pp. 155–168, 1997.
- [4] D. A. Miller, “Rationale and challenges for optical interconnects to electronic chips,” *Proc. IEEE*, vol. 88, no. 6, pp. 728–749, 2000.
- [5] D. A. Miller, “Device requirements for optical interconnects to silicon chips,” *Proc. IEEE*, vol. 97, no. 7, pp. 1166–1185, 2009.
- [6] L. Brusberg, M. Immonen, and T. Lamprecht, “Electro-optical circuit boards with single- or multi-mode optical interconnects,” in *Optical Interconnects for Data Centers*, Elsevier, 2017, pp. 287–307.
- [7] R. Soref, “The Impact of Silicon Photonics,” *IEICE Trans. Electron.*, vol. E91-C, no. 2, pp. 129–130, Feb. 2008, doi: 10.1093/ietele/e91-c.2.129.
- [8] R. A. Soref, S. J. Emelett, and W. R. Buchwald, “Silicon waveguided components for the long-wave infrared region,” *J. Opt. Pure Appl. Opt.*, vol. 8, no. 10, pp. 840–848, Oct. 2006, doi: 10.1088/1464-4258/8/10/004.
- [9] K. Tanabe, K. Watanabe, and Y. Arakawa, “III-V/Si hybrid photonic devices by direct fusion bonding,” *Sci. Rep.*, vol. 2, no. 1, p. 349, Dec. 2012, doi: 10.1038/srep00349.
- [10] Z. Wang, B. Tian, M. Pantouvaki, W. Guo, P. Absil, J. Van Campenhout, C. Merckling, and D. Van Thourhout, “Room-temperature InP distributed feedback laser array directly grown on silicon,” *Nat. Photonics*, vol. 9, no. 12, pp. 837–842, Dec. 2015, doi: 10.1038/nphoton.2015.199.
- [11] H. Liu, T. Wang, Q. Jiang, R. Hogg, F. Tutu, F. Pozzi, and A. Seeds, “Long-wavelength InAs/GaAs quantum-dot laser diode monolithically grown on Ge substrate,” *Nat. Photonics*, vol. 5, no. 7, pp. 416–419, Jul. 2011, doi: 10.1038/nphoton.2011.120.
- [12] X. Sun, A. Zadok, M. J. Shearn, K. A. Diest, A. Ghaffari, H. A. Atwater, A. Scherer, and A. Yariv, “Electrically pumped hybrid evanescent Si/InGaAsP lasers,” *Opt. Lett.*, vol. 34, no. 9, p. 1345, May 2009, doi: 10.1364/OL.34.001345.

- [13] A. W. Fang, H. Park, O. Cohen, R. Jones, M. J. Paniccia, and J. E. Bowers, “Electrically pumped hybrid AlGaInAs-silicon evanescent laser,” *Opt. Express*, vol. 14, no. 20, p. 9203, 2006, doi: 10.1364/OE.14.009203.
- [14] H. Park, A. W. Fang, S. Kodama, and J. E. Bowers, “Hybrid silicon evanescent laser fabricated with a silicon waveguide and III-V offset quantum wells,” *Opt. Express*, vol. 13, no. 23, p. 9460, 2005, doi: 10.1364/OPEX.13.009460.
- [15] J. Zheng, Z. Liu, C. Xue, C. Li, Y. Zuo, B. Cheng, and Q. Wang, “Recent progress in GeSn growth and GeSn-based photonic devices,” *J. Semicond.*, vol. 39, no. 6, p. 061006, Jun. 2018, doi: 10.1088/1674-4926/39/6/061006.
- [16] M. Bauer, J. Taraci, J. Tolle, A. V. G. Chizmeshya, S. Zollner, D. J. Smith, J. Menendez, C. Hu, and J. Kouvetakis, “Ge–Sn semiconductors for band-gap and lattice engineering,” *Appl. Phys. Lett.*, vol. 81, no. 16, pp. 2992–2994, Oct. 2002, doi: 10.1063/1.1515133.
- [17] J. Mathews, R. T. Beeler, J. Tolle, C. Xu, R. Roucka, J. Kouvetakis, and J. Menéndez, “Direct-gap photoluminescence with tunable emission wavelength in Ge_{1–y}Sn_y alloys on silicon,” *Appl. Phys. Lett.*, vol. 97, no. 22, p. 221912, Nov. 2010, doi: 10.1063/1.3521391.
- [18] R. Chen, H. Lin, Y. Huo, C. Hitzman, T. I. Kamins, and J. S. Harris, “Increased photoluminescence of strain-reduced, high-Sn composition Ge_{1–x}Sn_x alloys grown by molecular beam epitaxy,” *Appl. Phys. Lett.*, vol. 99, no. 18, p. 181125, Oct. 2011, doi: 10.1063/1.3658632.
- [19] H. Li, J. Brouillet, A. Salas, X. Wang, and J. Liu, “Low temperature growth of high crystallinity GeSn on amorphous layers for advanced optoelectronics,” *Opt. Mater. Express*, vol. 3, no. 9, p. 1385, Sep. 2013, doi: 10.1364/OME.3.001385.
- [20] N. Bhargava, M. Coppinger, J. Prakash Gupta, L. Wielunski, and J. Kolodzey, “Lattice constant and substitutional composition of GeSn alloys grown by molecular beam epitaxy,” *Appl. Phys. Lett.*, vol. 103, no. 4, p. 041908, Jul. 2013, doi: 10.1063/1.4816660.
- [21] S. A. Ghetmiri, W. Du, J. Margetis, A. Mosleh, L. Cousar, B. R. Conley, L. Domulevicz, A. Nazzal, G. Sun, R. A. Soref, J. Tolle, B. Li, H. A. Naseem, and S.-Q. Yu, “Direct-bandgap GeSn grown on silicon with 2230 nm photoluminescence,” *Appl. Phys. Lett.*, vol. 105, no. 15, p. 151109, Oct. 2014, doi: 10.1063/1.4898597.
- [22] K. P. Homewood and M. A. Lourenço, “The rise of the GeSn laser,” *Nat. Photonics*, vol. 9, no. 2, pp. 78–79, Feb. 2015, doi: 10.1038/nphoton.2015.1.
- [23] R. Soref, “Mid-infrared photonics in silicon and germanium,” *Nat. Photonics*, vol. 4, pp. 495–497, Aug. 2010, doi: 10.1038/nphoton.2010.171.

- [24] X. Wang, A. Cuervo Covian, L. Je, S. Fu, H. Li, J. Piao, and J. Liu, “GeSn on Insulators (GeSnOI) Toward Mid-infrared Integrated Photonics,” *Front. Phys.*, vol. 7, p. 134, Sep. 2019, doi: 10.3389/fphy.2019.00134.
- [25] K.-H. Kao, A. S. Verhulst, W. G. Vandenberghe, B. Soree, G. Groeseneken, and K. De Meyer, “Direct and Indirect Band-to-Band Tunneling in Germanium-Based TFETs,” *IEEE Trans. Electron Devices*, vol. 59, no. 2, pp. 292–301, Feb. 2012, doi: 10.1109/TED.2011.2175228.
- [26] L. Jiang, J. D. Gallagher, C. L. Senaratne, T. Aoki, J. Mathews, J. Kouvetakis, and J. Menéndez, “Compositional dependence of the direct and indirect band gaps in $\text{Ge}_{1-y}\text{Sn}_y$ alloys from room temperature photoluminescence: implications for the indirect to direct gap crossover in intrinsic and n -type materials,” *Semicond. Sci. Technol.*, vol. 29, no. 11, p. 115028, Nov. 2014, doi: 10.1088/0268-1242/29/11/115028.
- [27] B. E. A. Saleh and M. C. Teich, *Fundamentals of Photonics*. New York, USA: John Wiley & Sons, Inc., 1991. pp. 918–920.
- [28] M. Czerny and A. F. Turner, “Über den Astigmatismus bei Spiegelspektrometern,” *Z. Fur Phys.*, vol. 61, no. 11–12, pp. 792–797, Nov. 1930, doi: 10.1007/BF01340206.
- [29] V. Saptari, *Fourier transform spectroscopy instrumentation engineering*. Bellingham, WA: SPIE Optical Engineering Press, 2004. pp. 66–67.
- [30] P. R. Griffiths and J. A. De Haseth, *Fourier transform infrared spectrometry*, 2nd ed. Hoboken, N.J: Wiley-Interscience, 2007. pp. 19–21.
- [31] H. Aroui, J. Orphal, and F. Kwabia, “Fourier Transform Infrared Spectroscopy for the Measurement of Spectral Line Profiles,” in *Fourier Transform - Materials Analysis*, S. Salih, Ed. InTech, 2012. p. 74.
- [32] J. Margetis, S. Al-Kabi, W. Du, W. Dou, Y. Zhou, T. Pham, P. Grant, S. Ghetmiri, A. Mosleh, B. Li, J. Liu, G. Sun, R. Soref, J. Tolle, M. Mortazavi, and S.-Q. Yu, “Si-Based GeSn Lasers with Wavelength Coverage of 2–3 μm and Operating Temperatures up to 180 K,” *ACS Photonics*, vol. 5, no. 3, pp. 827–833, Mar. 2018, doi: 10.1021/acsp Photonics.7b00938.

Appendix A: Description of Research for Popular Publication

Silicon materials and their alloys rank amongst the most far-reaching technological contributions. Electronic devices have become an essential part of our daily lives and a vital tool for accomplishing almost every task. Consequently, high-performance silicon-based lasers and detectors have long been sought after, owing to the possibility of monolithic integration of photonics with high-speed Si electronics and the desire of widening the scope of Si technology innovations. Over the past few decades, high-resolution imaging laser radar has become an attractive option in several optoelectronics device applications.

Researchers have identified and demonstrated a new group-IV alloy material system named (Si)GeSn to revolutionize infrared imaging technology. (Si)GeSn is a disruptive technology that can meet the need for faster, lighter, higher signal-to-noise and energy-efficient infrared imaging devices at a much lower cost. The factors enabling the SiGeSn as a disruptive technology over all other infrared technologies include: (1) bandgap engineering capability, (2) significantly lower radiative and Auger recombination, (3) Si integration, and (4) complementary metal oxide semiconductor (CMOS) compatibility.

At the University of Arkansas, Solomon Ojo, a Microelectronics-Photonics student of Dr. Shui-Qing (Fisher) Yu of the Electrical Engineering department, has recently worked on research to design and test an electrically-pumped (Si)GeSn laser device operating at a world record temperature of 115 °C fabricated in a CMOS compatible process flow. Solomon had imagined the possibility of having an affordable smartphone with built-in IR cameras, which he believes can improve situational awareness, enhance safety with long-range detection and recognition capabilities.

The focus now is to study the light emitting diode (LED) design and develop a better

fabrication technique toward improving the device efficiency and obtaining electroluminescence (EL) at room temperature.

Appendix B: Executive Summary of Newly Created Intellectual Property

The new intellectual property created from this project is:

1. The workbench design for using an FTIR spectrometer with external laser sources to characterize grown samples/fabricated devices for RT PL, optical pumping, and EL with the same setup.

Appendix C: Potential Patent and Commercialization Aspects of Listed Intellectual Property Item

C.1 Patentability of Intellectual Property (Could Each Item be Patented)

The patentability of the listed intellectual property was considered.

1. The unique setup design and efficiency could be patented.

C.2 Commercialization Prospects (Should Each Item Be Patented)

1. The alignment and setup could easily be modified and replicated. FTIR spectrometers are commercially available for characterization of various materials and different approaches could be used for setup. The IP should not be patented.

C.3 Possible Prior Disclosure of IP

1. Not applicable.

Appendix D: Broader Impact of Research

D.1 Applicability of Research Methods to Other Problems

The characterization method employed in this thesis research could be used to study the fundamental structural, electrical, and optical properties of other materials and fabricated light-emitting devices such as group III-V laser devices.

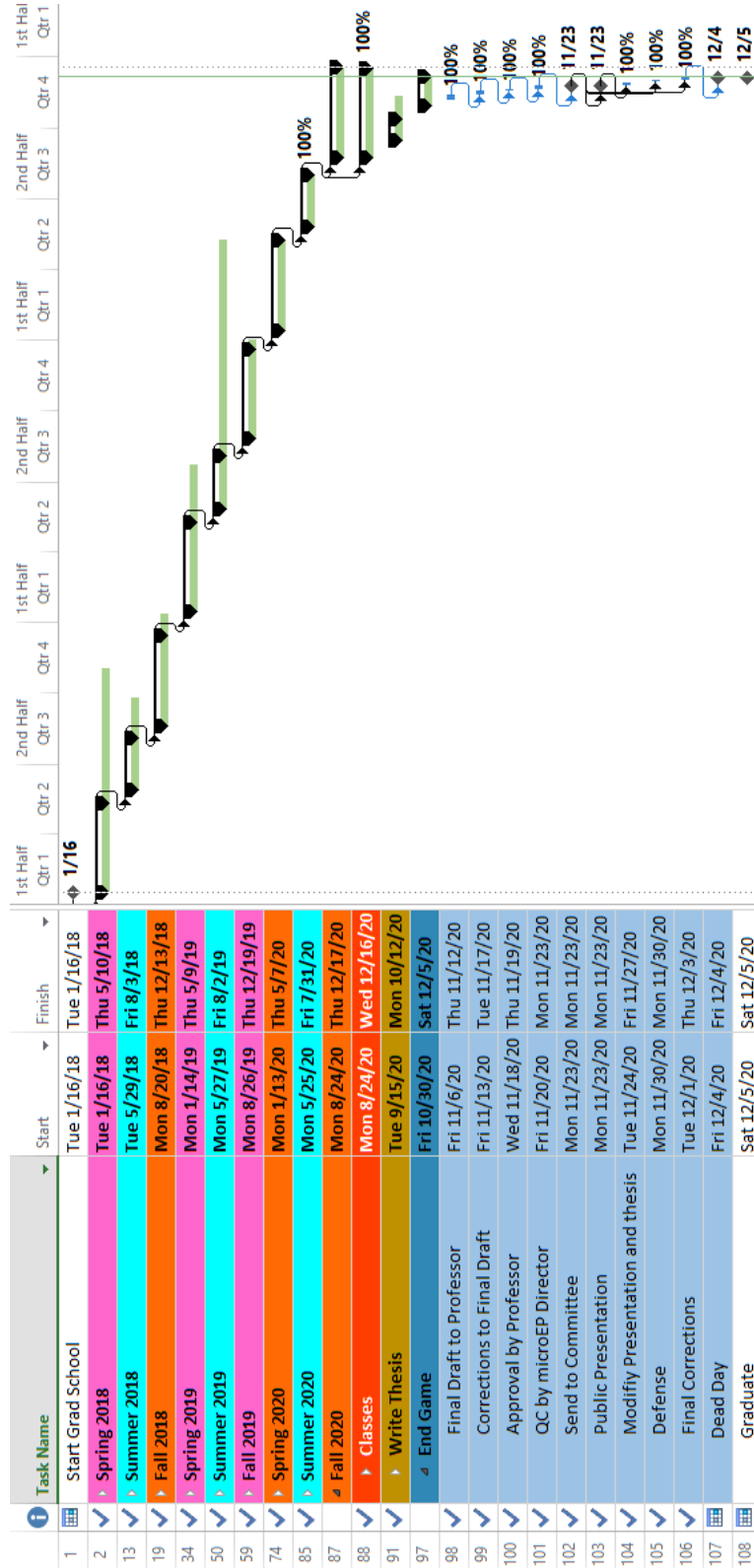
D.2 Impact of Research Results on U.S. and Global Society

High-resolution electroluminescence and photoluminescence have been demonstrated for a GeSn based laser. The results reported for the GeSn based laser on Si have shown improved characteristics required for on-chip integration. This would have a great impact on the U.S and global society as the GeSn laser material is further developed for large-scale manufacturing, utilizing state-of-the-art silicon image sensor circuits on the same chip and lowering the cost significantly. The outcome will make the (Si)GeSn material the dominating IR detector technology by replacing the expensive group III-V materials.

D.3 Impact of Research Results on the Environment

The development of GeSn based laser leads to the manufacturing of power-efficient optoelectronic devices, thereby significantly reducing dependence and high consumption of other natural sources of energy that negatively affect the environment.

Appendix E: Microsoft Project for MS MicroEP Degree Plan



Appendix F: Identification of All Software Used in Research and Thesis Generation

Computer #1:

Model Number: Lenovo 80XM

Serial Number: PF13VTHE

Location: Personal laptop

Owner: Dr. Shui-Qing Yu

Software #1:

Name: Microsoft 365 Apps for enterprise

Purchased by: Electrical Engineering Department, University of Arkansas

Software #2:

Name: Microsoft Project Professional 2013

Provided by: Electrical Engineering Department, University of Arkansas

Software #3:

Name: Zotero

Purchased by: Free download available from Zotero.org

Software #4

Name: OriginPro 2021 (student version)

Serial Number: GA3S4-6089-7245285

Purchased by Solomon Ojo

Software #5

Name: GNU Image Manipulation Program (GIMP)

Purchased by: Free download available from gimp.org

Computer #2:

Model Number: Dell Vostro

Serial Number: 52M6XK1

Location: ENRC Room 2923

Owner: Dr. Shui-Qing Yu

Software #1:

Name: SynerJY with built-in Origin software

Purchased by: Dr. Shui-Qing Yu

Computer #3:

Model Number: Dell Inspiron

Serial Number: 52M6XK1

Location: ENRC Room 2923

Owner: Dr. Shui-Qing Yu

Software #1:

Name: LabVIEW 2019 software

Purchased by: Electrical Engineering Department, University of Arkansas

Appendix G: All Publications Published, Submitted, and Planned

G.1. Articles in Refereed Journals

2020

- [6]. Zhou, Yiyin; **Ojo, Solomon**; Miao, Yuanhao; Tran, Huong; Grant, Joshua; Abernathy, Grey; Amoah, Sylvester; Bass, Jake; Salamo, G.; Du, Wei; Liu, Jifeng; Margetis, Joe; Tolle, John; Zhang, Yong-Hang; Sun, Greg; Soref, Richard; Li, Baohua; Yu, Shui-Qing “Electrically injected GeSn lasers with peak wavelength up to 2.7 μm at 90 K” Planned to be submitted to Advanced Optical Material.
- [5]. Grey Abernathy, Yiyin Zhou, **Solomon Ojo**, Bader Alharthi, Perry C. Grant, Wei Du, Joe Margetis, John Tolle, Andrian Kuchuk, Baohua Li, Shui-Qing Yu “Study of SiGeSn/GeSn single quantum well towards high-performance all-group-IV optoelectronics” Manuscript Status: Submitted. Journal of Applied Physics. Manuscript #JAP20-AR-06009.
- [4]. Seyedeh Fahimeh Banihashemian, Joshua M Grant, Abbas Sabbar, Huong Tran, Oluwatobi Olorunsola, **Solomon Ojo**, Sylvester Amoah, Mehrshad Mehboudi, Shui-Qing Yu, Aboozar Mosleh, Hameed A Naseem “Growth and characterization of low-temperature $\text{Si}_{1-x}\text{Sn}_x$ on Si using plasma enhanced chemical vapor deposition,” Opt. Mater. Express, vol. 10, no. 9, p. 2242, Sep. 2020, doi: 10.1364/OME.398958.
- [3]. Yiyin Zhou, Yuanhao Miao, **Solomon Ojo**, Huong Tran, Grey Abernathy, Joshua M Grant, Sylvester Amoah, Gregory Salamo, Wei Du, Jifeng Liu, Joe Margetis, John Tolle, Yong-Hang Zhang, Greg Sun, Richard A Soref, Baohua Li, Shui-Qing Yu “Electrically injected GeSn lasers on Si operating up to 100 K,” Optica, vol. 7, no. 8, p. 924, Aug. 2020, doi: 10.1364/OPTICA.395687.

2019

- [2]. Zhou Yiyin, Du Wei, Dou Wei, **Solomon Ojo**, Tran Huong, Ghetmiri Seyed, Liu Jifeng, Sun Greg, Soref Richard, Margetis Joe, Tolle John, Li Baohua, Chen Zhong, Mortazavi Mansour, Yu Shui-Qing “Optically Pumped GeSn Lasers Operating at 270 K with Broad Waveguide Structures on Si,” ACS Photonics, vol. 6, no. 6, pp. 1434–1441, 2019.

2018

- [1]. Joe Margetis, Yiyin Zhou, Wei Dou, Perry C. Grant, Bader Alharthi, Wei Du, Alicia Wadsworth, Qianying Guo, Huong Tran, **Solomon Ojo**, Grey Abernathy, Aboozar Mosleh, Seyed A. Ghetmiri, Gregory B. Thompson, Jifeng Liu, Greg Sun, Richard Soref, John Tolle, Baohua Li, Mansour Mortazavi, Shui-Qing Yu, “All group-IV SiGeSn/GeSn/SiGeSn QW laser on Si operating up to 90 K”, Applied Physics Letters 113, 221104 (2018)

G.2. Articles and Abstracts in Conference Proceedings

2020

- [4]. Yiyin Zhou, Yuanhao Miao, **Solomon Ojo**, Grey Abernathy, Wei Du, Greg Sun, Richard Soref, Jifeng Liu, Yong-Hang Zhang, Mansour Mortazavi, Baohua Li, and Shui-Qing Yu, “Direct bandgap electroluminescence from SiGeSn/GeSn double-heterostructure monolithically grown on Si,” in Conference on Lasers and Electro-Optics, OSA Technical Digest (Optical Society of America, 2020), paper SM3M.4.
- [3]. Grey Abernathy, Yiyin Zhou, **Solomon Ojo**, Yuanhao Miao, Wei Du, Greg Sun, Richard Soref, Jifeng Liu, Yong-Hang Zhang, Mansour Mortazavi, Baohua Li, and Shui-Qing Yu, “Study of gain for SiGeSn/GeSn/SiGeSn multiple quantum well lasers,” in Conference on Lasers and Electro-Optics, OSA Technical Digest (Optical Society of America, 2020), paper SM3M.5.

2019

- [2]. Yiyin Zhou, Wei Dou, Wei Du, **Solomon Ojo**, Huong Tran, Seyed Ghetmiri, Jifeng Liu, Greg Sun, Richard Soref, Joe Margetis, John Tolle, Baohua Li, Zhong Chen, Mansour Mortazavi, Shui-Qing Yu, “Si-based Mid-Infrared GeSn-Edge-Emitting Laser with Operating Temperature up to 260 K”, CLEO 2019 (San Jose): Applications and Technology, AW3P.3
- [1]. Yiyin Zhou, Joe Margetis, Grey Abernathy, Wei Dou, Perry C Grant, Bader Alharthi, Wei Du, Alicia Wadsworth, Qianying Guo, Huong Tran, Solomon Ojo, Aboozar Mosleh, Seyed A Ghetmiri, Gregory B Thompson, Jifeng Liu, Greg Sun, Richard Soref, John Tolle, Baohua Li, Mansour Mortazavi, Shui-Qing Yu, Investigation of SiGeSn/GeSn/SiGeSn Quantum Well Structures and Optically Pumped Lasers on Si, CLEO 2019 (San Jose): Science and Innovations, STu3N. 3.

G.3. Conference Presentations

2019

- [3]. Jake Bass, Grey Abernathy, Sylvester Amoah, Huong Tran, Samir Saha, **Solomon Ojo**, Oluwatobi Olorunsola, and Shui-Qing (Fisher) Yu, Towards Fully-Integrated Optical Systems, 2019 CHECCS IMWP Summer (meeting), August 11-13, Fayetteville, AR (2019)
- [2]. Yiyin Zhou, Wei Dou, Wei Du, **Solomon Ojo**, Huong Tran, Seyed Ghetmiri, Jifeng Liu, Greg Sun, Richard Soref, Joe Margetis, John Tolle, Baohua Li, Zhong Chen, Mansour Mortazavi, Shui-Qing Yu, Si-based Mid-Infrared GeSn-Edge-Emitting Laser with Operating Temperature up to 260 K, CLEO 2019 (San Jose): Applications and Technology, AW3P.3

- [1]. Yiyin Zhou, Joe Margetis, Grey Abernathy, Wei Dou, Perry C Grant, Bader Alharthi, Wei Du, Alicia Wadsworth, Qianying Guo, Huong Tran, **Solomon Ojo**, Aboozar Mosleh, Seyed A Ghetmiri, Gregory B Thompson, Jifeng Liu, Greg Sun, Richard Soref, John Tolle, Baohua Li, Mansour Mortazavi, Shui-Qing Yu, Investigation of SiGeSn/GeSn/SiGeSn Quantum Well Structures and Optically Pumped Lasers on Si, CLEO 2019 (San Jose): Science and Innovations, STu3N. 3.

Appendix H: Bruker IFS 66/S Standard operating procedure for Yu Lab

Standard Operation Procedure (SOP) for Bruker FTIR

Important Safety measure:

1. Wear the appropriately labeled goggle for the laser you are about to operate (at the entrance to lab 2933-A).
2. Turn on the switch that indicates laser operation is on once you access the lab.
3. Wear gloves.
4. Block the beam path on the FTIR table with the beam block near to the source.

Getting Started:

1. Open the N₂ bottle behind the FTIR table: (a little opening will do)



2. Turn on the power switch for the Bruker IFS electronics unit beneath the FTIR table:



3. Fill the LN₂ into the Dewar of the InSb detector (ignore step if it is a PbS detector)
4. Turn on the desktop computer.
5. Start the 532 nm (green) laser. (follow the SOP for Green Laser operation).

6. Switch on the 1064 nm laser. (follow the SOP for 1064 nm Laser operation).
7. Wait for a couple of minutes for the laser beam to stabilize.
8. Turn on the chopper: select appropriate frequency based on detector type.
9. Turn on the lock-in amplifier.
10. Confirm the FTIR spectrometer status light is green. If it is blinking red, check the Nitrogen bottle is properly opened, otherwise confirm if the bottle is empty.



11. Make sure the power meter is in the beam path as indicated below:



12. Turn on the detector. (Ensure all beam path are blocked to avoid damaging the detector)

Sample mounting:

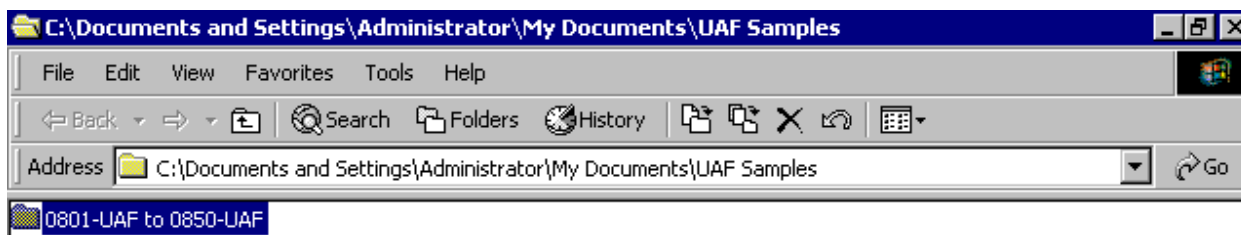
1. Apply small grease on the sample holder
2. Place the sample to measured accordingly.
3. Unblock the green laser to ensure the laser beam is hitting the right spot on the sample.
4. If the laser beam is not on the sample, adjust the sample and/or the sample holder only and not the beam path or laser source.

Log on to the computer:

1. Log on to the Windows Administrator account. No password is required.


2. On the desktop, select the  shortcut to UAF samples.

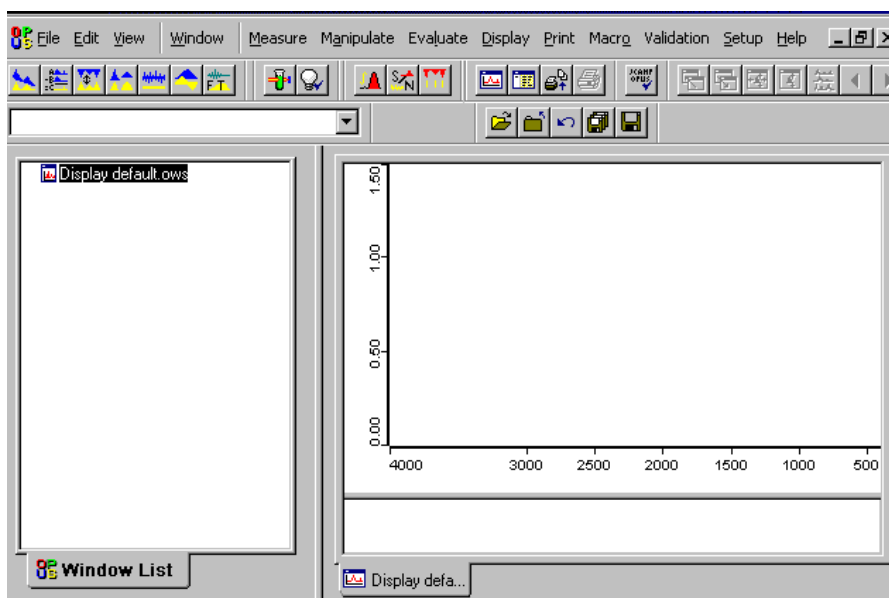
3. Select the main folder for the sample number range



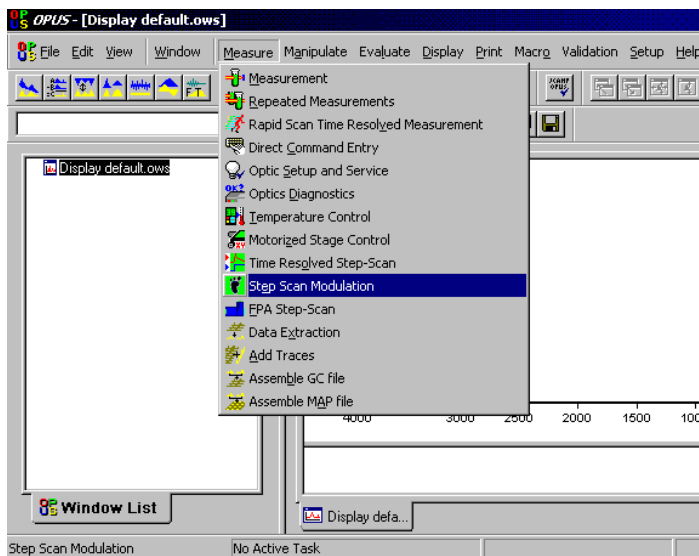
4. Create a sub-folder for the sample number to be measured e.g 0826-UAF

Start OPUS:

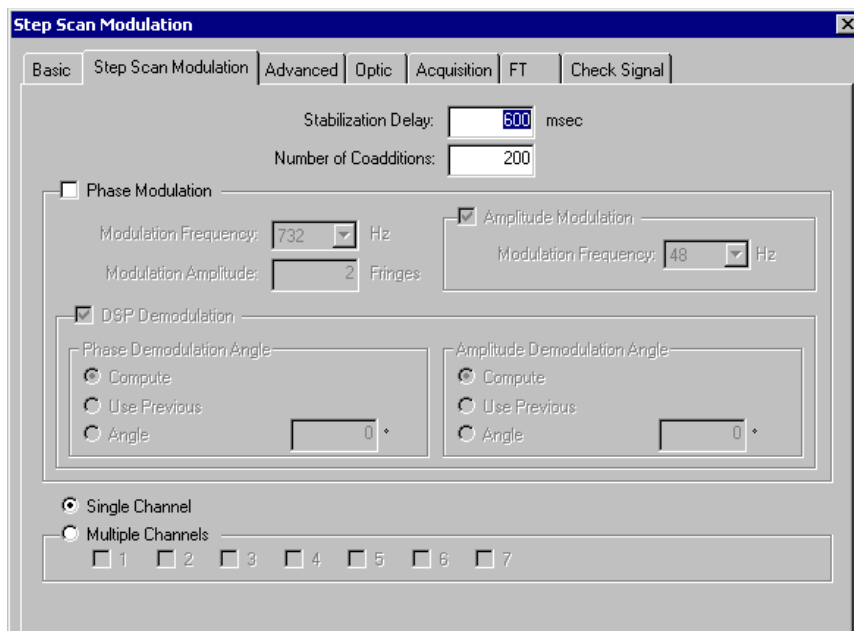
1. From the desktop, double click  to launch OPUS software.
2. The Login dialog box will appear and prompt for a password.
3. The default password is opus1
4. Once you log in, you will be assigned a workspace file as shown below:



5. Confirm the status light at the bottom left-hand corner is still green. If the light is red, it indicates there is a problem with the spectrometer. Please contact the FIR table manager.
6. Click on the “**M**easure” tab from the workspace file window and then select the “Step Scan Modulation”



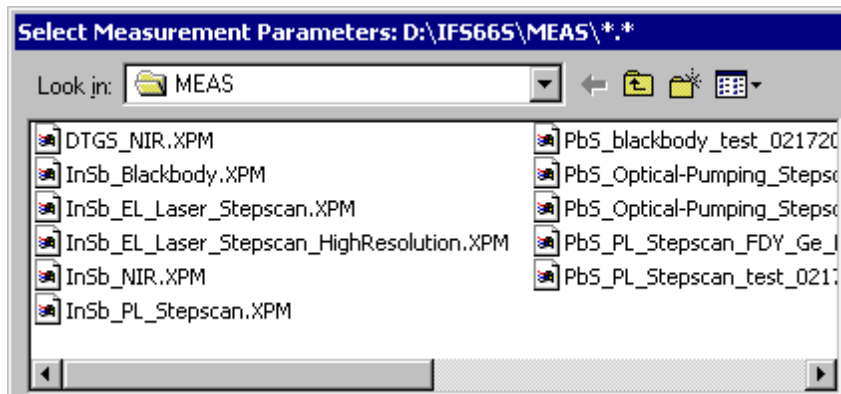
7. View the **Basic** tab.
8. Go to the “**Step Scan Modulation**” tab:



Avoid changing the settings. However, note that the “Stabilization Delay” should be equal to 6 times the “Time Constant” on the Lock-in amplifier.

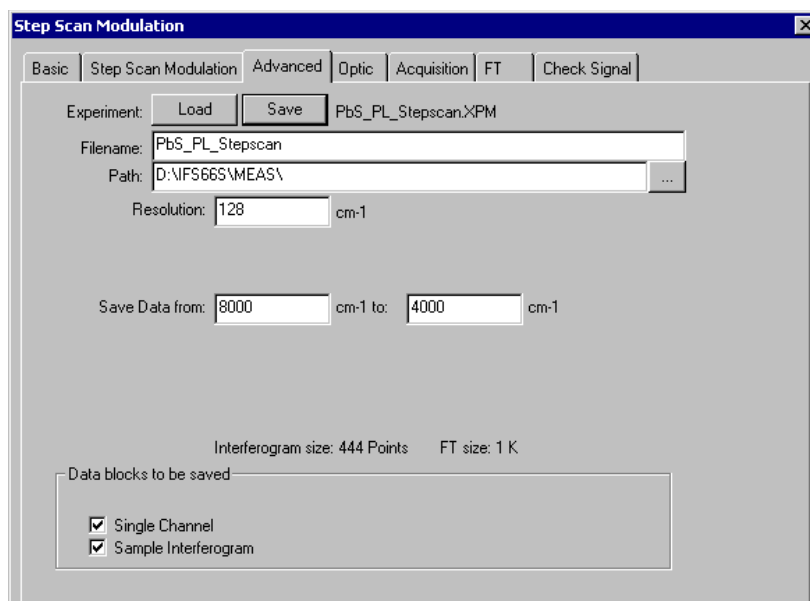
9. **Advance tab:**

- a. Click on “Load” to select the appropriate experiment file based on the detector type. Note that the settings for each detector type have been saved on the system already.



For example, when using a PbS detector for PL, select the PbS_PL_Stepscan....

- b. Do not alter the file name or path.
- c. Resolution: This has been set to 128 cm⁻¹ (only change if you need a higher resolution). Note: Higher resolutions will increase your Interferogram size (data points) and scan time.
- d. Enter a spectral range in wavenumber for spectrum data-blocks that you would like to save.



10. Optics tab:

Confirm setting is the same as shown below

The screenshot shows the 'Step Scan Modulation' dialog box with the 'Optic' tab selected. The settings are as follows:

Parameter	Value
Source Setting:	Laser; 9395.0 cm-1; 510 mW
Beamsplitter:	KBr
Aperture Setting:	2.0 mm
Measurement Channel:	External right (X3)
Detector Setting:	External A
Scanner Velocity:	0 ; 1.6 KHz
Sample Signal Gain:	Automatic
Delay after Device Change:	0
Delay Before Measurement:	0

11. Acquisition tab:

The screenshot shows the 'Step Scan Modulation' dialog box with the 'Acquisition' tab selected. The settings are as follows:

Parameter	Value
Wanted High Frequency Limit:	8000
Wanted Low Frequency Limit:	4000
Laser Wavenumber:	15799.90
Interferogram size:	444 Points
FT size:	1 K
Acquisition Mode:	Double Sided, Forward-Backward

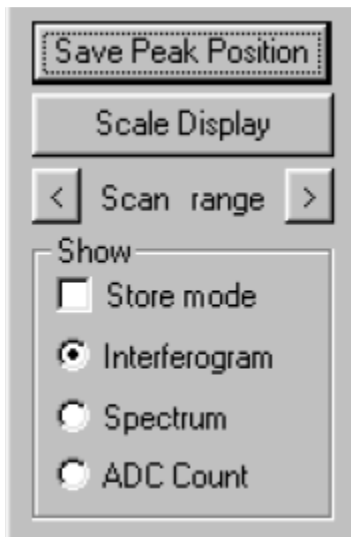
The “Wanted High Frequency Limit” and the “Wanted Low Frequency Limit” must be the same or within the range of the data-blocks selected in Advance tab.

12. FT tab (leave them unchanged):

The screenshot shows the 'Step Scan Modulation' dialog box with the 'FT' tab selected. The settings are as follows:

Parameter	Value
Phase Resolution:	32
Phase Interferogram Points:	444
Phase Correction Mode:	Power Spectrum
Apodization Function:	Blackman-Harris 4-Term
Zerofilling Factor:	2
Interferogram size:	444 Points
FT size:	1 K

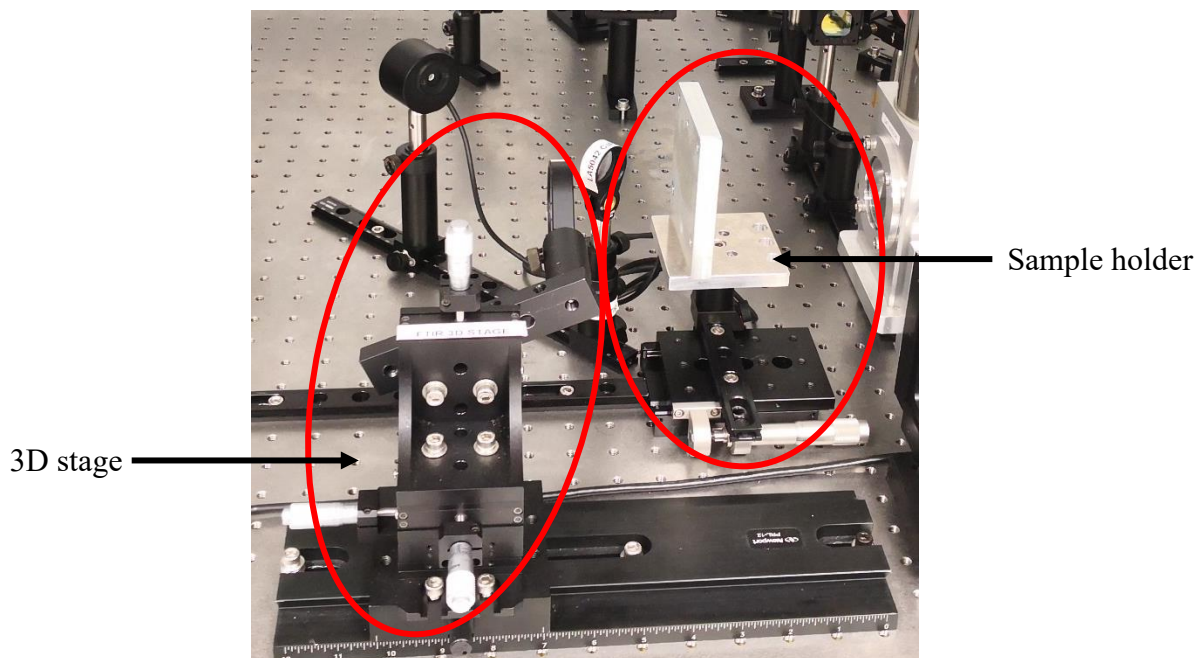
13. Check Signal tab.



Sample Measurement:

1. Unblock the laser beam. (To change laser source, flip appropriate mirror for the path)
2. Measure the laser power. Set to desired power if need be.
3. Optimize the sample measurement by adjusting the 3D stage and sample holder only.

Note: Do not touch the beam path or any other optics on the table as they have already been aligned and fixed.



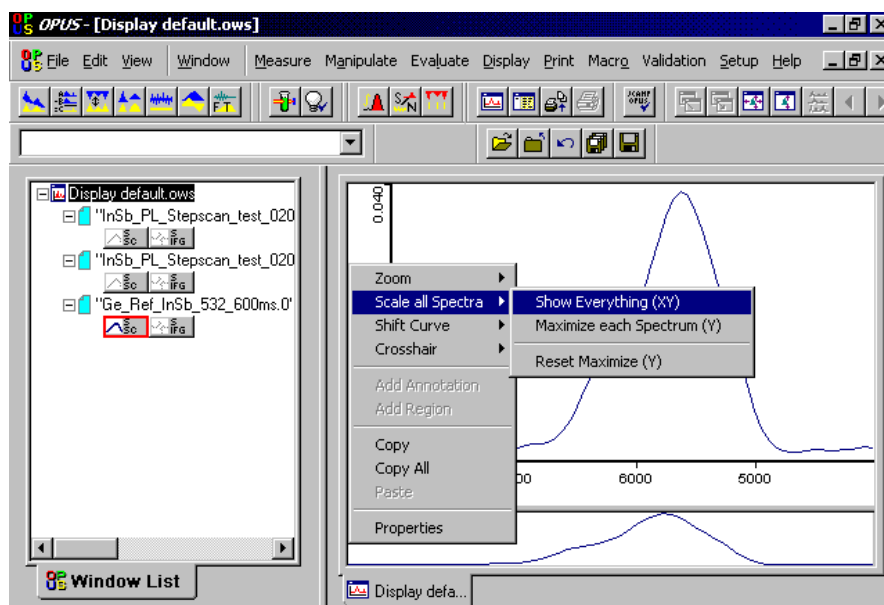
4. See optimized reading from the lock-in amplifier. If no signal reading is observed on the lock-in, check the following:
 - a. Confirm detector is on.
 - b. Ensure the laser block has been removed from the beam path.
 - c. Go to the **Optics tab** and compare the setting is the same as number 10 above.
 - d. Adjust the 3D stage and or the sample holder again.
5. Once the desired optimization is achieved, go to the **“Basic”** tab, and click on “Start Step Scan Modulation Measurement”



6. Wait for the measurement to complete. Note: The status light of the FTIR spectrometer will turn red during measurement.

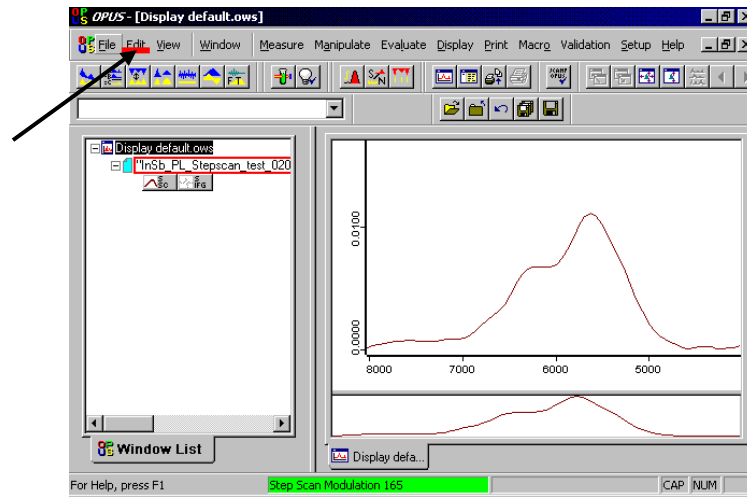
Save Spectra:

1. When the measurement is complete, display the whole spectrum using “Scale all Spectra”
 2. Save the spectrum using the **Save File As** command from the File tab
 3. Save as Data Point Table format (this will enable us to plot the result in Origin)
- i.

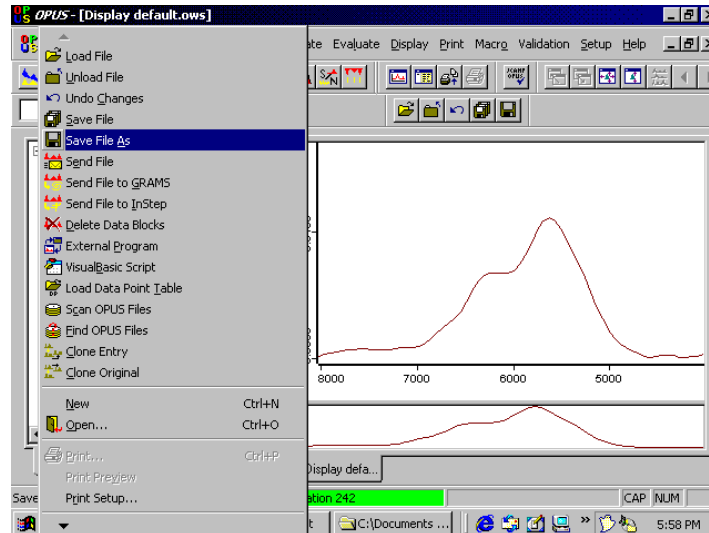


Note: Convert saved data from wavenumber to wavelength before plotting in Origin.
(check SharePoint for FTIR conversion excel template)

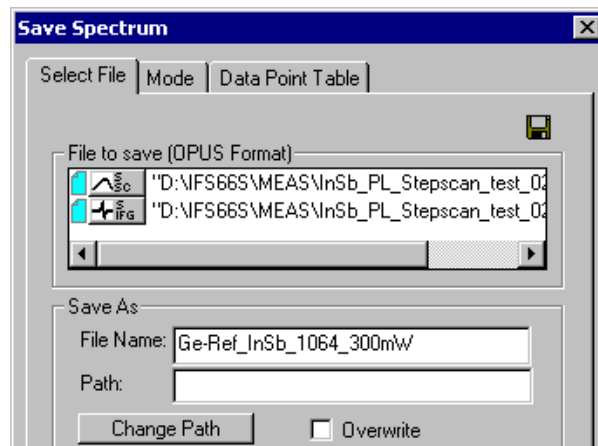
ii.



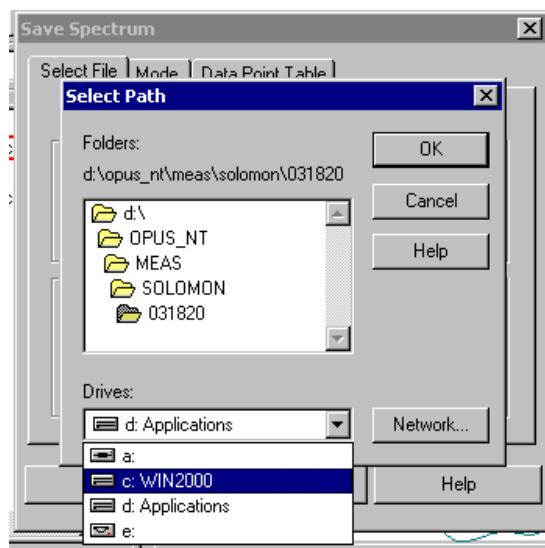
iii.



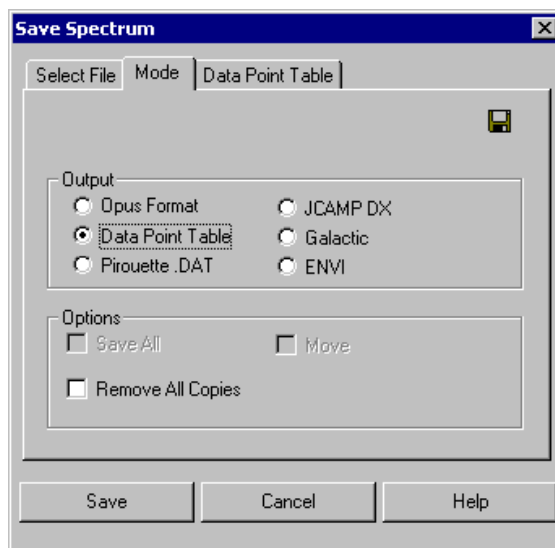
iv. Name the file accordingly. For example, 0XXX-UAF



v. Select path by navigating to the folder created in number 4 of **Log on to the computer**



vi. From the **Mode** tab, select the “Data Point Table” format and click save



Shut Down:

1. Exit the OPUS software.
2. Copy saved file from computer onto a USB for data processing and shutdown computer.
3. Turn off the Bruker IFS electronics unit beneath the FTIR table.
4. Close the N₂ bottle. (Ensure the electronics unit is turned off before this step).
5. Turn of all lasers following their standard shutdown procedure.
6. Turn off the lock-in amplifier and the chopper.

Appendix I: Edge Emitting LED/Lasers Fabrication Traveler

Traveler, Edge Emitting LEDs/Lasers (wide ridge)

0598-0600
FDY-XX1 XX2 XX3
ERW 1 024-026

Fab Lot # ERW

Start Date:

Due Date:

Mask Set: Edge Laser

Purpose: Edge emitting laser

Lot#: Edge Emitting Laser, Ridge Defined Edge Emitter, Wet Etch

Device #	Lot #	Growth info	Description
0598	ERW1024	FDY0XX1	Sn % composition, cap thickness & doping
0599	ERW1025	FDY0XX2	Sn % composition, cap thickness & doping
0600	ERW1026	FDY0XX3	Sn % composition, cap thickness & doping

OP/LINK	DESCRIPTION	PARAMETER	ESTIMATED TIME
1	Sample Clean		1 hour
2	1st alignment: mesa	Edge LED -1 half	3 hours
2	Mesa Etching		2 hours
3	2 nd alignment: Metal contacts	Edge LED -2 half	3 hours
4	Metal deposition & Lift-off		4 hours
5	Lapping		
			Total: 20 hours

Sample Pre-clean (Start)				
Date/ Time	1.1	Solvent Clean <input type="checkbox"/> Sonicator	<input type="checkbox"/> Acetone sonication for 5 minutes <input type="checkbox"/> Use Q-tip to gently clean surface in Acetone <input type="checkbox"/> Rinse with clean IPA <input type="checkbox"/> Rinse with Di water <input type="checkbox"/> N2 Dry /Dehydration bake, 100 °C for 2 minutes <input type="checkbox"/> Check under microscope <input type="checkbox"/> Repeat or use Remover PG at 80°C for 10 min if necessary	

Photolithography			
Date/ Time	2.1	Photolithography <input type="checkbox"/> Preset & precheck <input type="checkbox"/> HMDS <input type="checkbox"/> Spinner <input type="checkbox"/> Hot plate (Soft bake) <input type="checkbox"/> MJB-3 <input type="checkbox"/> Testing <input type="checkbox"/> Base hood <input type="checkbox"/> Hot plate (Hard bake) <input type="checkbox"/> Descum <input type="checkbox"/> Inspection Microscope	<input type="checkbox"/> 110°C & 130°C <input type="checkbox"/> Spin coater Recipe 4; 4000 rpm <input type="checkbox"/> 1.5-inch chuck w/ skirt <input type="checkbox"/> Blue tape <input type="checkbox"/> Apply HMDS Recipe 4; 4000 rpm <input type="checkbox"/> AZ4110 (target ~ 1.7 um) <input type="checkbox"/> 110°C (reading) /50 sec <input type="checkbox"/> Check accuracy with thermocouple Edge LED mask (1st half) <input type="checkbox"/> Beads removal at the edges <input type="checkbox"/> Mask orientation <input type="checkbox"/> Use bottom right corner for consistency <input type="checkbox"/> Determine exposure time PR Thickness: _____um (Profilometer) Energy: _____mJ/cm2 (Tk*45) Intensity: <u>4.52</u> mW/cm2 (From log) Exposure Time: <u>11</u> s (Energy/Intensity) <input type="checkbox"/> Develop using AZ300 MIF (around 45 sec) <input type="checkbox"/> Rinse in DI water <input type="checkbox"/> N2 Blow dry Develop time / Comments: 0XX1-FDY: _____ 0XX2-FDY: _____ 0XX3-FDY: _____ 130 °C (reading) /15 min <input type="checkbox"/> Check accuracy with thermocouple 3-minute run time Power: <u>200 Watts</u> O ₂ Gas Flow: <u>250 sccm</u> <input type="checkbox"/> Smallest Feature O.K.?

		<input type="checkbox"/> Profilometer <input type="checkbox"/> Mask cleaning	Resist thickness 0XX1-FDY: _____ 0XX2-FDY: _____ 0XX3-FDY: _____ <input type="checkbox"/> Remover PG at 80°C for 20 min	
--	--	---	---	--

Mesa Etching																								
	3.1	Wet etching <input type="checkbox"/> Acid bench	Recipe: HCL: H2O2: H2O=1: 1: 10 at 0°C H2O <u>200 mL</u> H2O2 <u>20 mL</u> HCL <u>20 mL</u> Target: <u>1400 nm for 60~68 min</u> <table border="1"> <thead> <tr> <th>Device #</th> <th>Time</th> <th>Thickness</th> <th>Rate</th> </tr> </thead> <tbody> <tr> <td>0598</td> <td></td> <td></td> <td></td> </tr> <tr> <td>0599</td> <td></td> <td></td> <td></td> </tr> <tr> <td>0600</td> <td></td> <td></td> <td></td> </tr> <tr> <td></td> <td></td> <td></td> <td></td> </tr> </tbody> </table>		Device #	Time	Thickness	Rate	0598				0599				0600							
Device #	Time	Thickness	Rate																					
0598																								
0599																								
0600																								
	3.2	Resist Removal <input type="checkbox"/> Matrix Asher (optional) <input type="checkbox"/> Inspection microscope <input type="checkbox"/> Profilometer	<input type="checkbox"/> Acetone or <input type="checkbox"/> PG remover, _____ minutes at 80°C 3-minute run time Power: <u>200 Watts</u> O ₂ Gas Flow: <u>250 sccm</u> <input type="checkbox"/> OK Etch depth Sample1: _____ Sample2: _____ Sample3: _____																					

2 nd alignment & define contacts (Start)			
Date/ Time	4.1	Solvent clean (if not continuous process)	<input type="checkbox"/> DI water <input type="checkbox"/> 5 min dehydration on hotplate at 95° C
	4.2	Photolithography Image reverse <input type="checkbox"/> HMDS <input type="checkbox"/> Spinner check <input type="checkbox"/> Spinner <input type="checkbox"/> Hot plate (Soft bake) <input type="checkbox"/> MJB-3 <input type="checkbox"/> Test <input type="checkbox"/> Hot plate (PEB) <input type="checkbox"/> MJB3 (Flooded exposure) <input type="checkbox"/> Descum <input type="checkbox"/> Base hood <input type="checkbox"/> Inspection Microscope	Recipe 3; 3000 rpm <input type="checkbox"/> Apply HMDS <input type="checkbox"/> Blue tape Recipe 3, 3000 rpm for 50 seconds <input type="checkbox"/> AZ5214(target ~ 1.8 um) <input type="checkbox"/> 2.5 inch chuck w/ skirt <input type="checkbox"/> Blue tape 95°C / 50 sec <input type="checkbox"/> Check accuracy with thermocouple <input type="checkbox"/> Beads removal at the edges Edge LED mask (2nd-half) <input type="checkbox"/> Mask cleaning PRS1000 / Acetone & IPA <input type="checkbox"/> Mask orientation <input type="checkbox"/> Use same corner as previous one for consistency <input type="checkbox"/> Determine exposure time PR Thickness: _____um (Profilometer) Energy: _____mJ/cm2 (Tk*27) Intensity: _____mW/cm2 (From log) Exposure Time: _____s (Energy/Intensity) 105 °C / 2 min <i>Check accuracy with thermocouple</i> <input type="checkbox"/> No Mask Needed <input type="checkbox"/> Determine exposure time Energy: _____>200_____mJ/cm2 (Tk*67.2) Exposure Time: _____ 60 _____s (Energy/Intensity) 3 minute run time Power: <u>200 Watts</u> O ₂ Gas Flow: <u>250 sccm</u> <input type="checkbox"/> Develop AZ300 MIF (around 30 seconds) <input type="checkbox"/> Rinse in DI water <input type="checkbox"/> N2 Blow dry Develop time / Comments Sample1: _____ Sample2: _____ Sample3: _____ <input type="checkbox"/> Smallest Feature O.K.?

Metal Deposition & Lift-off (Start)			
Date/ Time	5.1	Metal Deposition	<input type="checkbox"/> 10/350 nm Cr/Au <input type="checkbox"/> Inspection Microscope <input type="checkbox"/> Pumping down <input type="checkbox"/> Cr deposition <input type="checkbox"/> Au deposition
			<p>Samples: Pump down time: _____ min Base pressure: _____ mBar</p> <p>Reference value Cr : 100 Å @ 0.5-1 Å/sec Start current: _____ mA (in scale) Start pressure _____ mBar Start deposition rate: _____ Å/sec End pressure _____ mBar End deposition rate: _____ Å/sec Thickness: _____ Å</p> <p>Reference value Au : 3500 Å @ 1.5 Å/sec Start current: _____ mA (in scale) Start pressure _____ mBar Start deposition rate: _____ Å/sec Start Temperature: _____ End current: _____ mA (in scale) End pressure _____ mBar End deposition rate: _____ Å/sec End Temperature: _____ Thickness: _____ Å</p>
	5.2	Metal Liftoff	
		<input type="checkbox"/> Solvent Hood <input type="checkbox"/> Microscope	<input type="checkbox"/> Acetone <input type="checkbox"/> PG remover Temperature _____ Time _____ <input type="checkbox"/> Place in ultrasonic bath if necessary Acetone / Methanol / IPA / DI rinse Surface Cleanness <input type="checkbox"/> Pass <input type="checkbox"/> Fail Pattern OK? <input type="checkbox"/> Pass <input type="checkbox"/> Fail

Fabricated by:

Finish date: